## Mémoire

**Auteur :** Kolkman, Maxime
**Promoteur(s) :** Damblon, Christian
**Faculté :** Faculté des Sciences
**Diplôme :** Master en sciences chimiques, à finalité approfondie
**Année académique :** 2022-2023
**URI/URL :** http://hdl.handle.net/2268.2/17022

# Master thesis in chemistry

## Implementation and limits of fast 2D-NMR techniques: Ultrafast and Non-Uniform Sampling

Kolkman Maxime

Under the supervision of Pr. Christian DAMBLON

# <u>Content table</u>

## 0- Glossary

*Abbreviations*

- **DW**: dwell-time
- **EPI**: echo-planar imaging
- **expt**: experiment time
- **F1**: dimension related to $t_1$
- **F2**: dimension related to $t_2$
- **FID**: free induction decay
- **FT**: Fourier transformation
- **SW**: spectral window
- **$N_1$**: number of points acquired in the first dimension in conventional experiments
- **$N_2$**: number of points acquired in the second dimension in conventional experiments
- **$N_{conv}$**: number of points acquired in the conventional dimension in UF experiments
- **$N_{UF}$**: number of points acquired in the UF dimension in UF experiments
- **NUS**: non-uniform sampling
- **SNR**: signal-to-noise ratio
- **UF**: ultrafast

*Constants*

- **AL**: number of acquisition loop
- **CP**: Chirp Power
- **$D_1$**: relaxation delay
- **EL**: number of excitation loop
- **$G_a$**: acquisition gradient
- **$G_e$**: excitation gradient
- **IN**: number of interleaved scans
- **J**: coupling constant
- **k**: k-space position
- **$N_s$**: number of scans
- **$t_1$**: incrementation time for two dimensional sequences
- **$t_2$**: acquisition time in a sequence
- **$T_1$**: longitudinal relaxation time
- **$T_2$**: transversal relaxation time
- **$T_a$**: duration of one acquisition gradient $G_a$
- **$\gamma$**: gyromagnetic ratio
- **$\delta$**: chemical shift

# I-    Introduction

Nuclear Magnetic Resonance (NMR) is an analytical method considered to be one of the best for structural resolution of molecules. It provides a large amount of information describing connections between atoms of the studied molecules. NMR has also the advantages to be quantitative when correctly programmed, to be non-destructive and to be non-specific, meaning all molecules are detected simultaneously with the same efficiency. Moreover, NMR is highly reproducible, requires few sample preparations and is easy to automate. Therefore, NMR is adequate for a lot of biochemical fields, such as metabolomics, toxicology, the study of dynamical processes, the study of tissue materials, *et cetera*. (Reo, 2002; Welije *et al.,* 2006; Wishart, 2008; Giraudeau & Akoka, 2013; Marchand *et al.,* 2017; Markley *et al.,* 2017; Wishart, 2019; Martineau, Dumez & Giraudeau, 2020)

The main NMR sequence currently in use in most of these research fields is the $^1$H one dimensional (1D) spectrum. That sequence is simple, the acquisition is rapid, and it is easy to obtain quantitative signals. The pulse sequence consists only in a relaxation delay $D_1$, a non-selective 90° pulse and an acquisition step (*Figure 1*). A 90° pulse means the spins have a rotation of 90° from their initial position along the z-axis (axis of the permanent field $B_0$) and end in the xy plan. And a "non-selective" pulse is a pulse that excites the whole frequency range of the observed nucleus. The relaxation delay has different purposes. Its first one is to let the time to excited spins that are in the xy plan to recover to their initial position along the z-axis, and it is used to give time to the hardware to stabilize, mainly to avoid impact from heating.

The low complexity of the sequence, with a low number of pulses and delays, explains the rapidity of the experiment. The acquired signal is an evolution of the magnetisation through time. This is called a free induction decay (FID).
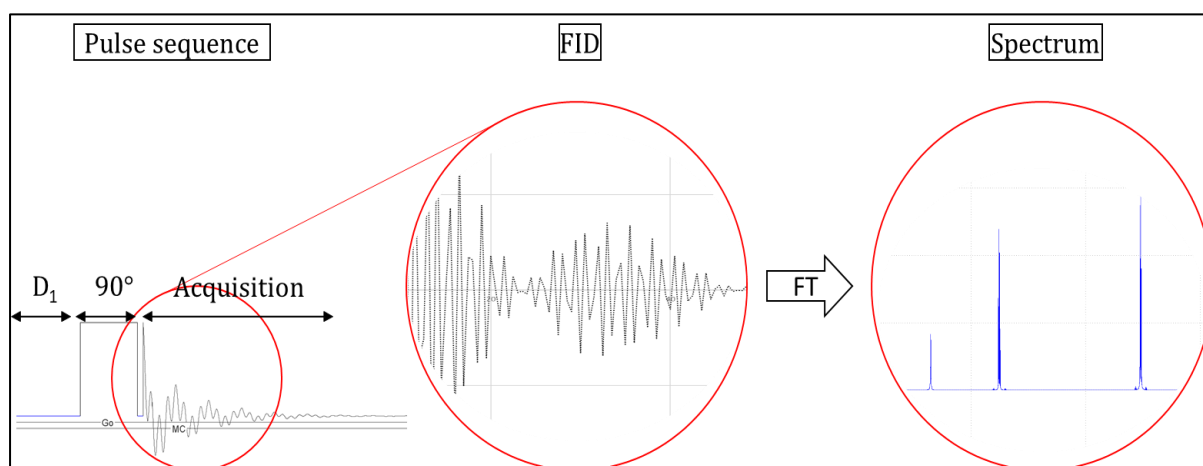


*Figure 1 - Experiment 1H one dimension: pulse sequence composed of a relaxation delay D1, a 90° pulse and the acquisition, free induction decay (FID) and spectrum after Fourier transform (FT) from left to right.*

But ¹H-spectra have a major drawback: there can be numerous overlapping signals. Figure 2 shows two cases. On the left side, the spectrum of ethanol, and on the right side, a more complex sample consisting of more than a dozen of metabolites. That latter spectrum has much more overlapping signals and suffers from a more difficult attribution and quantification. This is due to the small frequency window (SW) of the proton nucleus, about 12 ppm, and peaks are thus close to one another. Distinction between two neighbouring peaks can become difficult and quantification is harder to achieve. (Welije *et al.,* 2006; Giraudeau & Akoka, 2013; Marchand *et al.*, 2017; Markley *et al.*, 2017; Martineau, Dumez & Giraudeau, 2020; Le Guennec, Giraudeau and Caldarelli, 2014; Wishart, 2019)
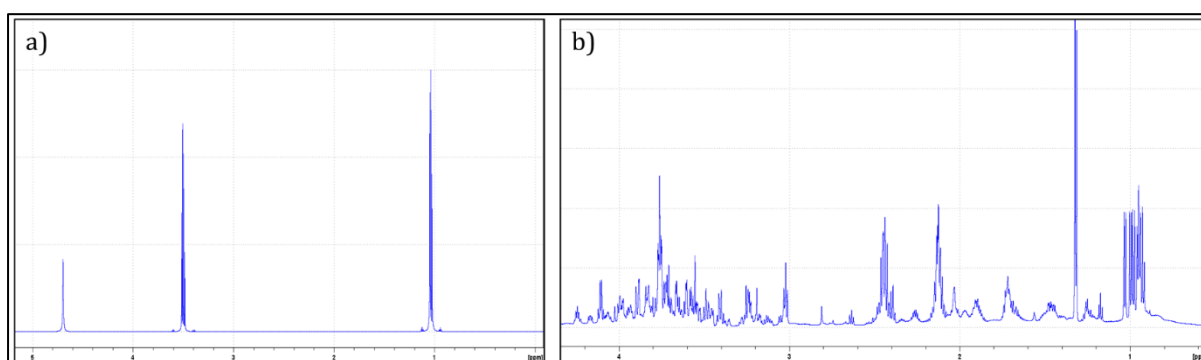


*Figure 2 - 1H spectrum for ethanol (a) and for a more complex mixture of molecules (b)*

Various solutions have been proposed in order to remediate to this lack of resolution, like pure shift NMR, NMR experiments with other nuclei (¹³C, ¹⁵N, ³¹P…) or two-dimensional (2D) experiments. (Giraudeau & Akoka, 2013; Marchand *et al.*, 2017; Martineau, Dumez & Giraudeau, 2020; Le Guennec, Giraudeau & Caldarelli, 2014)

Pure-shift NMR consists in suppressing all homonuclear couplings between neighbouring nuclei and thus changing all multiplets in singlets. This decreases the number of overlaps and allows a clearer view of the ¹H-spectrum. This "cleaning" eases identification and quantification. (Bowyer & Crouch, no date) It is used in ¹³C-spectra acquired with a homonuclear decoupling. All signals are singlets and easily distinguishable from one another.

NMR experiments with nuclei other than ¹H have wider SW and thus a better distinction between peaks. However, due to the low gyromagnetic ratio and the often low isotopic abundance (*Table 1*), the sensitivity is much lower for these experiments than for the ¹H-spectrum. As an example, carbon-13 has a gyromagnetic ratio 4 times lower than hydrogen and its abundance is about one percent. As the intensity of the signal depends proportionally to the isotopic abundance and to the gyromagnetic ratio cubed, the final intensity of carbon-13 is thus about 6400 times lower than the proton, which has an isotopic abundance near to a hundred percent. Moreover, the longitudinal relaxation time $T_1$ is also longer for nuclei others than ¹H. A longer $T_1$ means the

relaxation delay $D_1$ must be increased to let the magnetisation restore itself in its initial state before performing a second scan. This is even more necessary if the experiment is supposed to be quantitative. Therefore, with all these problems, quantification with such experiments require higher sample concentrations and longer experiment's time. (Giraudeau & Akoka, 2013)

| Nuclei | Gyromagnetic ratio γ $((1/2\,\pi)$ MHz.T$^{-1}$) | Ratio $\gamma\,/\,\gamma_H$ | Isotopic abundance (%) |
|---|---|---|---|
| $^1$H | 42.577 | 1 | 99.9885 |
| $^2$H | 6.536 | 0.154 | 0.0115 |
| $^{13}$C | 10.708 | 0.251 | 1.07 |
| $^{15}$N | -4.316 | -0.101 | 0.368 |
| $^{19}$F | 40.078 | 0.941 | 100 |
| $^{31}$P | 17.235 | 0.405 | 100 |

*Table 1 - Gyromagnetic ratio and isotopic abundance of observable nuclei in NMR (values come from Rosman & Taylor, 1999 and Bernstein, King & Zhou, 2004)*

2D experiments offer a much higher resolution compared to $^1$H-spectra thanks to the second dimension because signals are more easily discriminated. However, 2D-NMR experiments have different shortcomings which must be dealt with in order to extend the range of application fields of such methods. These shortcomings are numbered here below. (Giraudeau & Akoka, 2013; Marchand *et al.*, 2017; Martineau, Dumez & Giraudeau, 2020; Le Guennec, Giraudeau & Caldarelli, 2014)

### a. <u>Time</u>

The first problem with 2D-NMR is the long experiment duration compared to 1D--NMR. This time difference comes from the way the second dimension is acquired. (Giraudeau & Akoka, 2013)

The acquisition of a 1D spectrum is quite straightforward. All nuclei are excited and recorded at the same time. During the acquisition period, they are evolving at their specific Larmor frequency, which depends on their environment, and the magnetisation's intensity is monitored through time. Afterwards, a Fourier transformation (FT) is applied, transforming the temporal signal in a frequency spectrum (*Figure 1*). This cycle is repeated $N_s$ times, which is called the number of scans. One scan corresponds to one reading of the sequence of pulses and delays, and the results of all acquisition steps are summed up. This succession of steps is fast, but the experiment can be longer if the delay $D_1$ between successive scans needs to be adapted to the $T_1$ of the observed nucleus. Once excited, a nucleus recovers from its excited state back to its initial state, and this restoration follows an exponential function characterized by $T_1$. This time gives thus an idea about the delay needed to restore the magnetisation in its initial state. To have

repeatable and comparable results, it is important that the pulses of the successive scans are applied to the same initial state. Therefore, the delay $D_1$ needs to be adapted to the observed nuclei's $T_1$, and the experiment becomes longer if nuclei have a longer $T_1$. The duration of the spectrum acquisition could be summarized as:

Total duration = (sequence time + acquisition time + relaxation time) * $N_S$,

where the sequence time is the whole sequence of pulses and delays. In any case, a 1D spectrum can be achieved in less than 10 minutes, depending on the nucleus, the number of scans and the desired quality and resolution of the spectrum.
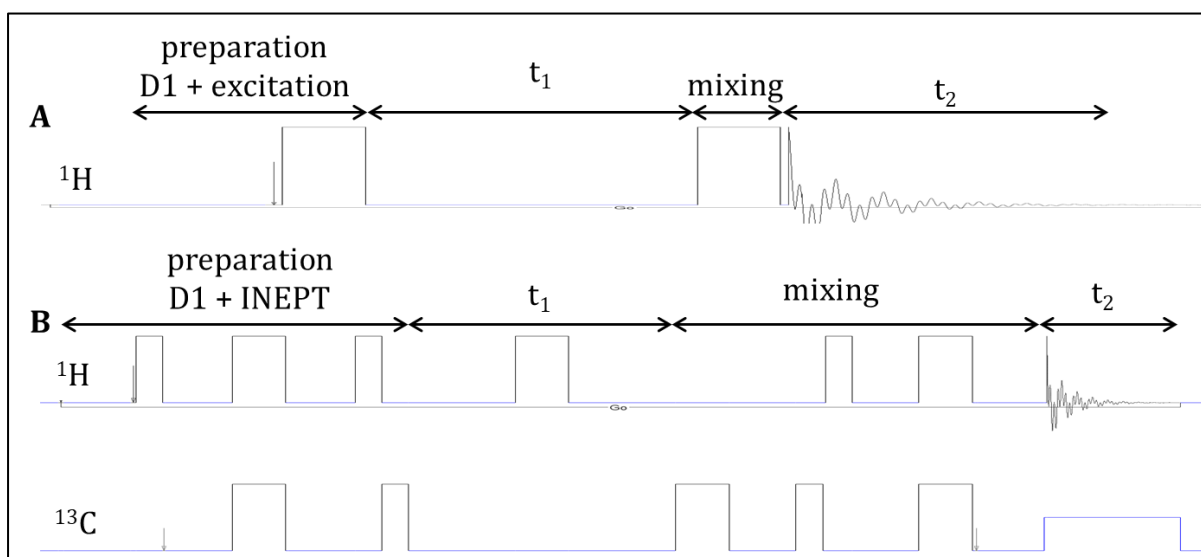


*Figure 3 - Pulse sequences for a COSY experiment (A) and a $^1H$-$^{13}C$-HSQC experiment (B), with their successive steps: preparation – evolution $t_1$ – mixing – acquisition $t_2$. These are the COSYPH and the HSQCPH sequences from Bruker.*

The acquisition of a 2D spectrum is more elaborated and requires the acquisition of numerous 1D spectra. The idea is to put one nucleus at a different step of its time evolution while a 1D spectrum for the other nucleus is acquired. To do as such, the time $t_1$ (*Figure 3*) is incremented at each scan. That incrementation is used to let the second nucleus evolve longer with various time, generating a different 1D-FID for each scan. This allows the point-per-point construction of the FID in the indirect dimension. A FT is then applied in the direct dimension F2 (related to $t_2$) on each 1D-FID individually and in the indirect dimension F1 (related to $t_1$) on all the 1D-FID (*Figure 4*).

As the time is directly proportional to both the number of scans (with a same $t_1$ value) and the number of $t_1$-incrementation, the time needed for this kind of experiment is much longer than for a simple 1D spectrum. It could be summarised as:

Total duration = (sequence time + acquisition time + relaxation time) * $N_S$ * $N_1$,

where the sequence corresponds to the whole sequence of pulses and delays. The factor $N_1$ represents the number of different 1D spectra that are acquired. Therefore, it represents the wanted resolution in the indirect dimension, the one obtained by the FT on all the 1D spectra. If a high-resolution spectrum is wanted, $N_1$ can be set up to 1024 or 2048.
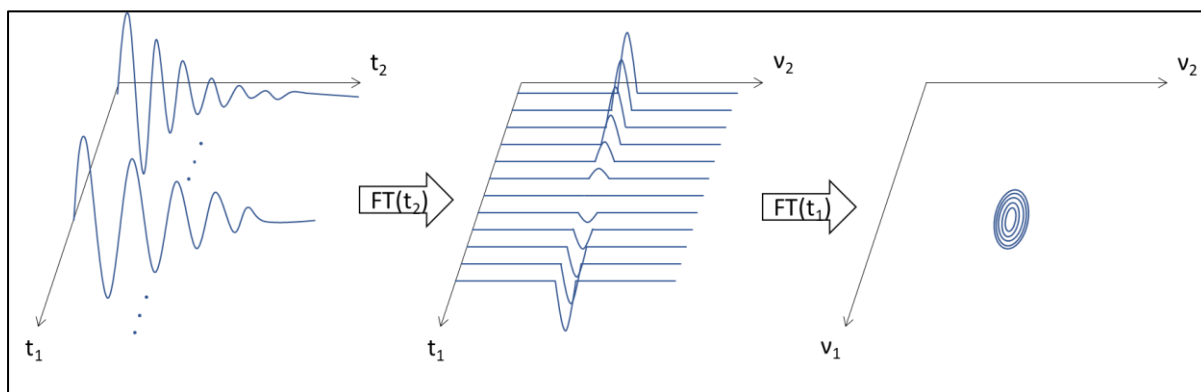


*Figure 4 - Acquired free induction decay (FID) and two-dimensional Fourier transform (FT), first in the direct dimension and then in the indirect one, for a 2D-spectrum.*

Compared to the 1D-spectra acquisition, the 2D-experiment has a longer total duration. Both $N_S$ and $N_1$ could be lowered to obtain a suitable total duration. However, it should be noted that all F1 FID contributes to the 2D overall signal-to-noise ratio (SNR). Therefore, if 128 scans are required to get a good enough 1D-spectrum in theory, 128 scans should be as well required for a 2D spectrum, that is for a 128 FID(F1) 2D spectra with one scan per FID. The practicality differs from the theory because of other considerations such as the artefact correction that requires to measure more than 1 scan per FID. In general, $N_S$ is high in the case of a 1D-acquisition because even with a high $N_S$ the experiment does not reach a too long duration, and for 2D-experiment, $N_S$ is often small.

The increase of experiment time is a real issue. The first consequence is the financial cost for one experiment. The cost increases with experiment time. The second consequence is the impossibility to study samples with a time-evolution like reactions or unstable molecules like with biological samples. Since they will change through the scanning, the spectrum will result from the sum of the initial and final states. (Giraudeau & Akoka, 2013; Marchand *et al.*, 2017; Martineau, Dumez & Giraudeau, 2020; Le Guennec, Giraudeau & Caldarelli, 2014)

Various research investigations towards methods allowing for more rapid experiments without impacting the resolution too much have been made. Different strategies have been adopted: reducing scan durations (SOFAST, ALSOFAST, BEST, ASAP, SMART), modifying the acquisition (Aliasing, NUS, Hadamard) and single-shot acquisition (Ultrafast (UF)).

## b. Quantification

In 2D experiments, peak volumes depend on numerous parameters (coupling constants J, relaxation times $T_1$ and $T_2$, pulse sequence delays...) and the dependency is not uniform for all peaks. $T_1$, as defined previously, characterizes the time needed for the magnetisation to restore itself in its original stable position along the z-axis. And $T_2$ describes the rapidity for the spins to lose their coherences in the xy plan. Peak volumes are therefore not directly proportional to the sample's concentration. (Giraudeau & Akoka, 2013; Marchand *et al.*, 2017; Martineau, Dumez & Giraudeau, 2020; Palmer *et al.*, 2015)

In addition, when quantitative conditions are required, the experiment time is even more increased. The delay $D_1$, allowing the complete restoration of the magnetisation on the initial state, must be longer than 5 times the longest $T_1$. Since the D1-increase reverberates $N_S*N_1$ times, this leads to huge increase in time and exacerbates problems due to longer experiment durations. Different solutions are possible. A first one is to determine all parameters impacting the volume of the peaks in order to calculate the absolute value of the concentration. This task is laborious and unconceivable for complex samples. (Giraudeau & Akoka, 2013) Another solution is to create a calibration curve, but that calibration would be specific for one compound in one spectrometer. (Marchand *et al.*, 2017) Other solutions more based on sequence modifications like $HSQC_0$, Q-HSQC and Q-QUIPU-HSQC exist. (Marchand *et al.*, 2017; Hu, Westler & Markley, 2011)

Because of that hindrance, 2D-NMR experiments are more used for identification and less for a quantification purpose. (Giraudeau & Akoka, 2013)

## c. Sensitivity

Compared to other analytical methods, NMR is characterised by a low sensitivity, which is due to the low population difference between the α and β spin-states. The limit of detection is about 1 to 5 μM and a volume of ~500μL is required. (Wishart, 2008; Marchand *et al.*, 2017) As mentioned above, sensitivity is even more of an issue with nuclei having low isotopic abundance and low gyromagnetic ratio like carbon-13. These can be real problems for investigations where some compounds have low concentration and/or where the sample volume cannot be imposed.

## d. Conclusion

To sum up, to extend the use of 2D-experiments in various areas, it is necessary to reduce the time of 2D-experiments and to optimise the sequence parameters to have the best sensitivity and resolution. Four solutions are currently used. (Martineau, Dumez & Giraudeau, 2020) The first one consists in reducing the SW of the indirect dimension by effecting aliasing/folding. The second option is the reducing of the time delay between two consecutive scans (SOFAST, ALSOFAST, BEST, ASAP, SMART). The third option

consists in using the scattered nature of the multi-dimensional NMR (non-uniform sampling (NUS), Hadamard). And the last option is the replacement of the time encoding by a spatial one (UF). However, all is a matter of compromise since the reduction of experiment time often induces a loss of sensibility or a loss of resolution. It is also necessary to study whether these faster experiments can be used in a quantitative way or if a quantitative experiment can have its total duration be reduced. The hereby document will focus on NUS and UF 2D experiments.

## II- Time-reduction solutions

The purpose here is to implement techniques allowing quicker 2D-NMR experiments. The selection will depend on the application range, the time duration improvement, the simplicity of implementation and the spectra quality (spectral width, resolution, missing signals) it offers.

Here is a quick presentation of various techniques proposing faster multidimensional NMR experiments. Time reduction is obtained in two different ways: reducing the duration of one scan (part a) or reducing the number of scans (part b) In general, these two kinds of techniques are compatible with one another.

### a. Relaxation time reduction

#### i. SOFAST

The band-Selective Optimised Flip-Angle Short-Transient (SOFAST) technique is a faster way to acquire 2D spectra. The experiment can last less than a minute.

The SOFAST technique is based on three points. (Schanda & Brutscher, 2005; Schanda, Kupče & Brutscher, 2005) The first one is the reduction of the sequence complexity. It is achieved by reducing the number of pulses. To minimize the loss of signals happening because of $B_1$ inhomogeneities and/or pulse' imperfections, the number of radio-frequency pulses is reduced as much as possible. $B_1$ refers to the magnetic field applied perpendicularly to $B_0$ and used to generate the rotation of the magnetisation. Secondly, the excitations do not generate 90° or 180° rotation but excites at the Ernst-angle. It has been shown that exciting at the Ernst-angle makes it possible to quicken experiments without hindering the sensitivity by unit time. (Ross, Salzmann & Senn, 1997) The formula for Ernst-angle is given by:

$$\cos (\alpha_{Ernst}) = \exp (-T_c/T_1)$$

with $T_c$ the duration of one scan (excitation + acquisition + relaxation). The Ernst-angle is the angle that gives the maximum SNR for a given pair of $T_1$ and $T_c$.

However, the use of Ernst-angle restricts the technique to HMQC experiments since HSQC are not compatible with Ernst-angle excitations. (Schanda & Brutscher, 2005)

The third and last modification is the optimisation of the longitudinal relaxation. Band-selective pulses are employed to excite only specific protons, which will have a reduced $T_1$ due to Nuclear Overhauser Effect (NOE) interactions with the non-excited protons surrounding them. NOE interactions are dipole-dipole interactions between two nuclei spatially close to one another. In the end, the lower $T_1$ makes it possible to lower the delay between two successive scans. Initially, the sequence has been created to excite amide protons from proteins but is it technically applicable for H-X. (Schanda & Brutscher, 2005; Schanda, Kupče & Brutscher, 2005)Due to the $T_1$ reduction, the SOFAST technique can use shorter delays between successive scans. This leads to a faster acquisition.

All these changes allow for quicker scans, and thus faster experiments while keeping a good enough sensitivity. Schanda and Brutscher (2005) showed a sensitivity by unit time increase of 300% in comparison with conventional sequences. Spectra are obtainable in less than a minute (37 seconds for Ross, Salzmann & Senn (1997), 5 seconds for Schanda & Brutscher (2005) and 16 seconds for Schanda, Kupče & Brutscher (2005)). As few sequence parameters are modified, and both acquisition and data treatment stay classic, the implementation of the SOFAST technique is simple. (Schanda & Brutscher, 2005)

ii. ALSO-FAST

The ALternate SOFAST (ALSO-FAST) is a variant of the SOFAST technique.

In contrast with SOFAST, non-selective pulses are used. In the SOFAST technique, the selectivity is achieved by exciting a small part of the proton frequency band. In the ALSOFAST sequence, all protons are excited, and the selectivity is obtained by applying frequency-selective inversion pulses on the second nuclei.

The modifications in the sequence allow the implementation of a technique that enhances sensitivity by collecting data on both x and y axis simultaneously. It shows a sensitivity enhancement compared to SOFAST, except at very short recovery times. That lesser sensitivity comes from the heating generated by the higher number of pulses. This increased number of pulses is the main disadvantage compared to the SOFAST technique. In addition to heating, it also means more radio-frequency inhomogeneities that generates dephasing. The experiment also suffers from longitudinal relaxation happening during the sequence, since the sequence lasts longer, and from unsuppressed J-couplings. Both leads the possible sensitivity problems. More information in (Mueller, 2008)

SOFAST and ALSOFAST could be complementary for the study of macromolecules with broad amide bands. (Mueller, 2008) However, the ALSO-FAST technique is not often mentioned in the literature.

### iii. BEST

Just as the SOFAST sequence, the Band-selective Excitation Short-Transient (BEST) strategy is to reduce the duration of one scan in order to achieve more scans. BEST allows the acquisition of 2D and 3D spectra. With BEST, 3D spectra can be acquired in less than an hour (15 minutes for Schanda, Van Melckebeke & Brutscher (2006) and 15 to 40 minutes for Lescop, Schanda & Brutscher (2007)).

The concepts are the same as for SOFAST experiments: a selective excitation of amide protons and NOE interactions with non-excited aliphatic protons to decrease the longitudinal relaxation time. However, compared to SOFAST, it does not use Ernst-angle excitations and can therefore be applied to HSQC sequences. On its own and for identical spectra, BEST-sequences can give a spectrum 5 to 7 times faster than a conventional sequence. (Schanda, Van Melckebeke & Brutscher, 2006)

### iv. ASAP

The Acceleration by Sharing Adjacent Polarisation (ASAP) allows the acquisition of HMQC or HSQC spectra for natural abundance nuclei with a reduced experiment's duration. The strategy is to excite carbon-13 directly bound protons and to keep the carbon-12 bound protons untouched. When the acquisition is finished, the polarisation of non-excited protons ($^{12}$C-H) is quickly transferred to protons bound to carbon-13. This transfer is achieved by the so-called "Hartmann-Hahn effect" (Hartmann& Hahn, 1962) Once the polarisation restored, the following scan can directly start. This transfer takes about 40 ms and is therefore much faster than a recovery delay of the order of few seconds. To increase the speed and the sensitivity even more, Ernst-angle excitation pulses can be applied. (Schulze-Sünninghausen, Becker & Luy, 2014)

However, the removal of delays can be problematic for the hardware as $^{13}$C decoupling continuous pulsing during acquisition will generate heating. Therefore, the combination with EXACT (Extended Acquisition Time) has been implemented. By adding delays in the acquisition period and collecting data points in chunks, the hardware gets time enough to cool down. Software like the one used for NUS data treatment is used to handle the obtained chunks. (Ndukwe, Shchukina, Kazimierczuk & Butts, 2016)

Schulze-Sunninghausen and co-workers obtained an HSQC spectrum in less than 30 seconds, and for a same experiment's duration, the ASAP-HSQC has an increased intensity compared to a conventional HSQC.

### v. SMART

SMAll Recovery Time Method's idea is to reduce the recovery delay after the acquisition and not allow the total restoration of the magnetisation in its initial state. (Vitorge, Bodenhausen & Pelupessy, 2010) It means that when performing a second scan, magnetisation from the previous scan is still present in the xy plan. It may interfere with

the current scan and generate artefacts. Pulse-field gradients are used at each scan to select the desired coherence, and each scan has gradients with different directions. These gradients, in addition to their selection purpose, are used to quench the remaining signal to avoid unwanted refocussing of signals from successive scans. These coherences reduction allows the use of shorter relaxation delays and thus reduce the experiment's duration. Vitorge, Bodenhausen and Pelupessy (2010) applied SMART on a COSY sequence. The recovery time was changed from 4 seconds to 10 milliseconds, reducing the experiment time from 36 minutes to 71 seconds.

SMART can be applied to any 2D sequence. However, because it does not allow total recovery of the magnetisation, SMART cannot be used for quantification. (Vitorge, Bodenhausen & Pelupessy, 2010) A last problem is that not all spectrometers have the possibility to generate magnetic field gradients on all three axes.

## b. <u>Acquisition variation</u>

### i. Aliasing/Folding

The concept of aliasing is to impose a smaller spectral width by taking longer $t_1$ increments. It will result in a spectrum folded on itself without losing signals. It means all signals are shifted into a reduced SW. (Jeannerat, 2000 & 2003) It can be used for two purposes. By keeping the same resolution, fewer points need to be acquired and the reduction of spectral width will give a shorter experiment's duration. Or, the number of sampled points can be increased, leading to an improved resolution. The spectrum can be folded up to 10 to 100 times and different techniques have been implemented to treat data. (Eggenberger, Pfändler & Bodenhausen, 1998; Jeannerat, 2000)

### ii. Hadamard

The Hadamard concept is to avoid acquiring the whole spectral width. Instead, a first and really fast classic FT spectrum is achieved to detect where correlations are present and, thereafter, the Hadamard sequence will focus on these specific frequencies. Multiple scans with selective irradiation are performed and a matrix is generated. Each line of the matrix corresponds to one scan, and each column corresponds to the frequency of a chemical site. The goal is to sample the F1 dimension in a non-linear way, and to avoid collecting information where there are none. It is therefore effective for nuclei with large SW like $^{13}C$, $^{19}F$ or $^{31}P$. (Ahmed, Rao & Abdussattar, 1971; Kowalski & Bender, 1973; Bletcha & Freeman, 1993; Kupče & Freeman, 2003)

The main advantage is the higher sensitivity. The same information is collected multiple times and the amount of collected information at one time is higher, all this leads to a higher sensitivity. An interesting analogy with weights has been presented by Marshall & Comisarow (1975) to understand it. Another major improvement is the rapidity of the experiment. Kupče & Freeman (2003) obtained a 2D-COSY spectrum with

the Hadamard technique in 45 seconds in comparison to a conventional spectrum acquired in 2h30. The sensitivity by unit time was not diminished. Other advantages are notable like the easiness to suppress the solvent peak, the small number of artefacts and the unnecessity to have a phase cycling. (Kupče & Freeman, 2003)

c. <u>Conclusion</u>

Since the objective is to find a technique which can be extended to the most possible applications, NUS has been chosen. As it will be presented in chapter IV, it is easy to implement, can be applied to all 2D-sequences and does not modify the acquired spectral window. Moreover, it can be used for two different purposes: faster experiments or higher-quality spectra.

BEST, SOFAST and ALSOFAST do not acquire the whole spectral width and cannot be applied to all sequence-types. Hadamard, SMART, aliasing and ASAP are more complex to implement than NUS.

UF (Chapter V) has also been selected since it proposes the highest time reduction. It has also been chosen because it is a non-conventional type of sequence which is conceptually different from all other NMR experiments. It indeed mixes MRI with NMR.

## III- Samples and experiments

Various samples were used for either NUS or UF experiments.

1) A sample of ethanol 1.71M in deuterated water ($D_2O$).
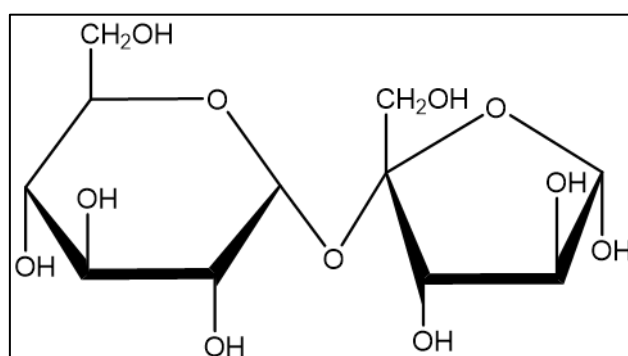2) A Bruker reference tube of sucrose (*Figure 5*) 2 mM in water.



*Figure 5 - Sucrose drawn with ChemDraw.*

3) A sample of a steroid: triamcinolone hexacetonide (THA) (*Figure 6*) 21.93mM in deuterated trichloromethane ($CDCl_3$). THA 1D-proton spectrum is displayed on figure 7.
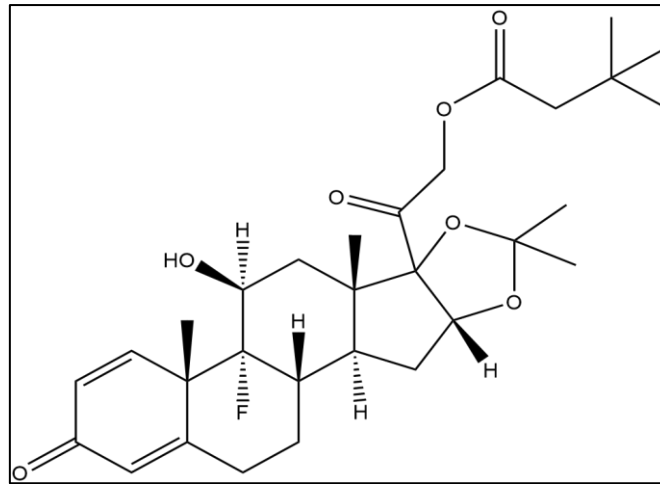
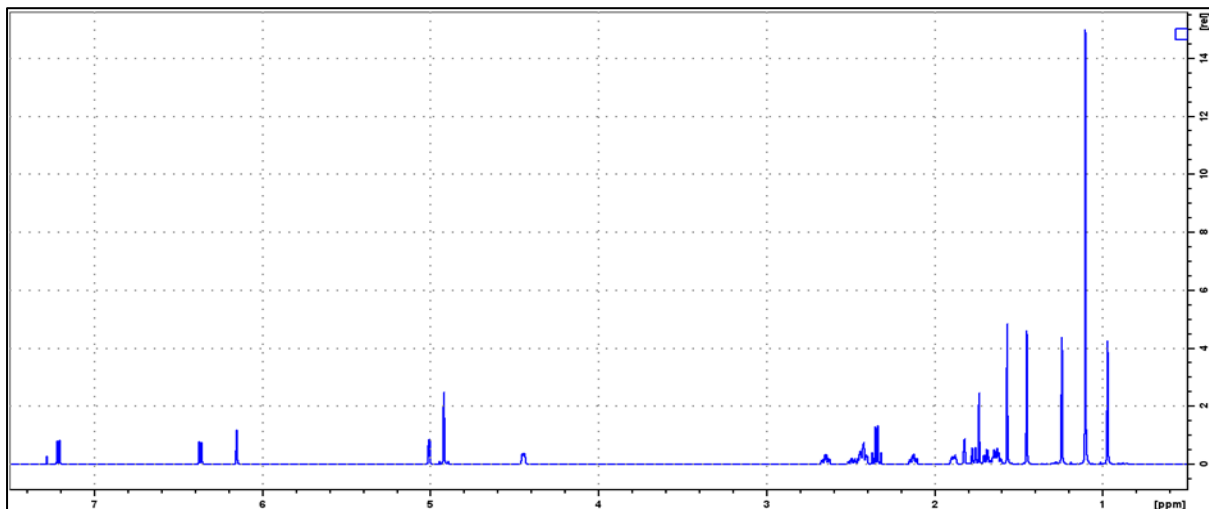*Figure 6 - Triamcinolone hexacetonide (THA) drawn with ChemDraw.*



*Figure 7 – Proton spectrum of the THA molecule*

4) An aqueous sample of 800µL with various metabolites:
   a. 2.3 mg of alanine (32.3 mM)
   b. 4.8 mg of 3,4-dihydroxyphenylalanine (30.4 mM)
   c. 3.2 mg of sucrose (11.7mM)
   d. 5.8 mg of 2-ethylhexan-1-ol (55.7 mM)
   e. 780µL of a phosphate buffer
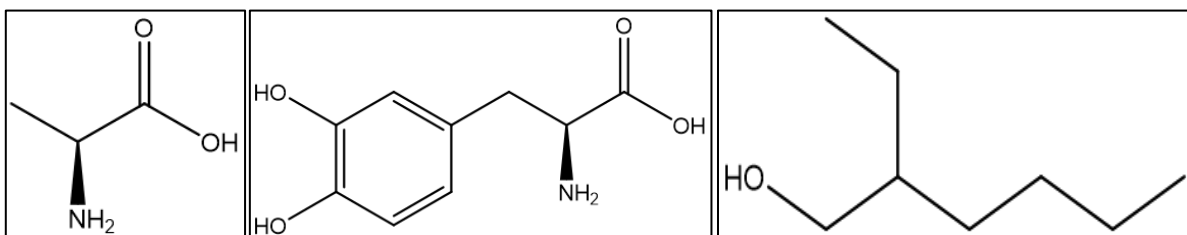   f. 20 µL of DSS 60mM (reference)



*Figure 8 – Alanine (left), 3,4-dihydroxyphenylalanine (middle) and 2-ethylhexan-1-ol (right)  drawn with ChemDraw.*

Conducted experiments relevant for the hereby document are summarized in the annexes (*Tables A1-A4*). Table A1 lists the NUS experiments conducted on THA 22mM, with COSY, HSQC and HMBC sequences. Table A2 summarizes the COSY-NUS experiments conducted on sucrose 2mM. Table A3 lists the UFCOSY experiments performed on ethanol 1.7M in $D_2O$ and THA 22mM in $CDCl_3$. Table A4 shows the PRUFCOSY experiments performed on sucrose 2 mM in $H_2O$ and the metabolites sample in $D_2O$ + $H_2O$. Lastly, table A5 summarises the conventional experiments used for comparison with the UF spectra.

All experiments were conducted on a Bruker Advance III 700MHz spectrometer, equipped with a Helium cooled probe (Cryoprobe™) and with a SampleJet. The COSY, HSQC and HMBC sequences come from the Bruker library. UF sequences were given by Patrick Giraudeau (Nantes).

## IV-    Non-Uniform Sampling (NUS)

### a.  Theory

The conventional acquisition is called uniform sampling and is ruled by the Nyquist theorem. This theorem states that, for a periodic signal to be correctly characterised, it must be sampled faster than twice the highest signal frequency. (Laughton & Warne, 2002; Palmer *et al.*, 2015) To respect that theorem, the uniform sampling proceeds by a constant $t_1$ incrementation to monitor the magnetisation evolution in the indirect dimension. And this $t_1$-increment is shorter than the half-period of the highest frequency of the signal. In contrast with uniform sampling, NUS does not follow Nyquist theorem and it does not need a constant $t_1$-incrementation. When performing NUS, only a small percentage of all time-points are measured, and these points are "randomly" scattered along the indirect dimension (*Figure 9*). The "time-increment" between two successive sample points is therefore not constant and the Nyquist theorem is thus not respected. As the number of points is limited, it results in a shorter experiment time. After the acquisition, an algorithm created for this task will calculate the unmeasured points of the FID. (Wishart, 2008; Palmer *et al.*, 2015) NUS can therefore be used to shorten the time of the experiment by reducing the number of sampled points. But it can also be used to increase the resolution while keeping the same duration for the experiment. In both cases, NUS allows a gain in sensitivity per unit time. (Wishart, 2008; Zambrello *et al.*, 2018)

The scattering of the points is not totally random. It has been shown that by sampling more points with $t_1 < 1.26*T_2$ and less points after $1.26*T_2$, the NUS-method has an improved sensitivity. (Palmer *et al.*, 2015) $T_2$ is the transverse relaxation time characterising the defocussing of the magnetisation on the xy-plane. By collecting less data after $1.26*T_2$, where the signal is less intense and noise relative more intense, SNR is improved. However, to improve resolution, it is necessary to sample points with a longer evolution time $t_1$. NUS, even if it favours low evolution time, will thus also sample points with longer $t_1$ to obtain a higher resolution. (Martineau, Dumez & Giraudeau, 2020; Palmer *et al.*, 2015)
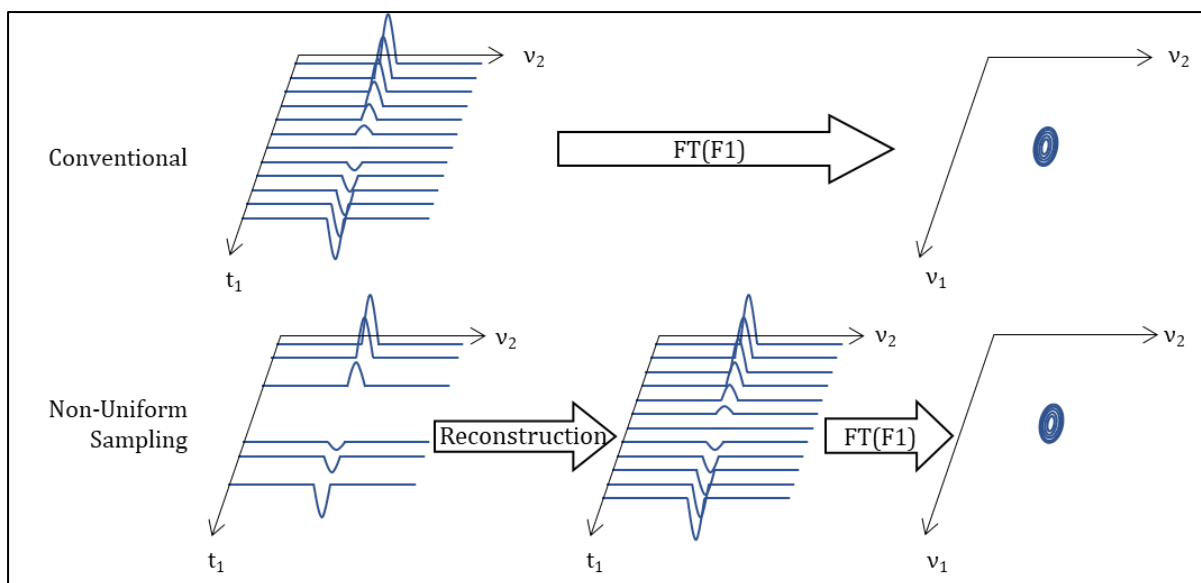
*Figure 9 – Comparison of the conventional acquisition and the acquisition modification proposed by NUS. To allow for a clearer view of the image a first Fourier transform along first dimension ($t_2$) has been considered before the reconstruction of NUS.*

Experiments with NUS have shown that appreciable spectra can be recorded when applying a 50% NUS with a HSQC-sequence, a 30% NUS with a COSY-sequence. The percentage represents the number of sampled points in comparison with uniform sampling. If a lower percentage is taken, $T_1$-noise and artefacts appear and/or the intensity of the peaks significantly decreases. The percentage varies from study to study as other teams acquired spectra with 25% of NUS. Different studies agree on the impact of a too low NUS percentage, but the percentage limit does not seem well defined. (Martineau, Dumez & Giraudeau, 2020; Marchand *et al.*, 2017; Le Guennec, Giraudeau & Caldarelli, 2014)

NUS can be applied for different purposes. Since it only modifies how the acquisition step proceeds, NUS can be applied on all multi-dimensional sequences and has no sample restriction.

## b. Implementation

Experiments conducted with NUS are listed in table A1 (in the annexes. Different figures present the results of these various experiments. The same template has been generated for all three experiment types (COSY, HSQC, HMBC). Only figures showing the most important results are shown here-below. The rest can be found in the annexes.

Before looking at the results, here is a quick reminder of the signals expected for all three experiments. COSY experiments show correlations between neighbouring protons that 2 or 3 chemical bonds apart and present a diagonal which does not give any correlation information. HSQC experiments show correlations between a proton and a carbon that are directly bonded. And HMBC experiments show correlations between protons and carbons that are up to 4 chemical bonds apart.

Results are shown here-after and are further discussed.

The first comparison concerns the impact of modifying the NUS percentage. Figures 10 (COSY), 11 (HMBC) and 12 (HSQC) compare each three spectra:

- No NUS,   $N_s = 1$, $N_2*N_1 = 2k*512$
- NUS 25%, $N_s = 1$, $N_2*N_1 = 2k*512$
- NUS 10%, $N_s = 1$, $N_2*N_1 = 2k*512$

A first comparison while keeping the same threshold for all three spectra is presented. Afterwards, the threshold levels of the spectra have been individually adapted for the best compromise between artefacts reduction and signals observation. A zoom offering more details can be seen in red in the last row of each figure. The figure for HSQC experiments (*Figure* 12) presents a difference. There was no need to adapt the threshold level to minimize the artefacts since there were none to get rid of. Therefore, two sets of spectra are present on the figure both compared at the same threshold level.
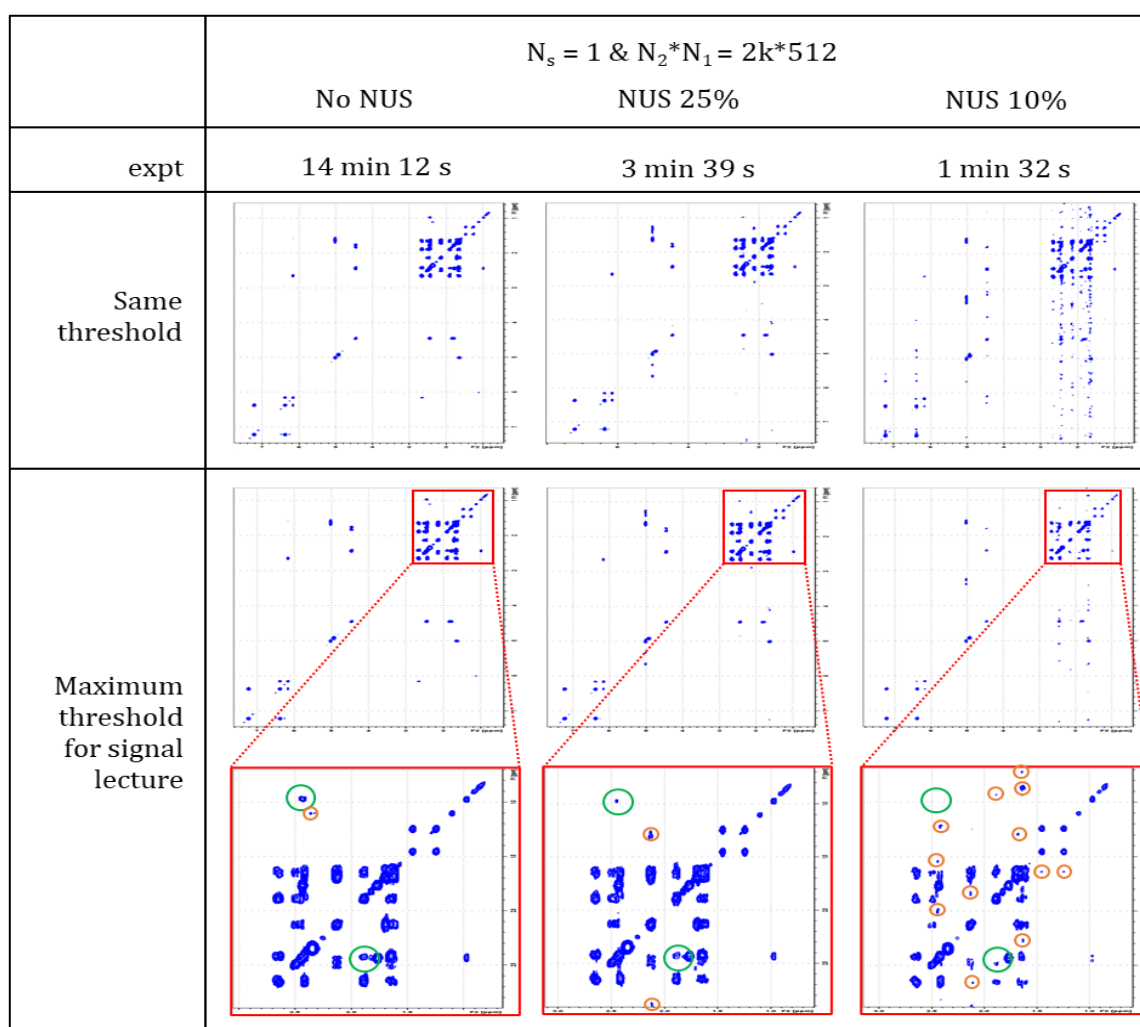


| | $N_s = 1$ & $N_2*N_1 = 2k*512$ | | |
| --- | --- | --- | --- |
| | No NUS | NUS 25% | NUS 10% |
| expt | 14 min 12 s | 3 min 39 s | 1 min 32 s |
| Same threshold | | | |
| Maximum threshold for signal lecture | | | |

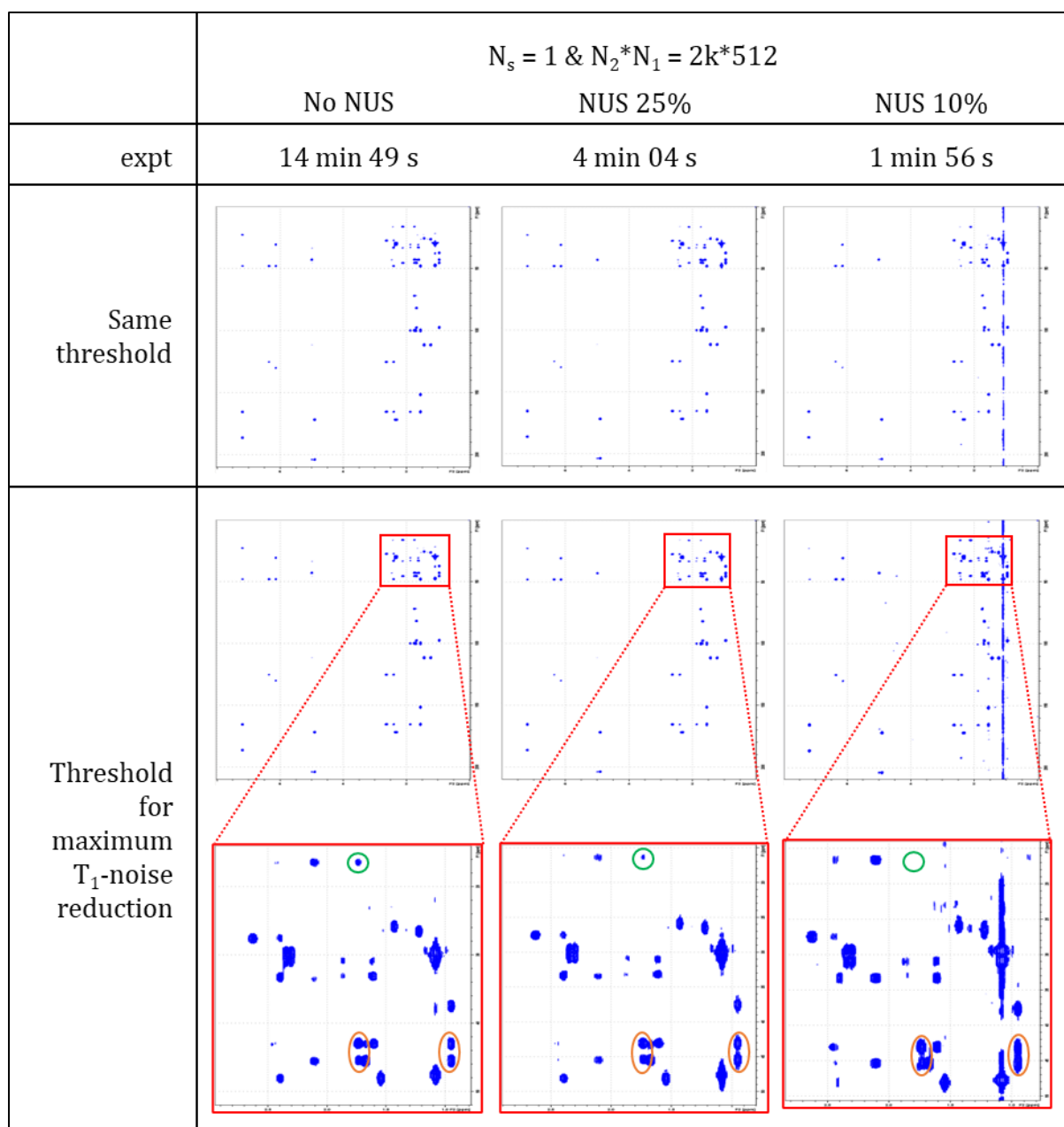*Figure 10 - Comparison of COSY spectra of a THA sample in CDCl₃ acquired with one scan and a resolution of 2k\*512, and various NUS percentages. Spectra are compared while having the same threshold (upper line) and while having an adapted threshold to ease the lecture of the spectra (bottom lines). A zoom on a crowded area is displayed in red. Green circles indicates signals that are lost when decreasing the NUS percentage and orange circles highlight the presence of T₁-noise and artefacts.*

| | $N_s = 1$ & $N_2*N_1 = 2k*512$ | | |
|---|---|---|---|
| | No NUS | NUS 25% | NUS 10% |
| expt | 14 min 49 s | 4 min 04 s | 1 min 56 s |
| Same threshold | | | |
| Threshold for maximum $T_1$-noise reduction | | | |



*Figure 11 - Comparison of HMBC spectra of a THA sample in CDCl₃ acquired with one scan and a resolution of 2k\*512, and various NUS percentages. Spectra are compared while having the same threshold (upper line) and while having an adapted threshold to ease the lecture of the spectra (bottom lines). A zoom on a crowded area is displayed in red.*
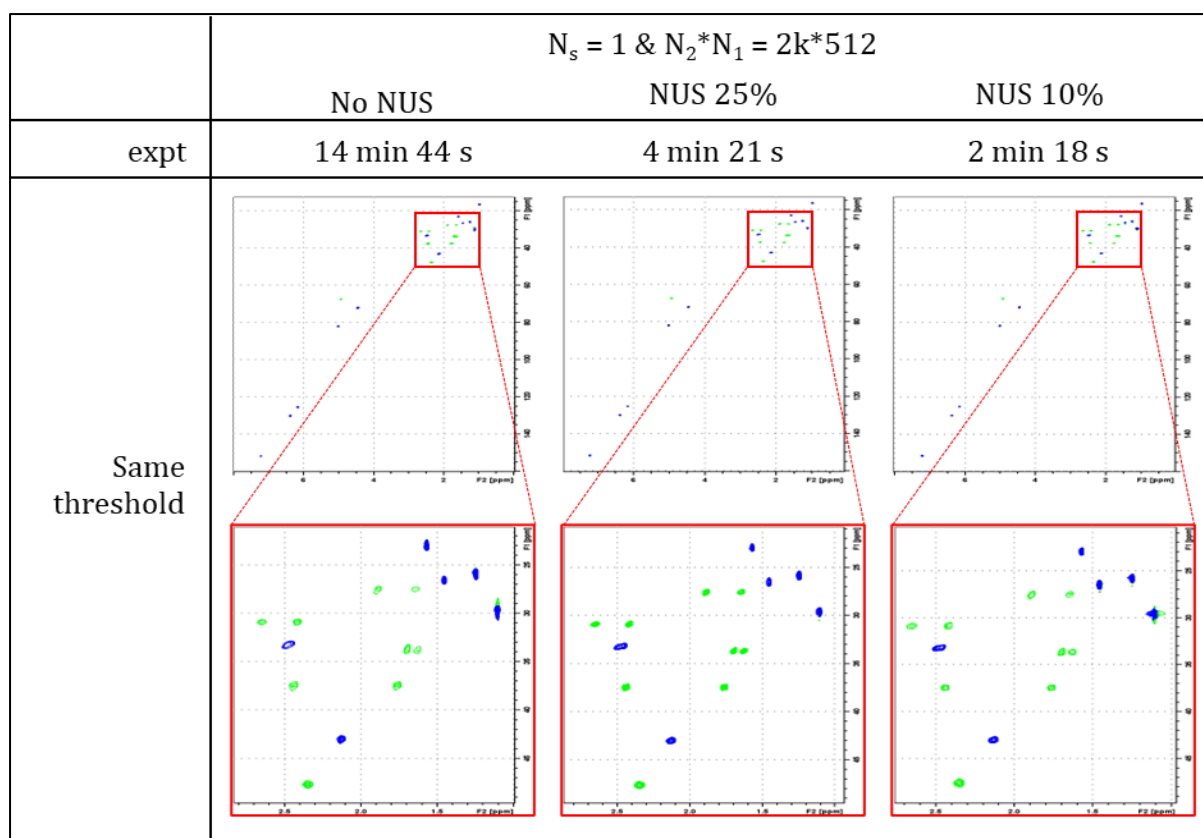
*Figure 12 - Comparison of HSQC spectra of a THA sample in CDCl₃ acquired with one scan and a resolution of 2k\*512, and various NUS percentages. Spectra are compared while having the same threshold (upper line) and while having an adapted threshold to ease the lecture of the spectra (bottom lines). A zoom on a crowded area is displayed in red.*

When analysing figure 10, the first observation is the appearance of vertical patterns on the right part of some spectra. They can also be observed on HMBC spectra (*Figure 11*) but not on HSQC spectra (*Figure 12*). These are more present when the percentage is lowered and appear at chemical shifts corresponding to intense singlets in the 1D-proton spectrum of THA (*Figure 7*). A second observation, which is easier to note when looking at the zoomed spectra, is the small number of missing signals (green circles). For all experiments, the NUS percentage presents no or little impact on the number of observed signals. At most, one or two signals are missing in the COSY and HMBC experiments. However, it is noteworthy to remember that both these experiments have their signals in pairs. Therefore, losing one or two signals may often not be a problem. But still, it is important to be careful with such losses. It is also important to state that the threshold level has a major impact on what is observable and what is not. The comparison between the HSQC spectra presents the least differences. It seems less impacted by the reduction of the NUS percentage. Orange circles are used to highlight issues: artefacts in figure 10 and loss of resolution in figure 11.

To further explore the impact of the NUS percentage, slices were extracted from the spectra used here-above and superposed. Columns were extracted: one at a chemical shift of a methyl's singlet and one where less noise is observable. Rows were extracted from the upper part of the spectra, where signals are more crowded. Figures below present the main observations. The rest of the superpositions can be found in the annexes

(*Figures A1-A11*). The same colour code is used through the figures: blue, red and green colours represent the various spectra respectively acquired without NUS, with NUS 25% and NUS 10%.

Figure 13 presents the superposition of columns extracted from the COSY spectra. The column has been extracted at 1.65 ppm, where an intense singlet is present. The figure shows the noise level and the number of artefacts both increase when the NUS percentage tends to lower values. However, signals are still intense enough to be discerned from the noise. For HSQC (*Figures A9-A11*), the intensity difference between signals and noise is even more significant. It is also observable that the hindrance caused by artefacts is of lower impact, and in fact barely not notable, in the case of rows. The problem is majorly present in the columns.
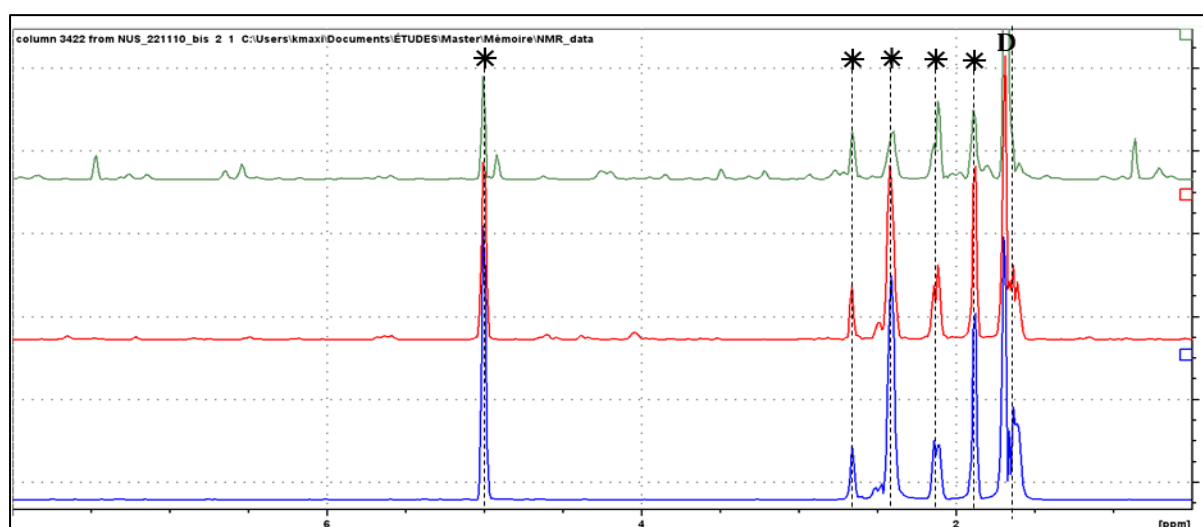


*Figure 13 – Superposition of the 1.65 ppm columns extracted from COSY spectra of a THA sample in CDCl$_3$ acquired without NUS (blue), with NUS 25% (red) or NUS 10% (green), all acquired with one scan, a resolution of 2k*512. These experiments lasted respectively 14 min 12s, 3 min 39s and 1 min 32s. Asterisks shows where the signals are, and D indicates the diagonal peak.*

Other figures have been constructed to study the impact of modifying the amount of data collected by comparing the following spectra:

- No NUS,   $N_s = 1$, $N_2*N_1 = 2k*512$ in blue       (reference)
- NUS 10%, $N_s = 1$, $N_2*N_1 = 2k*512$ in red
- NUS 10%, $N_s = 2$, $N_2*N_1 = 2k*512$ in green     (increase of $N_s$)
- NUS 10%, $N_s = 1$, $N_2*N_1 = 2k*1k$   in purple   (increase of $N_1$)

No matter which experiment sequence or whether it is a row or a column, increasing the number of scans does not seem to impact the intensities of signals or artefacts. However, increasing the resolution seems to have a more significant impact on the columns. Firstly, the resolution is improved in the second dimension. Secondly, the number of artefacts seems reduced. Lastly, increasing the resolution also increases the intensity of some signals. Figure 14 displays the superpositions of the columns extracted at 4.45 ppm from the COSY spectra. No intense singlet appears at 4.45 ppm in the 1D-proton spectrum. The other superpositions can be found in the annexes (*Figures A12-*

*A19*). The superposition is the one presenting the most notable differences. It is clearly observable that increasing $N_1$ induces both artefact reduction and signal increase.
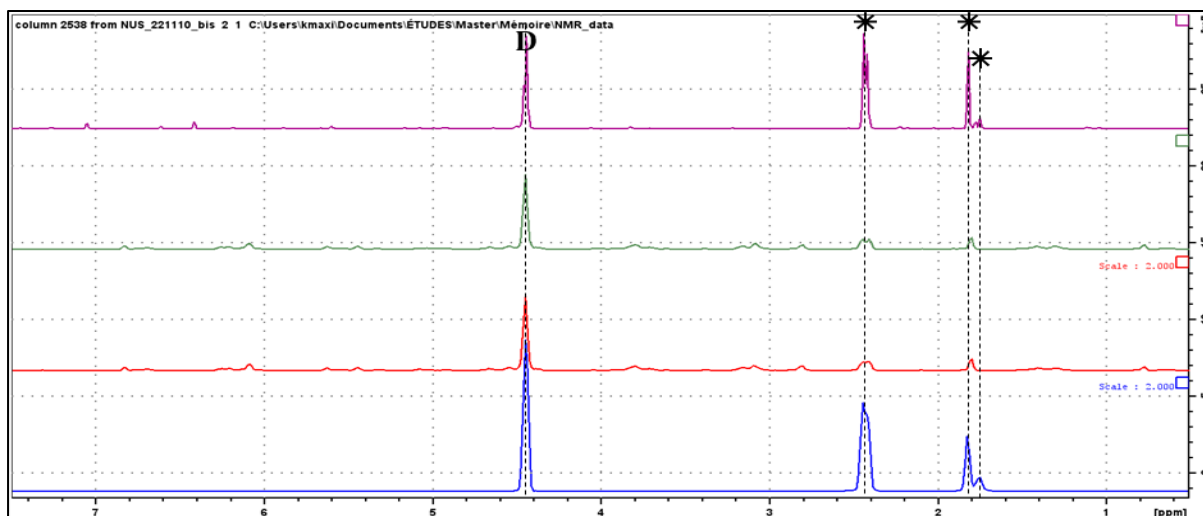


*Figure 14 - Superposition of the 4.45 ppm columns extracted from COSY spectra of a THA sample in CDCl₃ acquired with: no NUS, 1 scan, $N_2*N_1 = 2k*512$ in 14 min 1s (blue); NUS 10%, 1 scans, $N_2*N_1 = 2k*512$ in 1 min 32s (red); NUS 10%, 2 scans, $N_2*N_1$ in 2 min 56s (green); and NUS 10%, 1 scan, $N_2*N_1 = 2k*1k$ in 2 min 59s (purple). Asterisks show where the signals are, and D indicates the diagonal peak.*

Last figure type consists in superpositions of two 2D-spectra:

- No NUS, $N_s = 1$, $N_2*N_1 = 2k*512$ in blue
- NUS 10%, $N_s = 4$, $N_2*N_1 = 2k*1k$ in red

These spectra were acquired in similar amount of time, respectively 14 min 12s and 11 min 55s for the COSY spectra (*Figure 15*). All figures (*Figures 15, and A20 and A21 in the annexes*) present perfect superpositions, where no signals are lost and show an improved resolution in the second dimension. Figure 15 displays the superpositions for HMBC spectra.
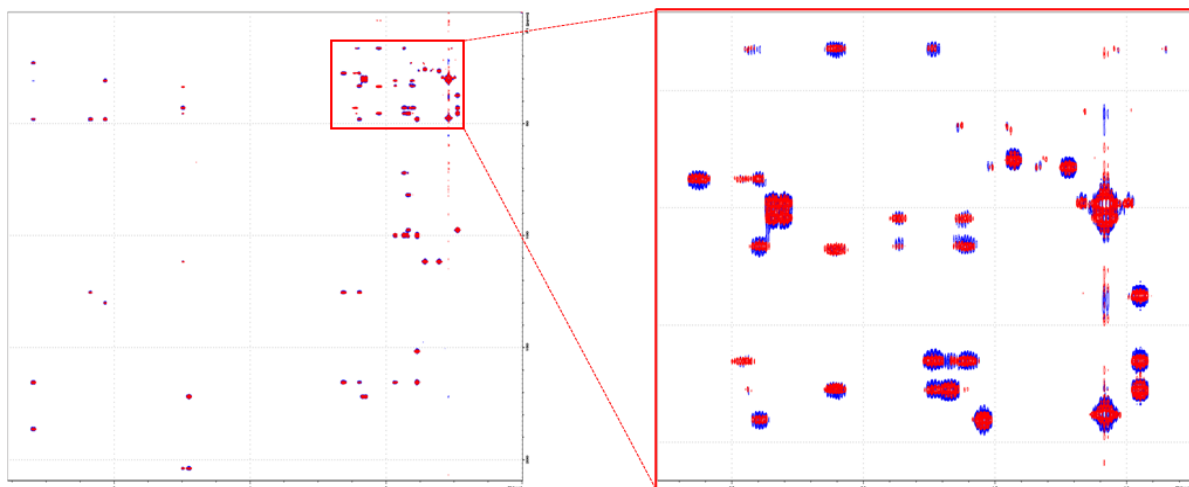


*Figure 15 – Superposition of HMBC spectra of a THA sample in CDCl₃ acquired with: no NUS, 1 scan, $N_2*N_1 = 2k*512$ in 14 min 49s (blue) and NUS 10%, 4 scans, $N_2*N_1 = 2k*1k$ in 11 min 55s (red). The red box on the right part is a zoom from the left superposition.*

To sum up, all three experiment types (COSY, HSQC, HMBC) show similar trends concerning NUS.

Firstly, it has not been discussed yet, but NUS proposes a simple technique with a promising time reduction. The shortest experiment durations were obtained for the spectra with 10% NUS, one scan and a resolution of 2k*512, and offers a factor nine of time reduction. This without modifying the sequence or SW.

Secondly, reducing the NUS percentage generates more artefacts and noise, and this is more significant in columns than in rows. As the NUS concept is to acquire less data in the second dimension and to recalculate it after the acquisition, it seems logic that such noise and artefacts, appear mostly on the columns. This is probably caused by mathematical errors due to the lower accuracy of the FID in the second dimension. It is noteworthy to mention the so-called $T_1$-noise patterns are mainly present on the right side of the spectra and more precisely, at the chemical shifts of intense singlets from methyls and tert-butyl functions. It is known that these intense singlets can hinder the lecture of spectra. THA is a complex molecule due to these functions but even though, signals on the spectra can be easily identified. It is also noticeable that HSQC spectra present less intense $T_1$-patterns than COSY and HMBC spectra. This is probably due to the fact the HSQC sequence used for the experiments has been perfectioned through the years. It has cleaning gradients and adiabatic pulses which reduces the number of artefacts generated during the acquisition of a spectrum. These improvements are not always possible for COSY and HMBC sequences and, therefore, the HSQC spectra acquired here present less problems than the COSY and HMBC ones.

Thirdly, the impact of $N_s$ and $N_1$ is different in a NUS experiment than in conventional acquisitions. In a conventional acquisition, increasing $N_1$ implies acquiring signal during a longer time, therefore acquiring more noise but improving resolution. Thus, increasing $N_1$ induces a lower SNR but a higher resolution. Modifications of $N_1$ results in carrying out the same acquisition multiple times. It leads to a higher SNR, without impacting the resolution. With NUS, all $t_1$ time-increments are not acquired. They are scattered over the whole acquisition time and $t_1$ shorter than $1.26*T_2$ are favoured. When $N_s$ is increased, the same $t_1$ are sampled multiple times. It does not modify the resolution and it increases SNR. However, as it does not acquire more "new" information, it does not modify the possible calculation errors and therefore the artefacts present in the NUS-spectra. When, $N_1$ is increased, the total acquisition time in the second dimension gets longer, thereby increasing the resolution. However, $t_1$-increments shorter than $1.26*T_2$ are still favoured. It means that the FID part where the signal has decayed due to its relaxation time $T_2$ is less sampled. Thus, less noise is measured, leading to a higher SNR. Thanks to the scattered and "random" screening of the signal in the second dimension, increasing $N_1$ can result in a higher SNR as well as in an improved resolution. As either $N_1$ or $N_s$ increase leads to higher experiment times, it should be better to increase the resolution instead of performing multiple scans when NUS is applied.

It is noteworthy to remind that the parameters have been pushed to the limits. As an example, most 2D experiments have a phase cycling which requires a higher number of scans, sometimes up to 16 scans. Phase cycling is used to reduce the formation of artefacts. Therefore, lowering each parameter to the minimum may cause a pile up of problems. Other experiments should be performed with longer experiment times without NUS and be compared with NUS experiments whose purpose is not to achieve faster acquisition but high-quality spectra.

NUS can be used for two major purposes. The first one is the possibility to acquire spectra in shorter times and the second one is to increase the SNR and/or the resolution of the spectra without . With the same parameters and 10% NUS, the time gain is about a factor 9. When having 10% NUS, it is possible to double the resolution and quadruple $N_s$ without time increase compared to spectra acquired without NUS. As doubling the resolution already renders a sufficient quality improvement and a factor 5 time reduction, it is a convenient solution for both faster and higher-resolution 2D-acquisition.

Here below are figures comparing zoomed area of spectra acquired with:

- No NUS, $N_s = 1$, $N_2*N_1 = 2k*512$ (reference)
- NUS 10%, $N_s = 1$, $N_2*N_1 = 2k*512$ (fastest)
- NUS 10%, $N_s = 1$, $N_2*N_1 = 2k*1k$ (higher resolution)

Figure 16 shows the COSY spectra, figure 17 the HSQC ones and figure 18 the HMBC ones. All figures shows that no signals are lost, that resolution is improved in the bottom-right spectra and that the time gain factor is about 5 or 9. The use of 10% NUS, with an increased resolution is what we recommend for fast COSY, HSQC and HMBC experiments.
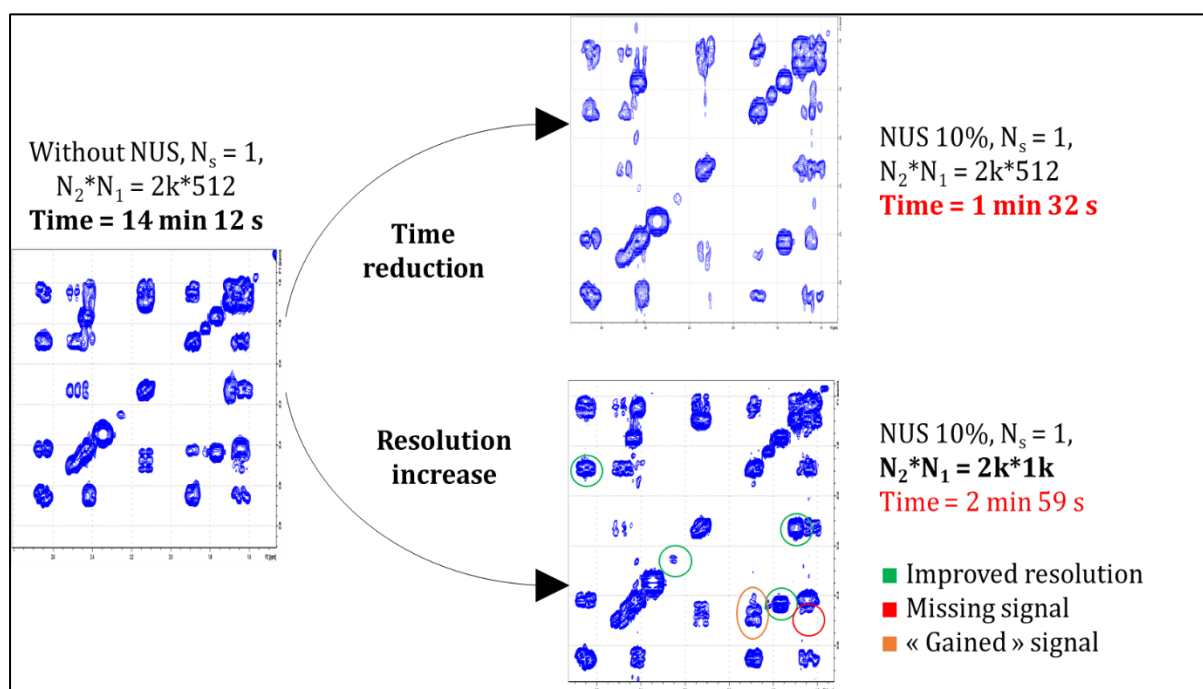


*Figure 16 – Comparison of COSY spectra of a THA sample in CDCl₃: the reference spectrum (14 min 12s) presented on the left, fastest NUS spectrum (1 min 32s) on the upper right part and the best compromise between time and resolution improvement (2 min 59s) on the lower right part.*

Without NUS, $N_s = 1$,
$N_2*N_1 = 2k*512$
**Time = 14 min 44 s**

**Time reduction**

**Resolution increase**

NUS 10%, $N_s = 1$,
$N_2*N_1 = 2k*512$
**Time = 2 min 18 s**
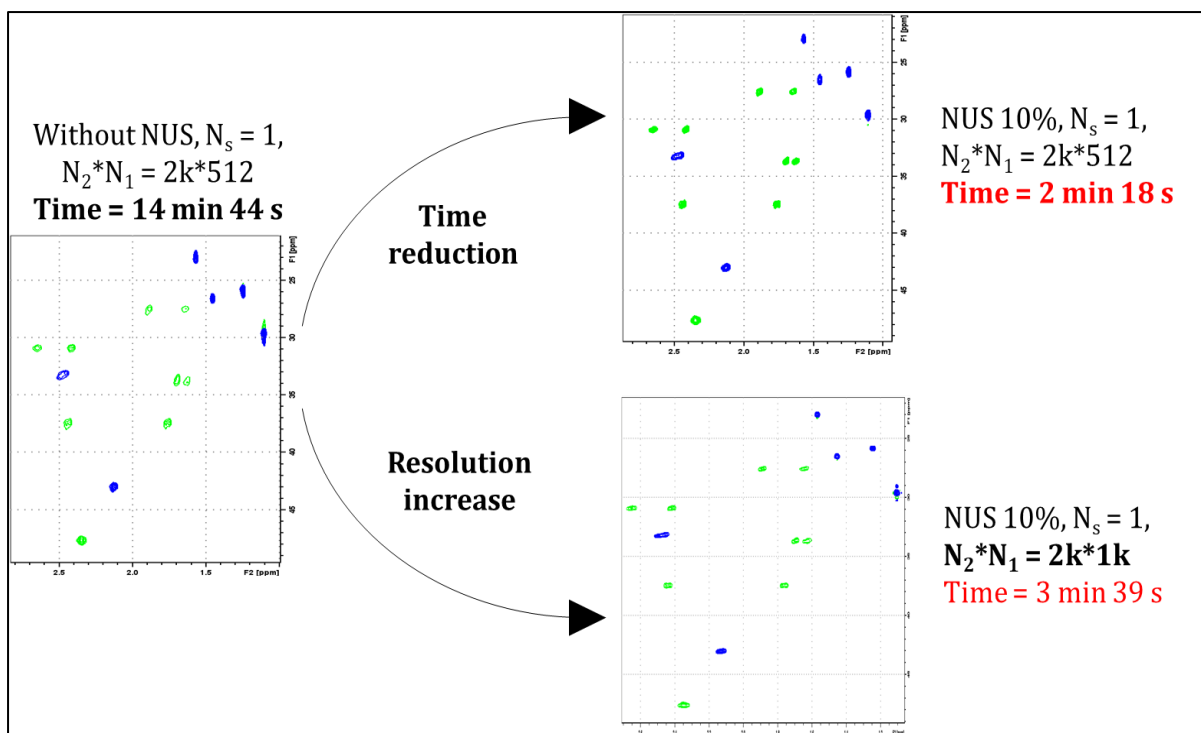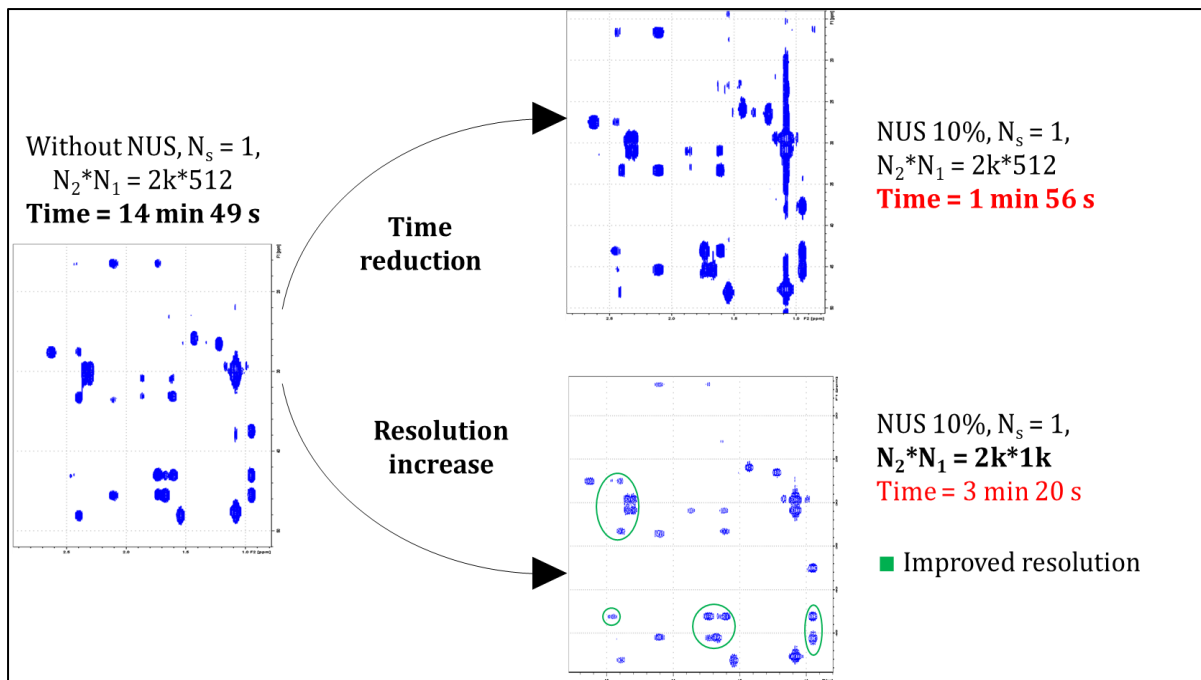
NUS 10%, $N_s = 1$,
$N_2*N_1 = 2k*1k$
Time = 3 min 39 s

*Figure 17 - Comparison of HSQC spectra of a THA sample in CDCl₃: the reference spectrum (14 min 44s) presented on the left, fastest NUS spectrum (2 min 18s) on the upper right part and the best compromise between time and resolution improvement (3 min 39s) on the lower right part.*



Without NUS, $N_s = 1$,
$N_2*N_1 = 2k*512$
**Time = 14 min 49 s**

**Time reduction**

**Resolution increase**

NUS 10%, $N_s = 1$,
$N_2*N_1 = 2k*512$
**Time = 1 min 56 s**

NUS 10%, $N_s = 1$,
$N_2*N_1 = 2k*1k$
Time = 3 min 20 s

■ Improved resolution

*Figure 18 - Comparison of HMBC spectra of a THA sample in CDCl₃: the reference spectrum (14 min 49s) presented on the left, fastest NUS spectrum (1 min 56s) on the upper right part and the best compromise between time and resolution improvement (3 min 20s) on the lower right part.*

NUS experiments were also performed on a sucrose 2mM sample, whose solvent is water. These experiments are listed in table A2. COSY spectra were acquired without NUS in 15'23", with NUS 25% in 3'55", NUS 10% in 1'38" and NUS 5% in 53". All spectra were acquired with 1 scan, a relaxation delay D1 of 1.5 seconds and a resolution of $N_2 * N_1$ =4k*512. Spectra are compared with same thresholds, adapted thresholds and zooms are presented in figure 19.

The same conclusions as for the THA sample can be asserted: $T_1$-noise patterns are observed, signals can be lost when the NUS percentage is decreased and both artefacts and noise are more present in spectra acquired with a lower NUS percentage. (*Figure 19*) However, no increased noise level is observed around the water signal. In fact, the water trace seems independent of the NUS percentage: both noise level and the width of the water band stay constant when the NUS percentage is modified.
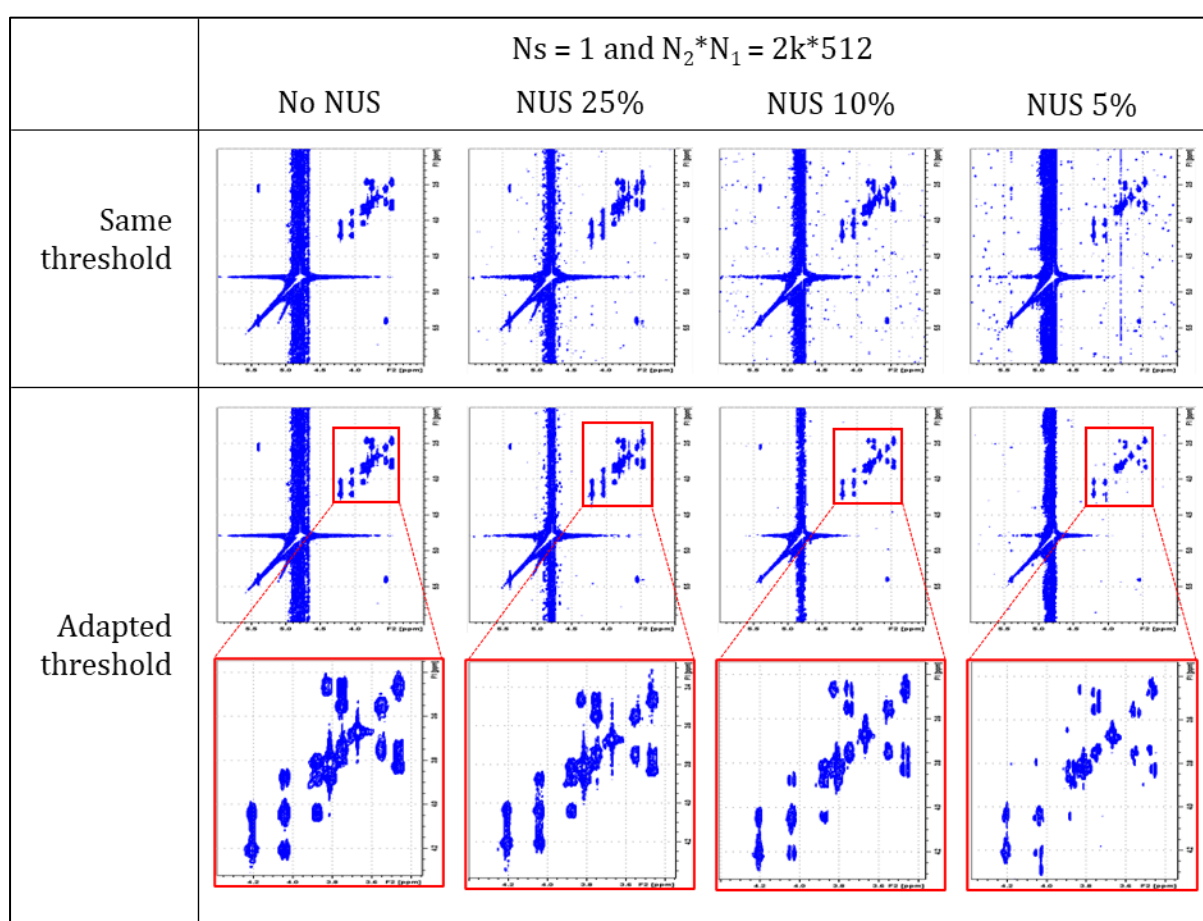


*Figure 19 - Comparison of COSY spectra of a sucrose2 mM sample in water acquired with one scan and a resolution of 2k*512, and various NUS percentages. Spectra are compared while having the same threshold (upper line) and while having an adapted threshold to ease the lecture of the spectra (bottom lines). A zoom on a crowded area is displayed in red.*

To sum up, NUS is highly recommended, whether the sample contains water or not. HSQC and HMBC experiments should be performed on aqueous sample. Even if water should not be observed, water is detected because of its high concentration. Sensitivity might be a problem for these experiments, and this should be further studied.

## V-      Ultrafast (UF) NMR

One of the main objectives of this work was to implement the UF technique on the spectrometer at the university of Liège. As it is an unorthodox method, the presented document has a pedagogical purpose and highlights the underlying concepts of this technique.

### a. Theory

#### i. Sequences

The UF method was proposed by Lucio Frydman and co-workers in 2002. (Frydman, Scherf & Lupulescu, 2002 & 2003) The basic idea is to remove the time incrementation obtained via multiple 1D experiment in the conventional 2D-sequence. This could be replaced  by an indirect time incrementation that would be acquired in one single scan. This would drastically reduce the time required to execute a 2D-experiment since the conventional $t_1$-incrementation induces a non-negligeable time increase. Conventional 2D-NMR experiments usually have the following global scheme:

$$[\text{Preparation - evolution } (t_1) – \text{mixing - acquisition } (t_2)] * N_s$$

with the incremented evolution time $t_1$ enabling different chemical shift evolutions at each scan, thereby constructing the FID in the indirect dimension.

In the UF sequence, there is no such step-by-step $t_1$-incrementation. All the different $t_1$-evolutions are now obtained from different spatial parts of the sample and are acquired in one single scan. One scan means a drastic experiment time reduction. This spatial differentiation is called "spatial-encoding" and is achieved by a so-called "slicing-method". The concept is to make each z-position correspond to one $t_1$-increment in the conventional sequences. To do so, magnetic field gradients along the z-axis are used to change the Larmor frequency along that axis. If each spatial point has its own Larmor frequency, it can be individually manipulated. The term "slice" will now be used instead of "spatial-point" because nuclei at the same height (z-position) behave the same way, therefore cutting the sample in "slices" (which can be seen in *figure 21* on page 31). In the end, a linear correlation between the magnetic field, thus the Larmor frequency, and the z-axis position emerges. The excitation and acquisition steps are the key components of the UF sequence.
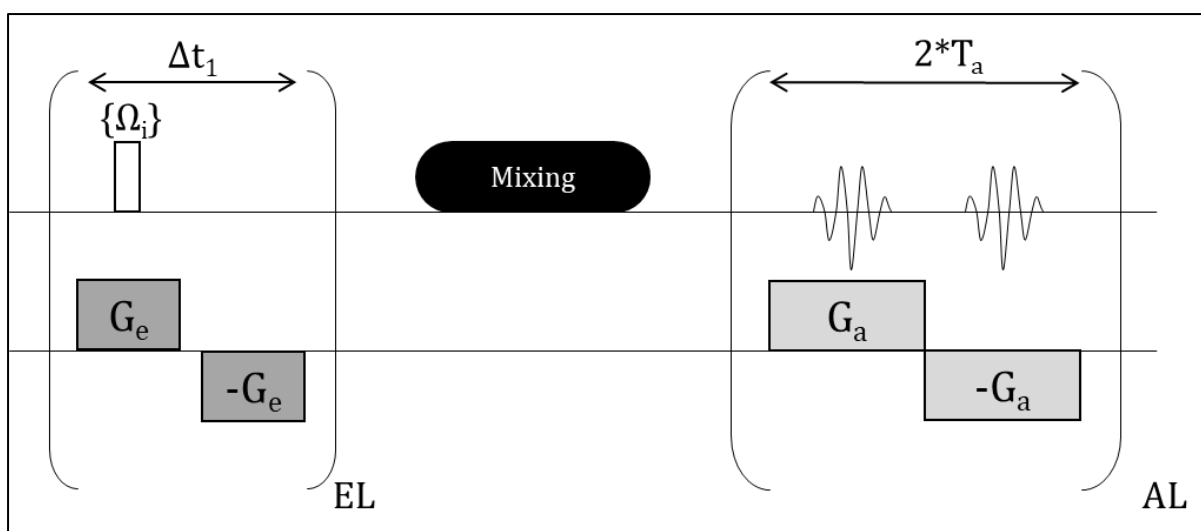
*Figure 20 - Ultrafast sequence proposed by Frydman and co-workers (2002): an excitation step composed of a succession of EL 90° pulses characterized by their frequency offset $\Omega_i$ while a pair of magnetic field gradients $\pm G_e$ is applied, followed by a mixing step and finally an acquisition step composed of AL pairs of magnetic field gradients $\pm G_a$, each one with a duration $T_a$.*

The first step of the sequence is the excitation (*left part of figure 20)*. A succession of EL (excitation loop) 90° pulses happens while a pair of opposite magnetic field gradients ($\pm G_e$) is active along the z-axis. Each pulse has its own frequency offset $\Omega_i$ and therefore excites one specific slice of the sample. The offset increment is of the order of 4 to 12 kHz. This step is performed while a pair of opposite magnetic field gradients are applied. As the application of a magnetic field gradient induces a dephasing, a second identical but opposite magnetic field gradient is added to counter this dephasing and to refocus the spins at the end of each lecture of the loop. Indeed, the magnetisation evolution is defined by its Larmor frequency and its evolution duration. The Larmor frequency is impacted by two phenomena: the magnetic field, which differ from slice to slice, and the chemical shift of each nucleus. The impact of the magnetic field variation gives spatial information, and the chemical shift variation gives spectroscopic information. In our case, only spectroscopic information is wanted and, therefore, the spatial information must be nulled. To do so, a pair of opposite magnetic field gradients is used, and the sum of their individual impact is equal to zero. In the end, the only impact of the magnetic field gradients is the generation of slices allowing the selective excitation, and the various magnetisation evolution are only impacted by the chemical shift and the evolution duration.

The slices are excited one by one in time and each of them will evolve during (EL+1-n)* $\Delta t_1$, with n the nth slice selected and $\Delta t_1$ the duration of one lecture of the excitation step (*Figure 21)*. These multiples of $\Delta t_1$ correspond to the different evolution durations needed to acquire the indirect dimension.
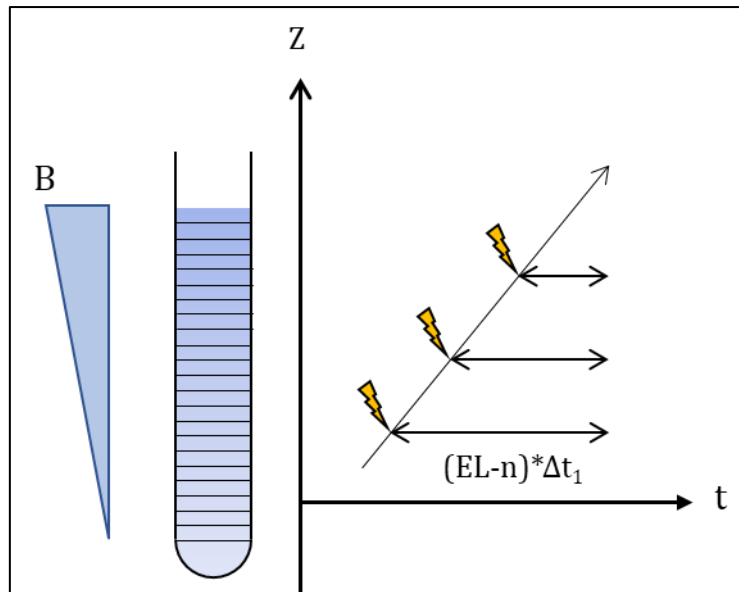
*Figure 21 - Sample divided in slices, each having its specific B value, individual excitation and distinct evolution duration (EL-n)\* $\Delta t_1$.*

To sum up, during the excitation step, magnetic field gradients allow specific spatial excitation. Each slice has the whole spectral width excited but its present its own evolution duration. Due to the specific evolution durations, slices present different dephasing and are therefore "phase-encoded". It means the phase information can be used to track the slice which the information comes from. Compared to the conventional sequence, one slice corresponds to one scan with a specific $t_1$-increment.

The second major part of the sequence is the acquisition loop, which follows the excitation and the mixing steps (r*ight part of figure 20*). All slices are acquired at the same time with an echo-planar imaging technique (EPI). EPI functions like MRI and decodes spectral information coming from various slices along the z-axis. (Mansfield, 1977; Ordidge & Mansfield, 1981; Ahn, Kim & Cho, 1986; Lhoste, *et al.*, 2022)  That step is composed by a loop of AL (acquisition loop) pairs of equal but opposite magnetic field gradients ($\pm G_a$) which are used to sweep through the k-space characterizing the sample. k-space is a concept used in MRI, where it is exploited to encode the space both in frequency and phase. Here, only the phase encoding is used along the z-axis.

During the excitation, the whole spectrum is excited on each slice, and each slice has its own evolution duration. Thanks to the application of a pair of opposite magnetic field gradients, nuclei only present evolution due to their chemical shifts. But as all slices evolve with different evolution durations, nuclei with the same chemical shift but from a different slice, have distinct phases. A k-value can be assigned for each chemical shift. This value represents the phase variation between nuclei having the same chemical shift but coming from successive slices.

It is defined as:

$$k_i = - C * \delta_i \qquad \text{with } C = \frac{\phi(z)}{\delta_i * z}$$

with $\delta_i$, the chemical shift of the $i^{th}$ nuclei, C an encoding constant and $\phi(z)$ the phase at a specific z-position. (Lhoste, *et al.*, 2022)

During the acquisition step, the magnetic field gradient $G_a$ is applied during a period $T_a$. $G_a$ generates a phase modulation and the longer it is applied, the more significant the modulation. This phase-modulation is also related to a k-value, which is defined by:

$$k(t) = A_p + \gamma_a \int_0^t G_a(n)dn$$

with $A_p$ the area of the prephasing gradients. (Lhoste, *et al.*, 2022)

Thus, during the time $T_a$, the k-values are sampled, from the lower ones up to the higher ones. When the k-value due to the temporal application of $G_a$ corresponds to the k-value of a particular chemical shift, an echo is observed.

$$k(t) = A_p + \gamma_a \int_0^t G_a(n)dn = k_i = - C * \delta_i$$

To conclude, during one magnetic field gradient $G_a$, chemical shifts $\delta$ are swept. This sweep is performed in one direction during a positive $G_a$ and in the other one when $G_a$ is negative. Each magnetic field gradient generates echoes for all chemical shifts. As these echoes come from the slicing method, it defines the UF dimension (which is related to $t_1$). The succession of magnetic field gradients enables a monitoring of these echoes through time which creates the other dimension (which is related to $t_2$). As this second dimension can be compared to the way a conventional acquisition is performed, it is called the conventional dimension. Data coming acquired during positive and negative $G_a$ are separately treated. The two data sets are put together by an adapted algorithm which then renders the final spectra.

The global scheme of the UF sequence becomes:

[Slice-selective preparation]$_{EL}$ – position-dependant evolution ($t_1$) –

position-independent mixing – acquisition with spatial decoding ($t_2$)

The following image (*Figure 22*) summarises the UF method proposed by Frydman and co-workers.
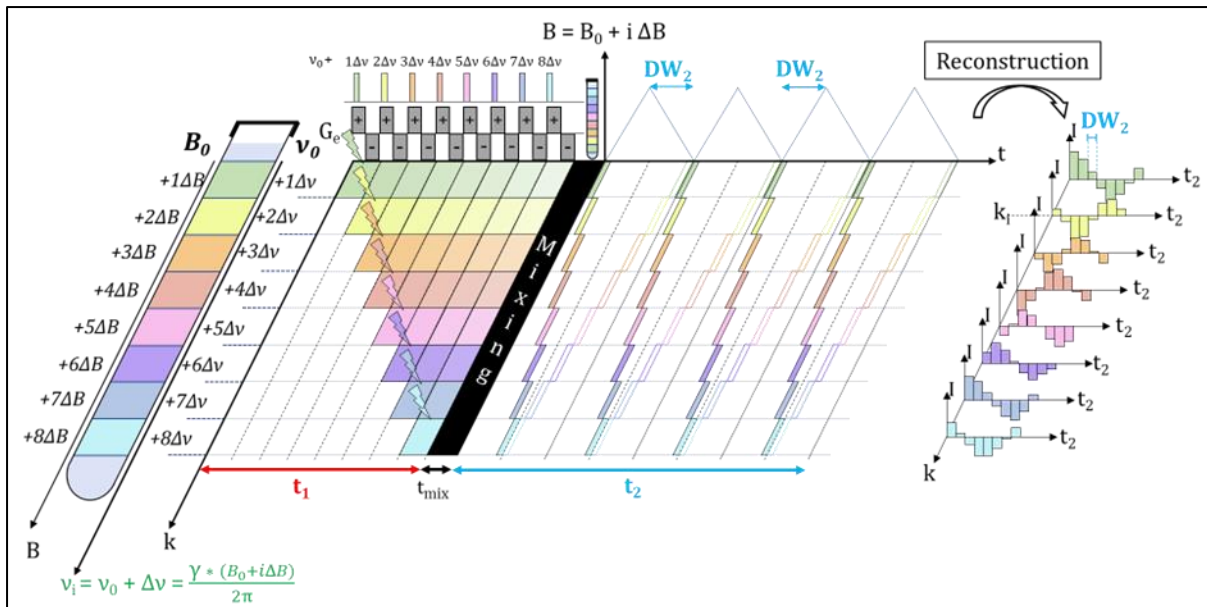
*Figure 22 - Graphical summary of the UF sequence proposed by Frydman. The sample tube is represented on the left part, with the various magnetic field and Larmor frequencies of the slices. During t₁, the excitation step occurs, with selective excitation and distinct time evolutions. After the mixing step starts the EPI-acquisition caracterized by t₂. Each slice is monitored at different moment, depending on how long the magnetic field gradients Gₐ have been applied, and renders one free induction decay (FID) after reconstruction. The right part of the figure displays the final outcome which correspond to the end-result expected for a conventional 2D-acquisition.*

The presented UF sequence is powerful, offering a major time reduction, but also has multiple drawbacks. (Frydman, Scherf & Lupulescu, 2002 and 2003; Pelupessy, 2003; Lhoste, *et al.*, 2022)) The first one is the lack of sensitivity compared to a conventional acquisition. In the latter, the whole sample is excited at each scan, implying that all nuclei are part of the entire signal. The intensity is thus much more important than in the UF method, where only nuclei present in one slice participate in a specific portion of the signal. Therefore, the SNR is lower for UF experiments. Moreover, in UF experiments, the frequency dispersion is higher than in a conventional experiment. It is indeed impacted by the spectral window, like a conventional experiment, but also by the frequency dispersion imposed by the magnetic field gradients. This higher frequency dispersion requires a larger receiver bandwidth, which in turn acquires more noise and reduces SNR. The second drawback is the requirement for perfectly squared pulses to excite the whole sample. If the pulses are not perfectly squared, an imperfect excitation is induced during the time the pulse is growing in intensity. The regions with imperfect excitations cannot be used and cause significant loss of signal. Third drawback is the presence of off-resonances effects like Bloch-Siegert shifts. Bloch-Siegert shifts happen when monochromatic irradiations, as with selective pulses, are used. With these pulses, some phase shifts are observable in a bandwidth much larger than the frequency window being excited. (Emsley & Bodenhausen, 1990) It therefore perturbs the linear correlation between δ and z-axis position. Final drawback is that pulses are too short to be perfectly selective.

Pelupessy (2003) proposed another pulse sequence which overcome some of the above mentioned drawbacks (*Figure 23*). Only the excitation step is modified. The train of EL 90° selective pulses is replaced by a first 90° non-selective pulse and two 180° chirp pulses. The 90° non-selective pulse happens while no magnetic field gradient is activated and excites all chemical shifts on the whole sample. Afterwards, a pair of two equal 180° chirp pulses are applied while a pair of equal but opposite magnetic field gradients ($\pm G_e$) are active. These so-called "chirp" pulses are adiabatic pulses which have a linear frequency ramp. They will pulse from lower frequencies up to higher ones. Since these pulses happen during the magnetic field gradients, they will excite the sample slice by slice.

The fact the magnetic field gradients are a pair can be justified by the same reasoning than for Frydman's sequence. The fact a pair of adiabatic pulses are present is due to a phase distortion generated when a chirp pulse is applied during a magnetic field gradient. (Ugurbil *et al.,* 1988) To overcome this drawback, a second adiabatic chirp is applied during the opposite magnetic field gradient. This creates an opposite distortion, therefore annihilating that problem. In the end, a linear correlation between phase-encoding and the z-axis is obtained.
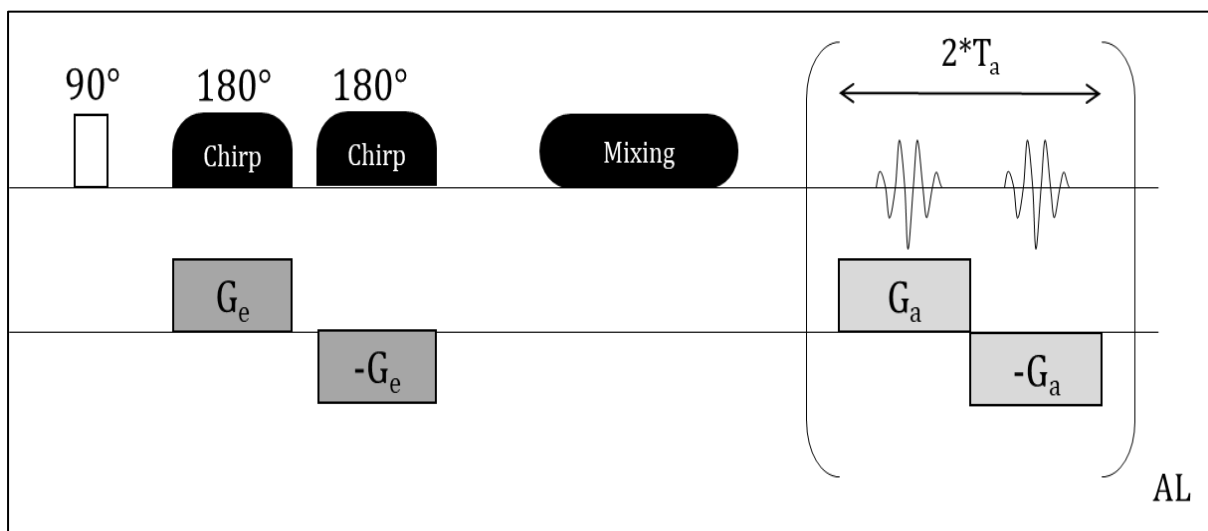


*Figure 23 - Ultrafast sequence proposed by Pelupessy (2003): a 90° non-selective pulse and a pair of adiabatic chirp pulses simultaneous with two opposite magnetic field gradients (Gpz0 & Gpz1), followed by a mixing step and the acquisition step composed of a pair of AL pairs of magnetic field gradients, each individual gradient with a duration $T_a$.*

The first chirp pulse will excite the sample bottom's up and the second one will refocus the slices from the upper ones to the lower ones (*Figure 24*). This means the time between both excitations is different for each slice. This corresponds to the $t_1$-incrementation found in the conventional sequence and to the multiples $N* \Delta t_1$ in Frydman's proposal. After the excitation and mixing steps, the acquisition is achieved just like in Frydman's sequence, with a loop of AL pair of magnetic field gradients ($\pm G_a$).
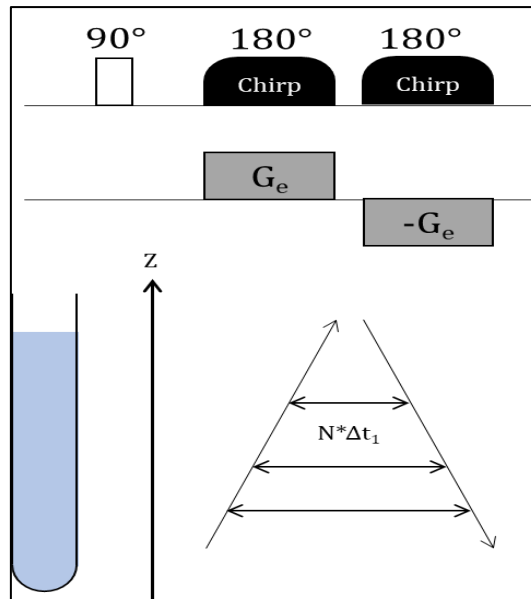
*Figure 24 - Time increments creation by the pair of adiabatic chirp pulses simultaneous with a pair of opposite gradients in the ultrafast sequence of Pelupessy.*

In comparison with Frydman's proposal, this method has three major advantages: the whole sample contributes to the signal (no problems due to imperfect square pulses), no off-resonance effects are detected, and the magnetic field gradients required are less intense. Still, the method is not perfect since some signals are lost. Firstly because of the diffusion losses during the duration of both excitation and acquisition steps and secondly because of the adiabatic pulses which are more sensitive to evolution losses related to $T_2$ and higher coupling constants J. (Pelupessy, 2003)

For further discussion, the sequence proposed by Frydman will be used in the images because it is easier to understand. However, all experiments have been performed with the sequence with chirp pulses and the equations therefore refers to the sequence proposed by Pelupessy.

## ii. General drawbacks

In general, the UF method presents two major drawbacks: a low resolution and a low sensitivity. (Frydman, Scherf, Lupulescu, 2002 and 2003; Pelupessy, 2003) The noise level increases with a factor $(2n)^{1/2}$, with n the number of points measured during one acquisition gradient $G_a$. Since there are two gradients, the total noise increases by a factor $n^{1/2}$ and thus SNR decreases by a factor $n^{1/2}$. Therefore, to increase the sensitivity, n should be lowered. However, this results in a lower resolution since it is inversely proportional to n. A compromise must be found between sensitivity and resolution. Currently, the pulse sequence proposed by Pelupessy (2003) offers the best sensitivity/resolution ratio and is the most frequently used. (Giraudeau & Akoka, 2010)

Another important drawback of the UF method is the lower spectral width (SW) in both dimensions. These are mostly limited by the power and the time-length of the acquisition magnetic field gradients. To increase the spectral width, the simplest solution is to increase the gradient power. Since only one scan is applied here, the hardware has the time to cool down and it may cause no harm. But it is paramount to act with care and to be sure not to damage the hardware by overheating. Other methods like aliasing are also workable solutions. It enables a refold of all signals on a smaller spectral width while keeping the same resolution. (Giraudeau & Akoka, 2010) The technique used here is called interleaving and is further developed at point iv.

The last major drawback is the appearance of artefacts which can appear because of the use of gradient-echo during the acquisition. Some phase shifts can appear at a local scale. (Posse & Aue, 1990; Hu & Le, 1996)

### iii. Applications

The UF method has been applied for different sequences like COSY, TOCSY, HSQC and HMBC, and spectra are usually obtained in less than a minute, very often within 10 seconds and sometimes even quicker than a second. (Shrot, Saphira & Frydman, 2004; Herrera A., *et al.*, 2010; Queiroz, Ferreira & Giraudeau, 2013) Research have also studied the appliance of the UF principle coupled with other methods to improve the sensitivity. It has been shown that the UF method can be coupled with Hadamard (Tal, Saphira & Frydman, 2009) and can be used with hyperpolarisation like DNP, which renders higher sensitivity by increasing the population difference between the α and β states. (Frydman & Blazina, 2007; Mishkovsky & Frydman, 2008; Giraudeau, Shrot & Frydman, 2009) Due to its characteristics, mainly its rapidity and the use of magnetic field gradients, the UF principle can also be a major tool in different studied areas such as real-time reactions, in vivo studies, NMR chromatography, n-dimensions experiments, faster MRI, exchange phenomena studies... (Saphira & Frydman, 2003; Shrot & Frydman, 2003; Frydman, 2006; Herrera A., *et al.*, 2010; Mankinen *et al.*, 2020)

From a quantitative perspective, the UF experiment has less $T_1$-noise than a conventional experiment. However, since it is faster, it is less sensitive. One solution might be to acquire different UF spectra and to sum them up. (Giraudeau & Akoka, 2013)

### iv. Interleaving

UF experiments have SW and resolution as drawbacks. These are defined by the following equations, with conv referring to the conventional dimension and UF to the UF dimension:

$$- \quad SW_{conv} = \frac{1}{2*T_a} \qquad\qquad - \Delta\nu_{conv} = \frac{1}{2*T_a*AL}$$

$$- \quad SW_{UF} = \frac{\gamma_a * G_a * T_a * L}{4\pi * T_{2CP})} \qquad\qquad - \Delta\nu_{UF} = \frac{1}{2 * T_{2CP}}$$

$$- \quad \gamma_a * G_a * L = 4\pi * \frac{SW_{conv} SW_{UF}}{\Delta\nu_{UF}}$$

with SW the spectral width, Δν the resolution, $G_a$ & $T_a$ the power and duration of the acquisition magnetic field gradient, γ the gyromagnetic ratio of the monitored nucleus, $T_{2CP}$ the combined duration of the two chirp pulses, AL the number of acquisition loops and L the sample length. (Lhoste, *et al.*, 2022)

SW and Δν in the conventional dimension can easily be compared with the formulae used in conventional sequences: SW = 1/(2*DW) and Δν = 1/(2*$t_{2,max}$) with DW the dwell-time and $t_{2,max}$ the maximum acquisition-time acquired in the $t_2$-dimension.
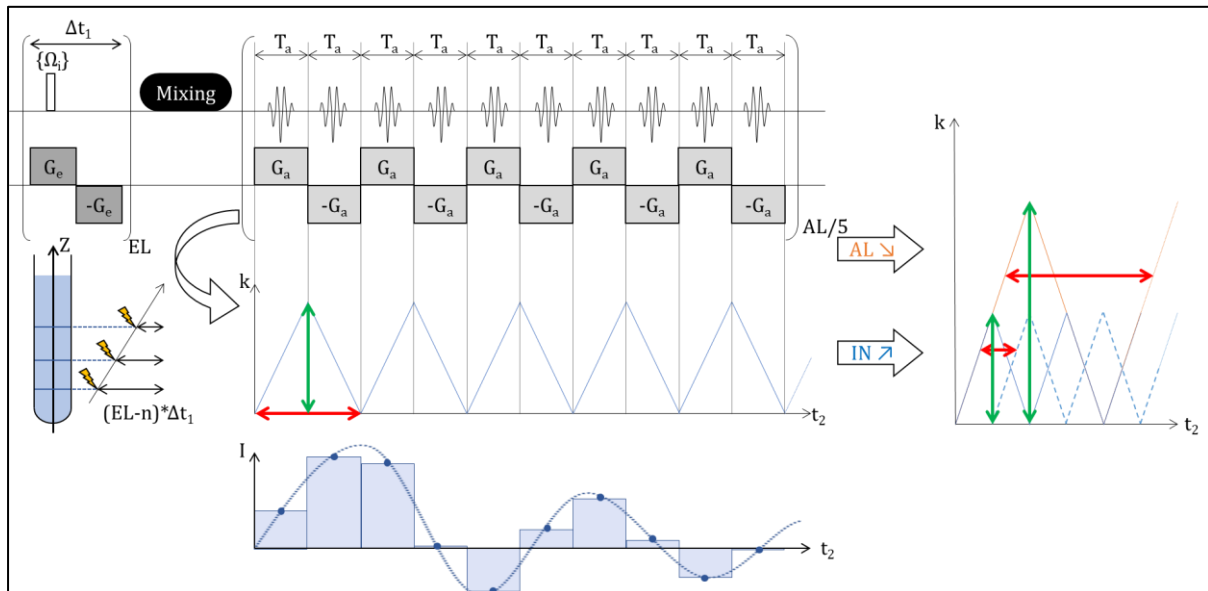


*Figure 25 – Summary of Frydman's UF sequence (up) and the successive excitations and acquisition of the various slices (middle). A conventional FID (bottom) gives a direct link between UF and conventional experiments. The right part of the figure describes the consequences of modifying the acquisition parameters, with AL the acquisition loop number and IN the interleaving number. The red double arrow shows the dwell-time along the time-axis $t_2$ (DW$_2$) and the green one shows the amplitude of the frequency range manipulated.*

Figure 25 shows the UF sequence on the upper part of the image. The part right beneath the sequence shows the sample tube, the successive excitations and the acquisition described as a screening of k through time $t_2$. The bottom part represents a conventional FID to give a direct comparison between the EPI acquisition and how a conventional FID is obtained. At last, the right part of the figure displays the impact of possible modifications of the acquisition parameters AL (in orange) and IN (in blue). IN stands for Interleaving Number.

As we consider the spatiotemporal space (k; $t_2$), the acquisition can be described as a zig-zag function, sweeping the k-domain while the time goes by. This sweeping happens in one direction then in the other one depending on the sign of the acquisition magnetic field gradient $G_a$. (*Figure 25*) $SW_{UF}$ is directly related to the k-domain which is sampled by the gradients (green lines in *figure 25*) and $SW_{conv}$ is equal to the inverse of the time between two parallel lines (2 * $DW_2$ (= 2*$T_a$) in red in *figure 25*) . To modify both SW, a first possible way is to modify AL, the number of acquisition loops (orange scenario in the right part of *figure 25*). As the total acquisition time along $t_2$ is maintained constant, AL has a direct impact on $T_a$:

$$T_a = t_{2,max}/(2*AL)$$

with $t_{2,max}$ the maximum $t_2$ value acquired, which is kept constant.

If AL is reduced, $T_a$ becomes longer and the k-domain range exploited increases (green line of the orange scenario in *figure 25*), resulting in a larger $SW_{UF}$. However, the time between two parallels (red line in the orange scenario in *figure 25*) increases too. Therefore, $SW_{conv}$ decreases because it is inversely proportional to that time. This can also be seen when looking at the equations of $SW_{UF}$ and $SW_{conv}$. Another possibility is the interleaving method (blue scenario in the right part of *figure 25*). It consists in repeating the experiment multiple times, with an increasing delay right before the acquisition step. This delay is equal to:

$$\frac{(i-1) \, * \, 2T_a}{IN}$$

with i, the $i^{th}$ scan and IN the number of interleaved scans.

Each of the acquisition starts thus at a different moment, meaning $DW_2$ (red line in the blue scenario in *figure 25*) decreases and thus $SW_{conv}$ increases. And $SW_{UF}$ is not modified since $G_a$ and $T_a$ keep the same values. $SW_{conv}$ becomes:

$$SW_{conv} = \frac{IN}{2T_a}$$

By combining these two strategies (increasing $T_a$ and conducting more scans), it is possible to enlarge both $SW_{UF}$ and $SW_{conv}$ . However, this technique can add some artefacts at distances $i*SW_{conv}/IN$ (i = 1,…IN), but these can be reduced by adding dummy scans or by using specific post-processing. (Lhoste, *et al.*, 2022) Increasing IN also means the sequence is repeated and the time of the experiment is increased by a factor IN.

## b. Implementation

All UFCOSY experiments are listed in table A3.

The employed sequence uses adiabatic chirp pulses for the space-encoding step. The first experiments were conducted on a simple sample (ethanol 1.71M in $D_2O$) to understand the sequence and the impact due to modifications of the acquisition

parameters. They were followed by experiments conducted on a more complex molecule: THA 22mM in CDCl₃. Lastly, the sequence was assessed on aqueous conditions: sucrose 2mM in water and a metabolite sample in D₂O with water added bit-by-bit.

After having calibrated the spectrometer as usual for conventional experiments, the preparations for the UF experiments start with the calibration of the excitation gradients and chirp pulses. Therefore, an experiment called "echograd" is used. That experiment displays the frequency excitation profile, meaning the bandwidth generated by the magnetic field gradients. The details of the calibration can be found in the annexes (*Page 64*), and a summary is presented right below.

The calibration starts by determining the frequency offset (O1P) of the chirp pulses. O1P represents the frequency on which the frequency bandwidth of the chirp pulse is centred. Since a major flaw of UF experiments is the SW of the spectrum, O1P is placed in the middle of the peaks, thus lowering the risk of missing signals. Afterwards, both power of the magnetic field gradient generating the slices ($G_e$) and the adiabatic chirp pulse (CP = chirp power) must be calibrated. The calibration is used to the generated bandwidth coincide with the excited one. If they coincide, the whole sample and the whole frequency band of the chirp are exploited (*middle part of figure 26*). If the frequency band generated by the magnetic field gradient is higher than the one excited by the pulse, a part of the sample is not excited (*left part of figure 26*). This leads to a loss of resolution since less slices are exploited. The reverse scenario will lead to a part of the chirp trying to excite "non-existing slices" (*right part of figure 26*).
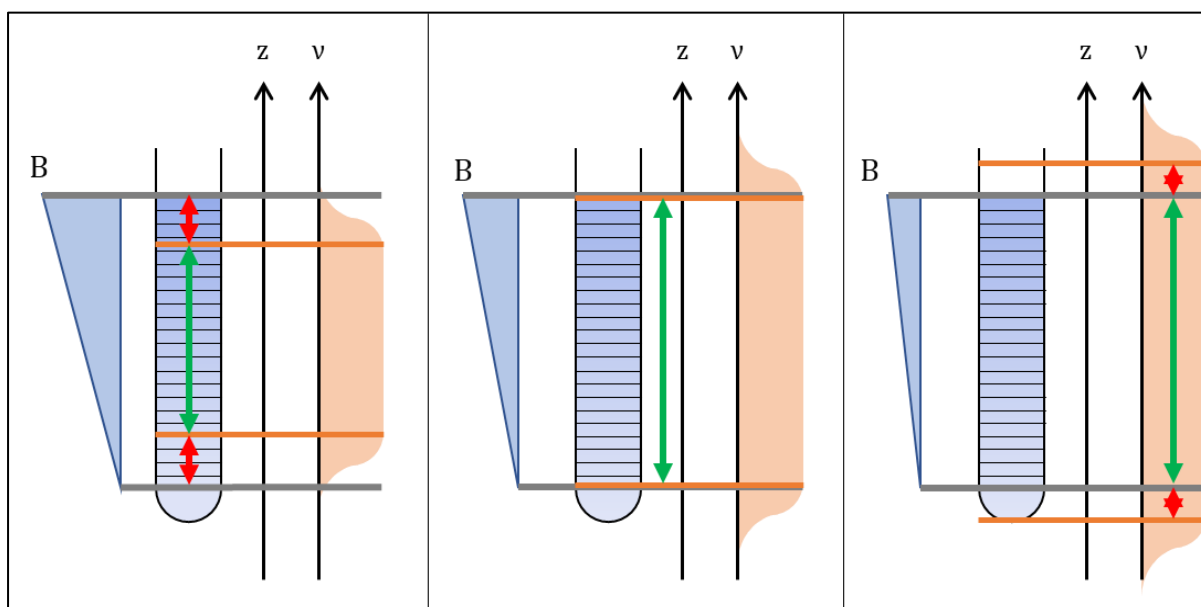


*Figure 26 - The frequency band generated by the gradient and the one excited by the chirp pulse must coincide, otherwise leading to a lesser situation. Middle scenario considers a perfect match. on the left side, the band frequency generated by the gradient is larger the one excited by the pulse. On the right part, the opposite scenario is displayed. The magnetic field gradient is shown on the left side of the sample tube and the chirp pulse is presented in orange on the right of the tube. Green arrows indicate what is really put to profit and red arrows indicate the parts that are not used.*

Once all these calibration steps are achieved, the UFCOSY experiment can be parametrised, using the values obtained by the echograd sequence (O1P = 3ppm, $G_e$ = 3.5% and CP = 17dB).

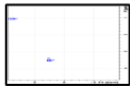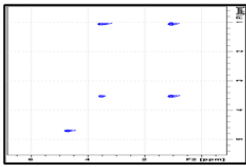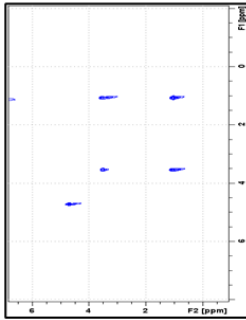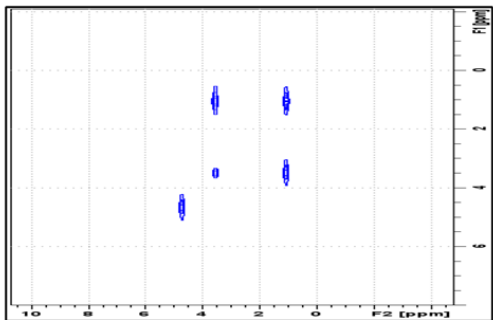| Parameters | $SW_{UF}$ (ppm) | $SW_{conv}$ (ppm) | Spectrum |
|---|---|---|---|
| $N_{conv}*N_{UF}$ = 256*512<br>IN = 1<br>AL = 128<br>expt = 14 s | / | / |  |
| $N_{conv}*N_{UF}$ = 512*1k<br>IN = 4<br>AL = 64<br>expt = 35 s | 7.7 | 5 |  |
| $N_{conv}*N_{UF}$ = 1k*1k<br>IN = 8<br>AL = 64<br>expt = 64 s | 7.7 | 10 |  |
| $N_{conv}*N_{UF}$ = 1k*2k<br>IN = 16<br>AL = 32<br>expt = 121 s | 15.5 | 10 |  |

*Table 2 - Parameters, experiment time and spectral width for various UFCOSY experiments on an EtOH sample. $SW_{UF}$ corresponds to the horizontal spectral window and $SW_{conv}$ to the vertical spectral window. All spectra have the same scale.*

$SW_{conv}$ is the vertical spectral width and $SW_{UF}$ is the horizontal one. The UF experiment with the parameters obtained by the echograd lasts 14 seconds (*first row of table 2*). However, as SW is too small in both dimensions, it is impossible to calibrate the spectrum due to the lack of signals. When both interleaving and AL modification are added, it is possible to acquire acceptable spectra, which are calibratable. Three spectra

are displayed in table 2. They were acquired with various AL and IN values therefore showing different SW and experiment time. Factors $N_{conv}$ and $N_{UF}$ are calculated and depends on AL and IN values. More information about the calculation of $N_{UF}$ and $N_{conv}$ can be found in the annexes (*Page 68*).

Last row of table 2 shows an experiment giving a spectrum with $SW_{conv}*SW_{UF}$ of 15.5ppm * 10ppm. Such large SW has no utility when monitoring protons, even more if this SW increase doubles the experiment time compared to the experiment rendering a spectrum with a $SW_{conv}*SW_{UF}$ of 10ppm * 7.7ppm, $SW_{UF}$ being horizontal and $SW_{conv}$ vertical. Besides the changes in SW, signals also have different shapes.
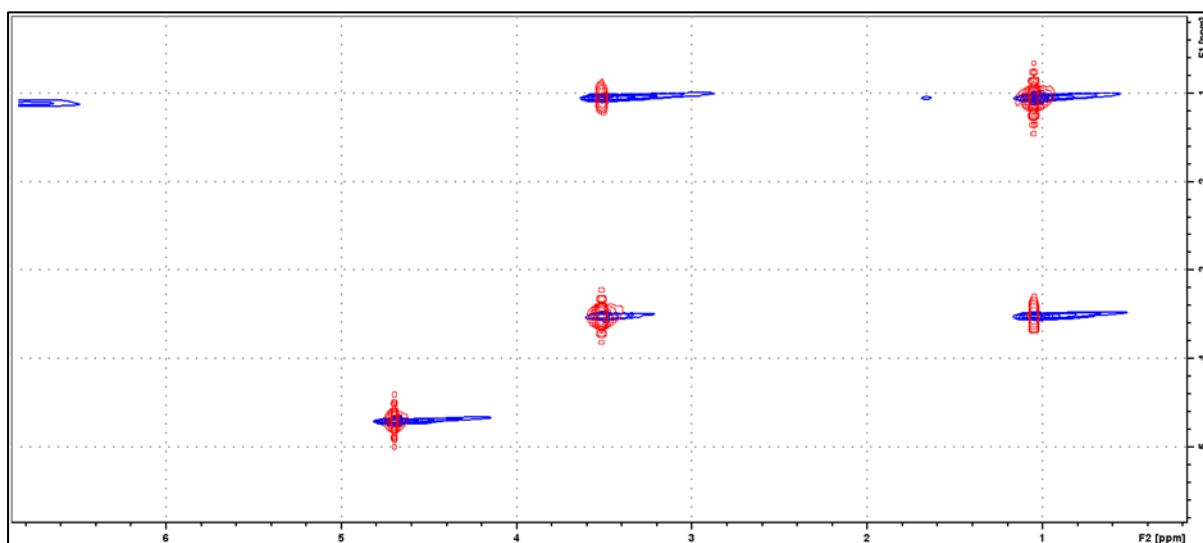


*Figure 27 – Superposition of COSY experiments for an ethanol sample. In blue, a UF spectrum acquired in 64 seconds with O1P = 3ppm, $G_e$ = 3.5%, CP = 17dB, $N_{conv}*N_{UF}$ = 1k*1k, IN = 8 and AL = 64. In red, a conventional COSY acquired in 112 seconds with one scan and $N_2*N_1$ =2k*64.*

The ethanol sample was also recorded with a conventional COSY experiment with one scan and $N_2*N_1$ = 2k*64 in 1 min 52s. (T*able A5 in the annexes)* A superposition of the conventional spectrum (red) with the one acquired by UFCOSY (blue) in 64 seconds (*third row of table 2*) demonstrates few differences (*Figure 27*). Firstly, UF signals are horizontally deformed but this does not hinder the lecture of the spectrum. However, in the case of a more complex molecule or mixture, signals overlapping could start hampering the analysis of the spectrum. Secondly, SW is wider for the conventional spectra. It is possible to increase SW for the UF experiments, resulting in an increase in time. However, as ethanol is a small molecule, the number of observable signals is low and both conventional as UF techniques give clear spectra. Both SW and artifacts could become a problem if a molecule presenting a larger chemical shift dispersion is sampled. Therefore, to explore the UFCOSY limits, a more complex molecule was used: THA 22mM in CDCl₃. The echograd calibrations for THA were O1P set to 4 ppm, $G_e$ to 3.5% and CP to 19dB. Figure 28 displays the UFCOSY spectrum generated by the UFCOSY sequence while using the parameters determined by the echograd calibration.
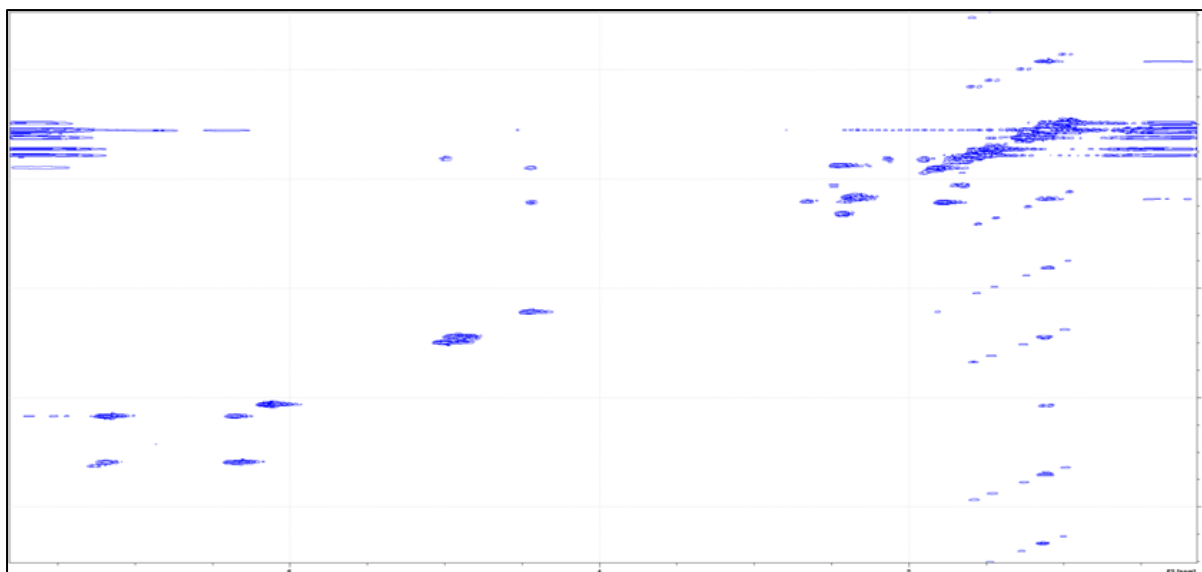
*Figure 28 - UFCOSY spectrum for a sample of THA in CDCl3. O1P = 4ppm, $G_e$ = 3.5%, CP = 19dB, $N_{conv}*N_{UF}$ = 1k\*1k, IN = 8 and AL = 64. The spectrum was acquired in 64 seconds and the spectral windows are ~8ppm\*10ppm.*

The notable repetitive traces on the column along 1.1 ppm of the spectrum are artefacts. The vertical repetition of the pattern is due to interleaving causing artefacts spaced by a distance i\*$SW_{conv}$/IN. The pattern that is repeated.

An extra time delay D10 can be added between the non-selective 90° pulse and the first gradient $G_e$. Various values of D10 have been attempted and 30ms was the optimal one. (*spectrum on figure 29*) The adding of D10 induces a reduction of the number of artefacts on the 1.1 ppm column.
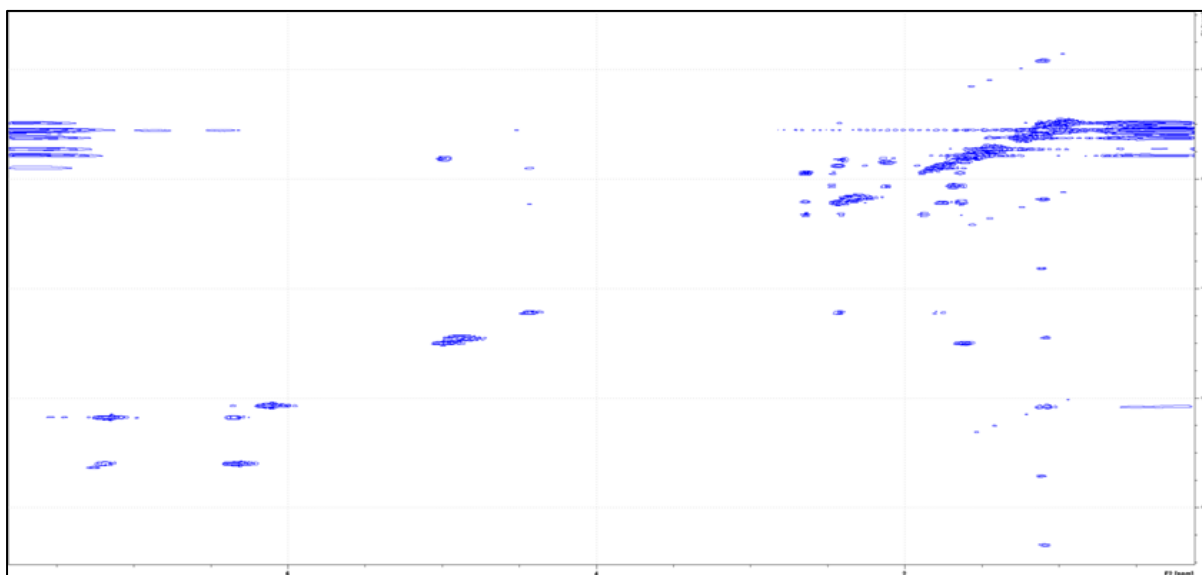


*Figure 29 - UFCOSY spectrum for a sample of THA in CDCl3. O1P = 4 ppm, $G_e$ = 3.5%, CP = 19dB, $N_{conv}*N_{UF}$ = 1k\*1k, IN = 8, AL = 64 and D10 = 30ms. The spectrum was acquired in 64 seconds and the spectral windows are ~8ppm\*10ppm.*

*Kolkman M.*

Spectra were also acquired using two scans instead of one. A small reduction of the artifacts on the 1.1ppm row is observable but no other significant changes are notable. The UF-spectrum acquired with D10 = 30ms and 2 scans will be presented in blue in figure 30, which is a superposition of both UF and conventional spectra.

A superposition of the UF spectra acquired in 64 seconds and a conventional experiment acquired in in 14 min 12s is presented. (*Figure 30*) The conventional COSY-spectrum was acquired with one scan and $N_2*N_1$ = 2k*512. (*Table A3 in the annexes*) The figure does not display the whole spectra. SW is wider in the conventional experiment than in the UF one. A zoom on the crowded area of the superposition is displayed on the right.
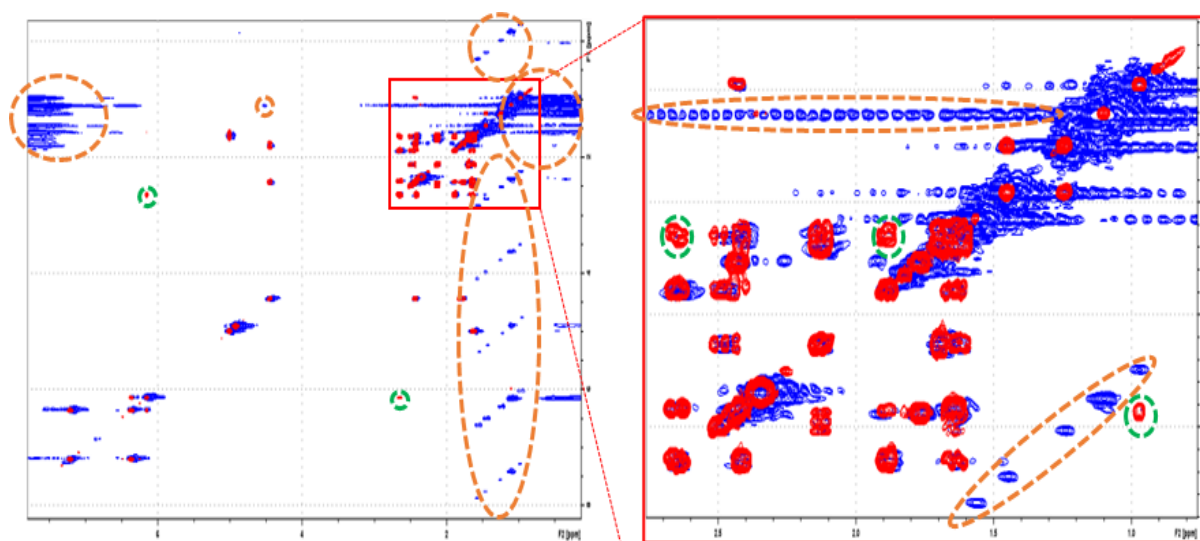


*Figure 30 - Superposition of two COSY spectra of THA, acquired with an UF experiment in blue (O1P = 4 ppm, $G_e$ = 3.5%, CP = 19 dB, $N_{conv}*N_{UF}$ = 1k*1k, IN = 8, AL = 64, D10 = 30ms, $N_S$ = 1 and an acquisition in 64 seconds) and a conventional COSY in red ($N_2*N_1$ = 2k*512, $N_S$ = 1 and an acquisition in 14 min 12 seconds). A zoom on the crowded part in present on the right. Orange circles highlight artefacts are and green circles indicate signals that hardly observed in the UF spectrum.*

Artefacts are observable on the left and right extremities of the spectrum and on the 1.1 ppm column and 1.1ppm row (*orange circles*). Green circles indicate signal that are not visible in the UF spectrum but well in the conventional spectrum.

Three observations are notable. First, the number of signals lost in the UF spectrum is low. Secondly, the number of artefacts is significant, and their size make them a concerning problem. Third, the signals are larger in the UF spectrum. The addition of the two last observations hinders the lecture when signals are crowded. Therefore, the application of UF experiments might be limited when a high resolution is required. It may be interesting to use UF experiments to make real-time analysis, but its use towards high-resolution and structural analysis seems less probable.

The following step in the UF implementation is the application of UF-experiments on an aqueous sample. Therefore, an UFCOSY sequence with presaturation (PRUFCOSY) was used. Some details about the implementation of the presaturation can be found in the annexes. The sequence was tested on a sucrose 2 mM sample. (*experiments in table A4*) First, a conventional 1D-proton experiment was performed with a presaturation and the presaturation power was used for a UF experiment (about 46dB). As the water signal was observable, higher powers were used, up to 25 dB. As the spectrum kept being the same, no further experiments were achieved. Figure 31 displays the UF-spectrum acquired for the sucrose 2mM sample with a presaturation power of 25dB. The water signal and its replica due to interleaving are observable, and so are artefacts present on the edges of the spectrum. A last observation is the presence of horizontal lines at the water "signals" chemical shifts.
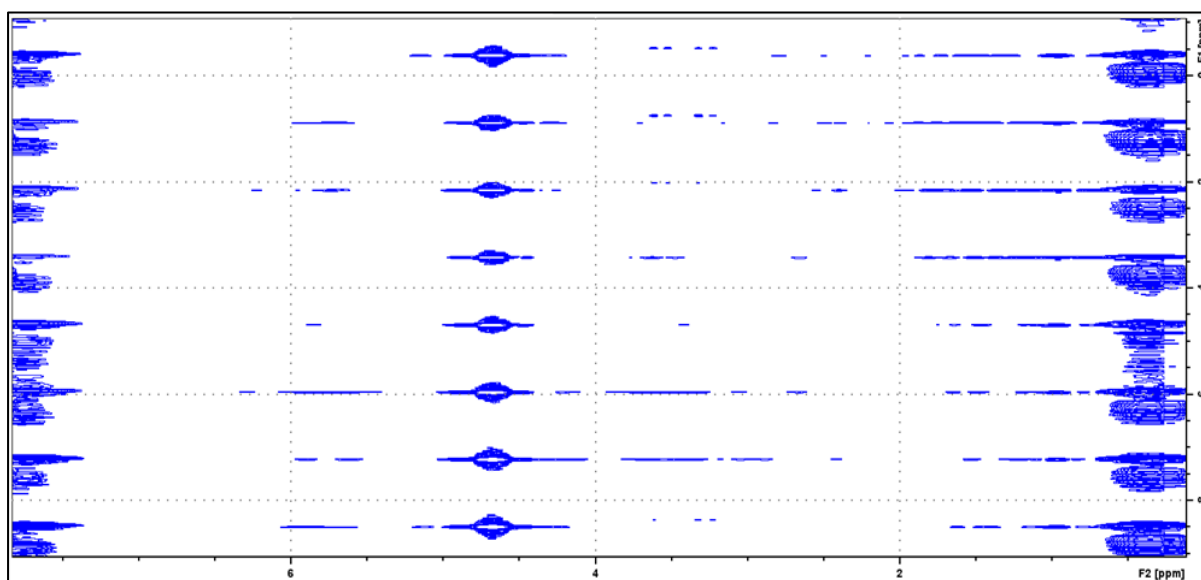


*Figure 31 - UF experiment conducted on a sample of sucrose 2mM in water. Parameters were the following: $N_{conv}*N_{UF}$ = 1k * 1k, AL = 64, IN = 8, $N_s$ = 1, presaturation power of 25dB and duration = 71 s.*

To further explore the possibilities proposed by the PRUFCOSY sequence, a sample containing metabolites at concentrations between 12 and 55mM in $D_2O$ was produced. A conventional COSY experiment with presaturation has been performed to give a reference spectrum (*Figure 32*). Then, little amount of water has been added and PRUFCOSY experiments have been carried out. (*experiments in table A4 in the annexes*)

Figure 33 presents the spectra obtained for various additions of water. As the added amount increases, the number of artefacts increases too, and they become more intense. This results in a relative decrease of the signal's intensity, sometimes to the point that they become unobservable. It is important to note the presaturation power has been kept constant.
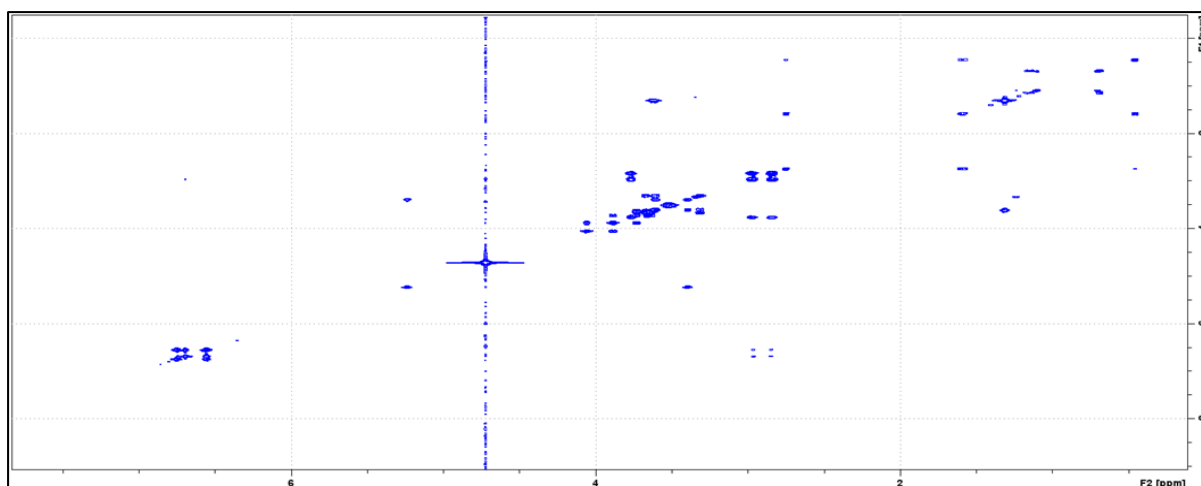
*Kolkman M.*

*Figure 32 - Conventional COSY spectrum for a sample of metabolites (alanine 32 mM, 3,4-dihydroxyphenylalanine 30 mM, sucrose 12mM and 2-ethylhex-1-ol 55mM) in 600μL D2O acquired without NUS, with $N_2*N_1$ = 4k*1k and NS = 2. The acquisition took 1 h 2 min.*
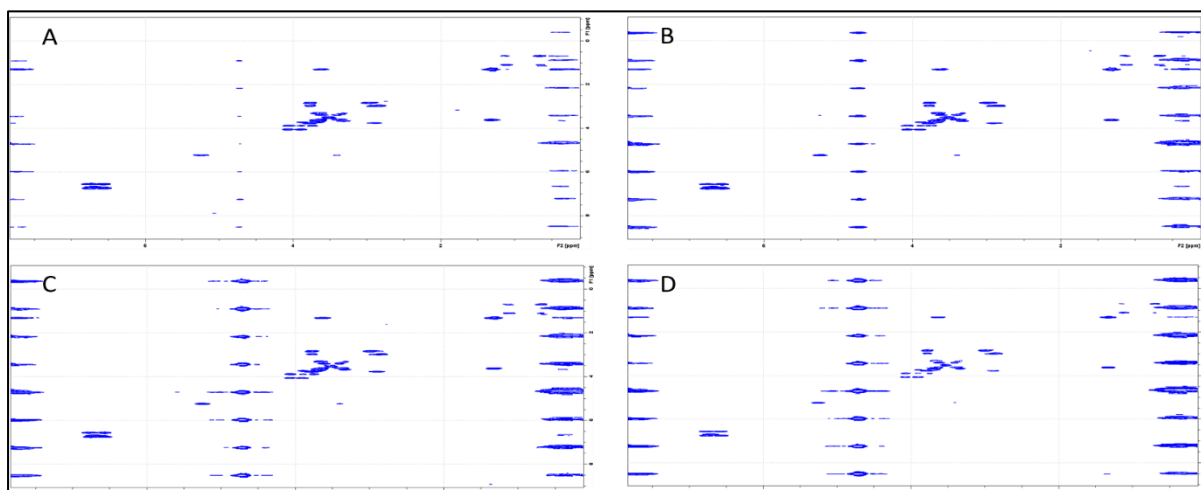


*Figure 33 - PRUFCOSY spectra of a sample of metabolites (alanine 32 mM, 3,4-dihydroxyphenylalanine 30 mM, sucrose 12mM and 2-ethylhex-1-ol 55mM) in 600 μL D2O with an adding of 10 μL (A), 70 μL (B), 130 μL (C) and 200 μL (D). All experiments were achieved in 71 seconds with O1P = 4 ppm, $G_e$ = 3.5%, CP = 12dB, $N_{conv}*N_{UF}$ = 1k*1k , IN = 8, AL =64 and $N_s$ = 1.*

A superposition (*Figure 34*) of the conventional COSY spectrum acquired before any addition of water and the PRUFCOSY experiment recorded after the addition of 200 μL of water shows the lost signals in the PRUFCOSY spectrum (green and orange circles). The orange circles are signals of DSS, which is less concentrated than the other metabolites. Since UF has a lack in sensitivity, it is coherent DSS is the first molecule to be unobservable. The green circles are lost signals for the other metabolites, sucrose and 3,4-dihydroxyphenylalanine to be more precise. It is also notable that horizontal lines begin to appear in the PRUFCOSY spectra and that signals are wider in the PRUFCOSY spectrum. Concerning experiment duration, the PRUFCOSY experiment is about fifty times faster. However, it is noteworthy to point out that the conventional experiment has

been done only once, with the parameters set such that a high resolution was obtained. Time improvement is possible. Moreover, the conventional spectrum is used as a reference, indicating the positions of signals. As it has not been acquired once water has been added, spectrum-quality and experiment time are not meant to be compared conventional and UF experiments.
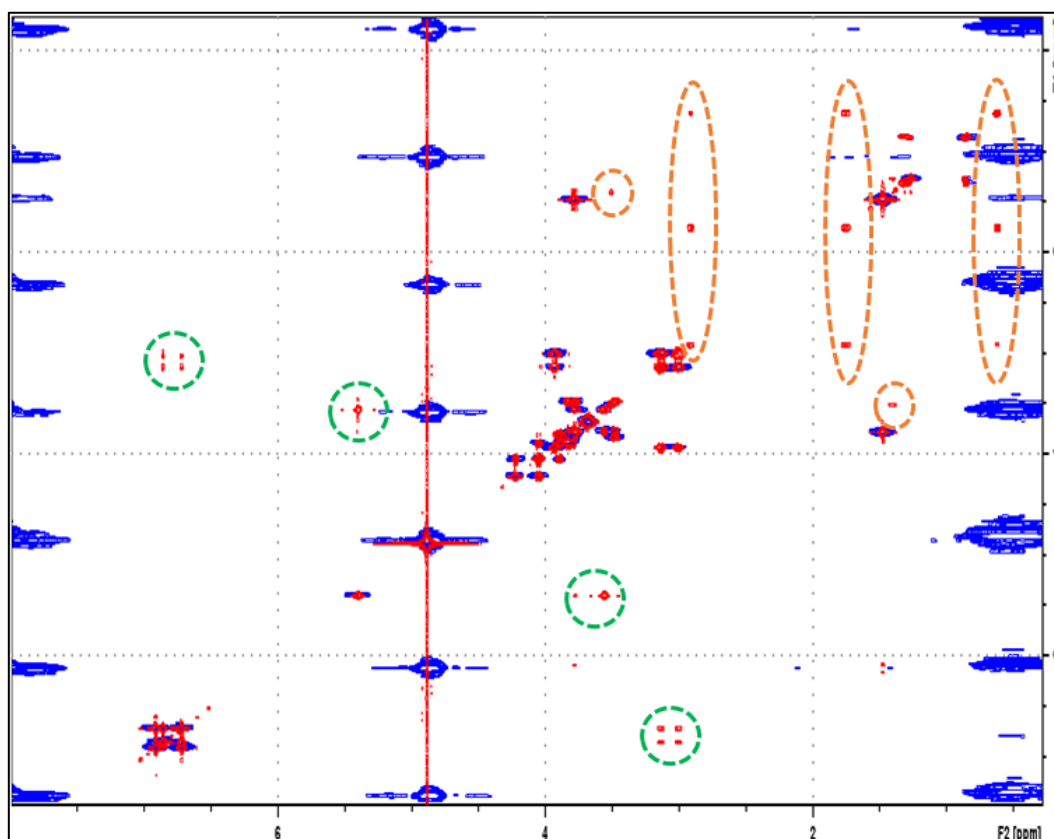


*Figure 34 - Superposition of the conventional COSY experiment recorded when water was not yet added (red) and the PRUFCOSY spectrum (blue) recorded after the addition of 200 µL of water. Green circles indicate lost signals which are visible in the red spectrum but not observed in the blue one. Orange circles are signals of DSS that are visible in the conventional experiment and not in the UF experiment.*

As water signals are still observable, we cannot state with conviction the PRUFCOSY has performed as expected. However, the power of the presaturation has not been calibrated when water was added, the presaturation has not been optimised. Other experiments should be achieved, and with care as both presaturation and UFCOSY sequence can generate heat and damage the hardware. The addition of both must be treated with caution. Another noteworthy point to mention is the fact the UF sequence without presaturation has not been tried on the sample once water was added. Therefore, no conclusion concerning the use of the PRUFCOSY can be asserted.

## VI-   Conclusion

During this document, two types of NMR experiment have been tested in various conditions. Non-Uniform Sampling (NUS) has first been applied on a molecule with numerous correlations: triamcinolone hexacetonide (THA). COSY, HSQC and HMBC sequences have been attempted and promising results have been found. The time reduction proposed by NUS can reach a factor 9 without hindering the resolution and the sensitivity of the spectrum. The main problem of NUS is the appearance of artefacts, majorly $T_1$-noise patterns which can hinder the lecture of the spectrum. NUS has also been applied to a COSY sequence on a water sample. The water vertical noise was not modified, and the spectra presented all the expected signals. One important feature of NUS is the possibility to be used to obtain higher quality spectra in the same amount of time. A promising compromise between both strategies (fastest as possible and higher quality) has been found by applying NUS 10% with a resolution increased by a factor 2. This leads to a factor 5 time reduction. NUS is a simple tool that can be applied to all multi-dimensional sequences without requiring specific calibrations and should therefore be employed. For the future, sensitivity limits and the impact of the NUS percentage on it could studied by testing different concentrations.

Spatial encoding or ultrafast (UF) is the second technique that has been implemented. The theoretical time reduction offered by UF is more significant than most fast-NMR technique. However, it presents inherent flaws which can be overcome but engendering an experiment duration increase. UF has been applied to different samples and conditions. All spectra present the same characteristics: artefacts at the edges, artefacts generated by interleaving, larger signals and occasional signal loss. If it does not render high-resolution spectra, it still can be used in different NMR field, in particular in real-time analysis, NMR chromatography, n-dimensions experiments, faster MRI. Its use in watery conditions has not been fully assessed. Further research towards extended application of the spatial encoding concept, like specific conditions and other sequences should be attempted.

## VII-   Acknowledgements

## VIII- Bibliography

Aguilar J. A., Nilsson M. Bodenhausen G. and Morris G. A. (2012) 'Spin echo NMR spectra without J modulation', *Chemical Communications,* 48, pp. 811-813. doi: 10.1039/c1cc16699a

Ahn C. B., Kim J. H. and Cho Z. H. (1986) 'High-speed spiral echo planar NMR imaging', *Transactions on Medical Magnetic,* 5, 1, pp. 2-7.

Ahmed N., Rao K. R. and Abdussattar A. L. (1971) 'BIFORE or Hadamard Transform', *IEEE Transactions on Audio and Electroacoustics,* 19, 3, pp. 225-234. doi: 10.1109/TAU.1971.1162193

Andersen N. S. and Köckenberger W. (2005) 'A simple approach for phase-modulated single-scan 2D NMR spectroscopy', *Magnetic Resonance in Chemistry*, 43, pp. 795-797. doi: 10.1002/mrc.1624

Bernstein M. A., King K. F. and Zhou X. J. (2004), *« Handbook of MRI pulse sequences »*, Elsevier Academic Press, pp. 960.

Bletcha V. and Freeman R. (1993) 'Multi-site Hadamard NMR spectroscopy', *Chemical Physics Letters,* 215, 4, pp. 341-346. doi: 10.1016/0009-2614(93)85725-4

Bowyer P. and Crouch R., *An introduction to pure shift NMR*, Jeol USA Inc.

Castanãr L., Sistaré E., Virgili A., Williamson R. T. and Parella T. (2014) 'Suppression of phase and amplitude J(HH) modulations in HSQC experiments', *Magnetic Resonance in Chemistry,* 53, pp. 115-119. doi: 10.1002/mrc.4149

Eggenberger U., Pfändler P. and Bodenhausen G. (1988) 'Folding and pattern recognition in two-dimensional NMR spectra', *Journal of Magnetic Resonance',* 77, pp. 192-196. doi: 10.1016/0022-2364(88)90047-9

Emsley L. and Bodenhausen G. (1990) 'Phase shifts induced by transient Bloch-Siegert effects in NMR', *Chemical Physics Letters,* 168, 3, 4, pp.297-303. doi: 10.1016/0009-2614(90)85614-I

Farjon J., Milande C., Martineau E., Akoka S. and Giraudeau P. (2018) 'The FAQUIRE approach: FAst, QUantitative, hIghly Resolved and sEnsitivy Enhanced ^{1}H, ^{13}C data', *Analytical Chemistry,* 90, 1845-1851. doi: 10.1021/acs.analchem.7b03874

Freeman R. and Kupče E. (2003) 'New methods for fast multidimensional NMR', *Journal of Biomolecular NMR*, 27, pp. 101-113.

Frydman L., Scherf T. and Lupulescu A. (2002) 'The acquisition of multidimensional NMR spectra within a single scan', *Proceedings of the Natural Academy of Sciences of the USA*, 99, pp. 15858-15862. doi: 10.1073/pnas.252644399

Frydman L., Lupulescu A. and Scherf T. (2003) 'Principles and features of single-scan two-dimensional NMR spectroscopy', *Journal of the American Chemical Society*, 125, pp. 9204-9217. doi: 10.1021/ja030055b

Frydman L. (2006) 'Single-scan multidimensional NMR', *Comptes Rendus Chimie,* 9*.* doi: 10.1016/j.crci.2005.06.014

Frydman L. and Blazina D. (2007) 'Ultrafast two-dimensional nuclear magnetic resonance spectroscopy of hyperpolarized solutions', *Nature*, 3, pp. 415-419. doi: 10.1038/nphys597

Giraudeau P., Shrot Y. and Frydman L. (2009) 'Multiple ultrafast, broadband 2D NMR spectra of hyperpolarized natural products', *Journal of the American Chemical Society*, 131, pp.13902-13903. doi: 10.1021/ja905096f

Giraudeau P. and Akoka S. (2010) 'A new gradient-controlled method for improving the spectral width of ultrafast 2D NMR experiments', *Journal of Magnetic Resonance*, 205, pp. 171-176. doi: 10.1016/j.jmr.2010.05.002

Giraudeau P. and Akoka S. (2013) 'Fast and ultrafast quantitative 2D NMR: Vital tools for efficient metabolomics approaches', *Advances in Botanical Research*, 67, pp. 99-158. doi: 10.1016/B978-0-12-397922-3.00003-4

Hartmann S. R. and Hahn E. L. (1962) 'Nuclear double resonance in the rotating frame', *Physical Review*, 128, 5, pp. 2042-2053. doi: 10.1103/PhysRev.128.2042

Heikkinen S., Toikka M. M., Karhunen P. T. and Kilpeläinen I. A. (2003) 'Quantitative 2D HSQC (Q-HSQC) via suppression of J-dependence of polarisation transfer in NMR spectroscopy: application to wood lignin', *Journal of American Chemical Society,* 125, pp. 4362-4367. doi: 10.1021/ja029035k

Herrera A., Fernández-Valle E., Gutiérrez E. M., Martínez-Álvarez R., Molero D, Pardo Z. D. and Sáez E. (2010) '2D ultrafast HMBC: a valuable tool for monitoring organic reactions', *Organic Letters*, 12, 1, pp. 144-147. doi: 10.1021/ol902532f

Hu K., Westler W. M. and Markley J. L. (2011) 'Simultaneous quantification and identification of individual chemicals in metabolite mixtures by two-dimensional extrapolated time-zero 1H-13C HSQC ($HSQC_0$)', *Journal of the American Chemical Society*, 133, pp. 1662-1665. doi: 10.1021/ja1095304

Hu X. and Le T. H. (1996) 'Artifact reduction in EPI with phase-encoded reference scan', *Magnetic Resonance in Medicine*, 36, pp. 166-171. doi: 10.1002/mrm.1910360126

Jeannerat D. (2000) 'High resolution in the indirectly detected dimension exploiting the processing of folded spectra', *Magnetic Resonance in Chemistry'*, 38, pp. 415-422. doi: 10.1002/1097-458X(200006)38:6<415::AID-MRC665>3.0.CO;2-U

Jeannerat D. (2003) 'High resolution in heteronuclear ^{1}H-^{13}C NMR experiments by optimizing spectral aliasing with one-dimensional carbon data', *Magnetic Resonance in Chemistry,* 41, pp. 3-17. doi: 10.1002/mrc.1118

Kowalski B. R., Bender C. F. (1973) 'The Hadamard Transform and spectral analysis by pattern recognition', *Analytical Chemistry,* 45, 13, pp. 2234-2239. doi: 10.1021/ac60335a007

Kupče E. and Freeman R. (2003) 'Two-dimensional Hadamard spectroscopy', *Journal of Magnetic Resonance,* 162, pp. 300-310. doi: 10.1016/S1090-7807(02)00196-9

Kupče E. and Freeman R. (2007) 'Fast multidimensional NMR by polarisation sharing', *Magnetic Resonance in Chemistry*, 45, pp. 2-4. doi: 10.1002/mrc.1931

Laughton M. A. and Warne D. F. (2002), Chapter 11 (11.8.8.1) 'Electrical measurements', in *Electrical engineer's reference book, sixteenth edition*, Newnes ISBN: 978-0-7506-4637-6

Le Guennec A., Giraudeau P. and Caldarelli S. (2014) 'Evaluation of fast 2D NMR for metabolomics', *Analytical Chemistry*, 86, pp. 5946–5954. doi: 10.1021/ac500966e

*Kolkman M.*

Lescop E., Schanda P. and Brutscher B. (2007) 'A set of BEST triple-resonance experiments for time-optimized protein resonance assignment', *Journal of Magnetic Resonance,* 187, pp. 163-169. doi: 10.1016/j.jmr.2007.04.002

Lhoste C., Lorandel B., Praud C., Marchand A., Mishra R., Dey A., Bernard A., Dumez J-N. and Giraudeau P. (2022) 'Ultrafast 2D NMR for the analysis of complex mixtures', *Progress in Nuclear Magnetic Resonance Spectroscopy,* 130-131, pp. 1-46. doi: 10.1016/j.pnmrs.2022.01.002

Mankinen O., Zhivonitko V. V., Selent A., Mailhiot S., Komulainen S., Prisle N. L., Ahola S. and Telkki V-V. (2020) 'Ultrafast diffusion exchange nuclear magnetic resonance', *Nature Communications*, 11:3251. doi: 10.1038/s41467-020-17079-7

Mansfield P. (1977) 'Multi-planar image formation using spin echoes', *Journal of Physics C: Solid State Physics,* 10, 3, pp.55-58.

Marchand J., Martineau E., Guitton Y., Dervilly-Pinel G. and Giraudeau P. (2017) 'Multidimensional NMR approaches towards highly resolved and high-throughput quantitative metabolomics', *Current opinion in Biotechnology*, 43, pp. 49-55. doi: 10.1016/j.copbio.2016.08.004

Markley J. L., Brüschweiler R., Edison A. S., Eghbalnia H. R., Powers R., Raftery D. and Wishart D. S. (2017) 'The future of NMR-based metabolomics', *Current Opinion in Biotechnology,* 43, pp. 34-40. doi: 10.1016/j.copbio.2016.08.001

Marshall A. G. and Comisarow M. B. (1975) 'Fourier and Hadamard transform methods in Spectroscopy', *Analytical Chemistry,* 47, 4, pp. 491-504. doi: 10.1021/ac60354a028

Martineau E., Dumez J-N. and Giraudeau P. (2020) 'Fast quantitative 2D NMR for metabolomics and lipidomics: a tutorial'*, Magnetic Resonance in Chemistry*, 58, pp. 390-403. doi: 10.1002/mrc.4899

Mauve C., Khlifi S., Gilard F., Mouille G. and Farjon J. (2016) 'Sensitive, highly resolved, and quantitative $^1$H-$^{13}$C NMR data in one go for tracking metabolites in vegetal extracts', *Chemical Communications,* 52, pp. 6142-6145. doi: 10.1039/c6cc01783e

Mishkovsky M. and Frydman L. (2008) 'Progress in hyperpolarized ultrafast 2D NMR spectroscopy', *ChemPhysChem*, 9, pp. 2340-2348. doi: 10.1002/cphc.200800461

Mueller L. (2008) 'Alternate HMQC experiments for recording HN and HC-correlation spectra in proteins at high throughput', *Journal of Biomolecular NMR',* 42, pp. 129-137. doi: 10.1007/s10858-008-9270-2

Ndukwe I. E., Shchukina A., Kazimierczuk K. and Butts C. P. (2016) 'Rapid and safe ASAP acquisition with EXACT NMR', *Royal Society of Chemistry,* 52, pp. 12769-12772. doi: 10.1039/c6cc07140f

Ordidge R. J. and Mansfield P. (1981) 'Rapid biomedical imaging by NMR', *British Journal of Radiology,* 54, pp. 850-855. doi: 10.1259/0007-1285-54-646-850

Palmer M. R., Suiter C. L., Henry G. E., Rovnyak J., Hoch J. C., Polenova T. and Rovnyak D. (2015) 'Sensitivity of nonuniform sampling NMR', *Journal of Physical Chemistry B*, 119, pp. 6502-6515. doi: 10.1021/jp5126415

Pelupessy P. (2003) 'Adiabatic single two-dimensional NMR spectroscopy', *Journal of the American Chemical Society,* 125, pp. 12345-12350. doi: 10.1021/ja034958g

Posse S. and Aue W. P. (1990) 'Susceptibility artifacts in spin-echo and gradient-echo imaging', *Journal of Magnetic Resonance*, 88, pp. 473-492. doi: 10.1016/0022-2364(90)90282-e

Queiroz L. H. K. Junior, Ferreira A. G. and Giraudeau P. (2013) 'Optimization and practical implementation of ultrafast 2D NMR experiments', *Química Nova*, 36(4), pp. 577-581

Reo N. V. (2002) 'NMR-based metabolomics', *Drug and Chemical Toxicology,* 25, 4, pp. 375-382. doi: 10.1081/DCT-120014789

Rosman K. J. R. and Taylor P. D. P. (1999) « Report of the IUPAC subcommittee for isotopic abundance measurements », *Pure and Applied Chemistry*, 71, pp. 1593-1607.

Ross A., Salzmann M. and Senn H. (1997) 'Fast-HMQC using Ernst angle pulses: An efficient tool for screening of ligand binding to target proteins', *Journal of Biomolecular NMR,* 10, pp. 389-396. doi: 10.1023/A:1018361214472

Saphira B. and Frydman L. (2003) 'Arrayed acquisition of 2D exchange NMR spectra within a single scan experiment', *Journal of Magnetic Resonance*, 165, pp. 320-324. doi: 10.1016/j.jmr.2003.09.006

Schanda P. and Brutscher B. (2005) 'Very fast two-dimensional NMR spectroscopy for real-time investigation of dynamic events in proteins on the time scale of seconds', *Journal of American Society,* 127, pp 8014-8015. doi: 10.1021/ja051306e

Schanda P., Hupče E. and Brutscher B. (2005) 'SOFAST-HMQC experiments for recording two-dimensional heteronuclear correlation spectra of proteins within a few seconds', *Journal of Biomolecular NMR,* 33, pp. 199-211. doi: 10.1007/s10858-005-4425-x

Schanda P., Van Melckebeke H. and Brutscher B. (2006) 'Speeding up three-dimensional protein NMR experiments to a few minutes', *Journal of American Society,* 128, pp. 9042-9043. doi: 10.1021/ja062025p

Schulze-Sünninghausen D., Becker J. and Luy B. (2014) 'Rapid heteronuclear single quantum correlation NMR spectra at natural abundance', *Journal of the American Society',* 136, pp. 1242-1245. doi: 10.1021/ja411588d

Shrot Y. and Frydman L. (2003) 'Single-scan NMR spectroscopy at arbitrary dimensions', *Journal of the American Chemical Society*, 125, pp. 11385-11396. doi: 10.1021/ja0350785

Shrot Y., Saphira B. and Frydman L. (2004) 'Ultrafast 2D NMR spectroscopy using a continuous spatial encoding of the spin interactions', *Journal of Magnetic Resonance*, 171, pp. 163-170. doi: 10.1016/j.jmr.2004.08.001

Tal A., Saphira B. and Frydman L. (2009) 'Single-scan 2D Hadamard NMR spectroscopy', *Angewandte Chemie*, 121, pp. 2770-2774. doi: 10.1002/ange.200805612

Ugurbil K., Garwood M., Rath A. R. and Bendall R. (1988) 'Amplitude- & frequency/phase modulated refocusing pulses that induce plane rotations even in the presence of inhomogeneous B1 fields', *Journal of Magnetic Resonance*, 78, pp. 472-497.

Vitorge B., Bodenhausen G. and Pelupessy P. (2010) 'Speeding up nuclear magnetic resonance spectroscopy by the use of SMAll Recovery Times – SMART NMR', *Journal of Magnetic Resonance,* 207, pp. 149-152. doi: 10.1016/j.jmr.2010.07.017

Weitzel A., Samol C., Oefner P. J. and Gronwald W. (2020) 'Robust metabolite quantification from J-compensated 2D $^1$H-$^{13}$C-HSQC experiments', *Metabolites,* 10, 449. doi: 10.3390/metabo10110449

Welije A. M., Newton J., Mercier P., Carlson E. and Slupsky C. M. (2006) 'Targeted profiling: Quantitative analysis of $^1$H NMR metabolomics data', *Analytical Chemistry,* 78, 13, pp. 4430-4442. doi: 10.1021/ac060209g

Wishart D. (2008) 'Quantitative metabolomics using NMR', *Trends in analytical chemistry*, 27(3). doi: 10.1016/j.trac.2007.12.001

Wishart D. S. (2019) 'NMR metabolomics: A look ahead', *Journal of Magnetic Resonance,* 306, pp. 155-161. doi: 10.1016/j.jmr.2019.07.013

Yao S., Meikle T. G., Sethi A., Separovic F., Babon J. J. and Keizer D. W. (2018) 'Measuring translational diffusion of N-enriched biomolecules in complex solutions with a simplified H-N HMQC-filtered BEST sequence', *European Biophysics Journal,* ?? doi: 10.1007/s00249-018-1311-5

Zambrello M. A., Schuyler A. D., Maciejewski M. W., Delaglio F., Bezsonova I. and Hoch J. C. (2018) 'Nonuniform sampling in multidimensional NMR for improving spectral sensitivity', *Methods.* doi: 10.1016/j.ymeth.2018.03.001

# IX-  Annexes

### a. Experiments

Conducted experiments relevant for the hereby document are summarized in the following tables. 1k stands for 1024 and 2k for 2048. NUS experiments in table A1 were performed on a THA 22mM in CDCl$_3$ sample. COSY experiments in table A2 were performed with NUS on a sucrose 2mM in water sample.

| Experiment | NUS percentage | N$_2$ | N$_1$ | Number of scans and time | | | | | Figures |
|---|---|---|---|---|---|---|---|---|---|
| COSY | / | 2k | 512 | N$_s$ = 1 14 min 12 s | | | | | 10, 13, 14, 16, A1, A2, A12, A13, A20 |
| | 50 | 2k | 512 | N$_s$ = 1 7 min 10 s | N$_s$ = 2 14 min 11 s | | | | |
| | 25 | 2k | 512 | N$_s$ = 1 3 min 39 s | N$_s$ = 2 7 min 10 s | N$_s$ = 4 14 min 11 s | | | |
| | | | 1k | N$_s$ = 1 7 min 17 s | N$_s$ = 2 14 min 26 s | | | | |
| | 10 | 2k | 512 | N$_s$ = 1 1 min 32 s | N$_s$ = 2 2 min 56 s | N$_s$ = 4 5 min 44 s | | | |
| | | | 1k | N$_s$ = 1 2 min 59 s | N$_s$ = 2 5 min 49 s | N$_s$ = 4 11 min 29 s | | | |
| HSQC | / | 2k | 512 | N$_s$ = 1 14 min 44 s | | | | | 12, 17, A9-A11, A17-A19, A21 |
| | 50 | 2k | 512 | N$_s$ = 1 7 min 49 s | N$_s$ = 2 14 min 44 s | | | | |
| | 25 | 2k | 512 | N$_s$ = 1 4 min 21 s | N$_s$ = 2 7 min 49 s | N$_s$ = 4 14 min 44 s | | | |
| | | | 1k | N$_s$ = 1 7 min 50 s | N$_s$ = 2 14 min 46 s | | | | |
| | 10 | 2k | 512 | N$_s$ = 1 2 min 18 s | N$_s$ = 2 3 min 42 s | N$_s$ = 4 6 min 31 s | | | |
| | | | 1k | N$_s$ = 1 3 min 39 s | N$_s$ = 2 6 min 25 s | N$_s$ = 4 11 min 57 s | | | |
| HMBC | / | 2k | 64 | | | | | N$_s$ = 16 29 min 07 s | 11-15, 18, A3-A8, A14-A16, A21 |
| | | | 128 | | | | N$_s$ = 8 29 min 08 s | | |
| | | | 512 | N$_s$ = 1 14 min 49 s | | | | | |
| | 50 | 2k | 512 | N$_s$ = 1 7 min 39 s | N$_s$ = 2 14 min 49 s | | | | |
| | 25 | 2k | 512 | N$_s$ = 1 4 min 04 s | N$_s$ = 2 7 min 39 s | N$_s$ = 4 14 min 49 s | | | |
| | | | 1k | N$_s$ = 1 7 min 40 s | N$_s$ = 2 14 min 50 s | | | | |
| | 10 | 2k | 512 | N$_s$ = 1 1 min 56 s | N$_s$ = 2 3 min 23 s | N$_s$ = 4 6 min 18 s | N$_s$ = 8 12 min 08 s | | |
| | | | 1k | N$_s$ = 1 3 min 20 s | N$_s$ = 2 6 min 12 s | N$_s$ = 4 11 min 55 s | | | |

*Table A1 - Experiments conducted on a THA 22mM in CDCl$_3$ sample. Various experiment types, with different parameters (NUS percentage, resolution and number of scans) and their durations are listed. Last column indicates the figure to which the experiment is referred.*

| Experiment | NUS percentage | $N_2$ | $N_1$ | Number of scans and time | Figures |
|---|---|---|---|---|---|
| COSY | / | 4k | 512 | $N_s = 1$<br>15 min 23 s | 19 |
|  | 50 |  |  | $N_s = 1$<br>7 min 44 s |  |
|  | 25 |  |  | $N_s = 1$<br>3 min 55 s |  |
|  | 10 |  |  | $N_s = 1$<br>1 min 38 s |  |
|  | 5 |  |  | $N_s = 1$<br>53 s |  |

*Table A2 – COSY experiments conducted on a sucrose 2mM in water sample. Their various parameters (NUS percentage, resolution and number of scans) and their durations are listed. Last column indicates the figure to which the experiment is referred.*

Table A3 presents the UFCOSY experiments carried out on either an ethanol 1.71M in $D_2O$ and a THA 22mM in $CDCl_3$.

| Sample Frequency offset Excitation gradient Chirp pulse power | IN | AL | D10 | IN and time | | | | | Figures |
|---|---|---|---|---|---|---|---|---|---|
| EtOH 10% in $D_2O$<br>O1P = 3 ppm<br>$G_e$ = 3.5%<br>CP = 17 dB | 128k | 128 | 10 µs | IN = 1<br>14 s | IN= 2<br>21 s |  |  |  | Table 2 |
|  |  | 64 | 10 µs |  | IN = 2<br>21 s | IN = 4<br>35 s | IN = 8<br>64 s |  |  |
|  |  | 32 | 10 µs |  |  | IN = 4<br>35 s | IN = 8<br>64 s | IN = 16<br>121 s |  |

| Sample | N | IN | AL | D10 | $N_s$ and time | | | | Figures |
|---|---|---|---|---|---|---|---|---|---|
| THA 22mM in $CDCl_3$<br>O1P = 4 ppm<br>$G_e$ = 3.5%<br>CP = 19 dB | 128k | 8 | 64 | 10 µs | $N_s = 1$<br>64 s |  |  |  | 28 |
|  |  |  |  | 15 ms | $N_s = 1$<br>64 s |  |  |  |  |
|  |  |  |  | 30 ms | $N_s = 1$<br>64 s | $N_s = 2$<br>122 s |  |  | 29-30 |
|  |  |  |  | 35 ms | $N_s = 1$<br>64 s | $N_s = 2$<br>122 s |  |  |  |
|  |  |  |  | 40 ms | $N_s = 1$<br>64 s |  |  |  |  |

*Table A3 - UFCOSY experiments conducted on two types of samples: ethanol 1.71M in $D_2O$, THA 22mM in $CDCl_3$. Parameters and experiment time are indicated. Last column shows the figure to which the experiment is related.*

Table A4 lists the PRUFCOSY experiments conducted on a sucrose 2 mM in water or an metabolites sample (Alanine 32.3 mM, 3,4-dihydroxyphenylalanine 30.4 mM, sucrose 11.7 mM and 2-ethylhexan-1-ol 55.7 mM.

| Sample | N | IN | AL | D10 | $N_s$ and time | Presaturation power | Figures |
|---|---|---|---|---|---|---|---|
| Sucrose 2mM in water O1P = 4 ppm $G_e$ = 3.5% CP = 12 dB | 128k | 8 | 64 | 10 µs | $N_s$ = 1 71 s | 46.27 dB | |
| | | | | | | 40 dB | |
| | | | | | | 35 dB | |
| | | | | | | 30 dB | |
| | | | | | | 28 dB | |
| | | | | | | 25 dB | 31 |

| Sample | N | IN | AL | D10 | Time | Added amount water | Figures |
|---|---|---|---|---|---|---|---|
| Metabolites in $D_2O$ + $H_2O$ O1P = 4 ppm $G_e$ = 3.5% CP = 12 dB | 128k | 8 | 64 | 10 µs | $N_s$ = 1 71 s | / | |
| | | | | | | + 1 µL | |
| | | | | | | + 5 µL | |
| | | | | | | + 10 µL | 33 |
| | | | | | | + 15 µL | |
| | | | | | | + 25 µL | |
| | | | | | | + 35 µL | |
| | | | | | | + 50 µL | |
| | | | | | | + 70 µL | 33 |
| | | | | | | + 130 µL | 33 |
| | | | | | | + 200 µL | 33 & 34 |

*Table A4 - PRUFCOSY experiments conducted on two types of samples: sucrose 2mM in water and metabolites (alanine, 3,4-dihydroxyphenylalanine, sucreose and 2-ethylhexan-1-ol) in $D_2O$. Parameters and experiment time are indicated. Last column shows the figure to which the experiment is related.*

Table A5 lists conventional COSY-experiments that were conducted to make comparisons with the UF experiments.

| Sample | $N_2$ | $N_1$ | Number of scans and time | | Figures |
|---|---|---|---|---|---|
| EtOH 10% in $D_2O$ | 2k | 32 | | $N_s$ = 2 1 min 52 s | |
| | | 64 | $N_s$ = 1 1 min 52 s | | 27 |
| THA 22mM in $CDCl_3$ | 2k | 512 | $N_s$ = 1 14 min 12 s | | 30 |
| Metabolites in $D_2O$ + $H_2O$ | 4k | 1k | | $N_s$ = 2 1h 02 min 08 s | 32 & 34 |

*Table A5 - Conventional experiments executed to be compared with the UF experiments. Last column indicates the figure to which the experiment is referred.*

b. <u>NUS results</u>

Here below are the superpositions of slices used to compare COSY, HSQC and HMBC experiments performed with NUS and that are not displayed in the here-above document. Figures A1-A11 show superpositions of slices extracted from spectra acquired with different NUS percentages and for all three experiment types: COSY (*Figures A1-A2*), HMBC (*Figures A3-A8*) and HSQC (*Figures A9-A11*). HMBC superpositions go by pairs: a superposition and its zoom on the noise level. HSQC superpositions are presented differently from the others (COSY and HMBC). Due to the low noise level, the superposed slices are closer to one another and horizontally shifted to avoid the superposition of the signals. This makes it possible to zoom more.
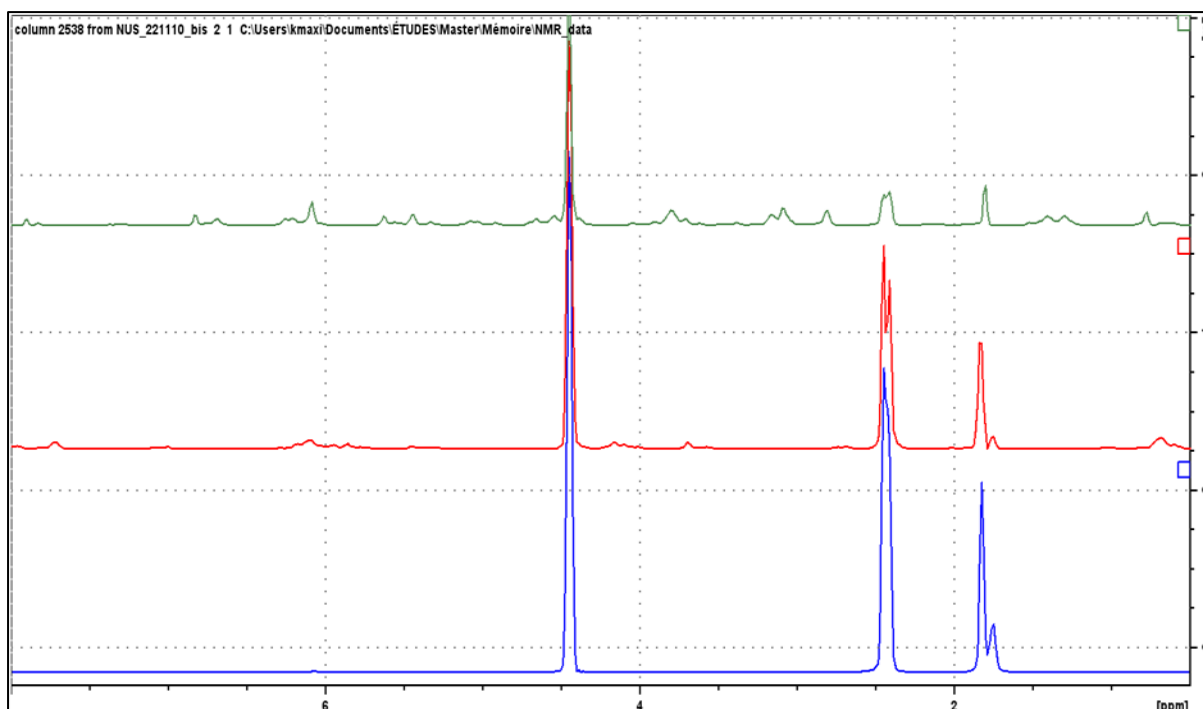
*Figure 19 - Superposition of the 4.45 ppm columns extracted from COSY spectra of a THA sample in CDCl₃ acquired without NUS (blue), with NUS 25% (red) or NUS 10% (green), all acquired with one scan, a resolution of 2k*512. These experiments lasted respectively 14 min 12s, 3 min 39s and 1 min 32s.*
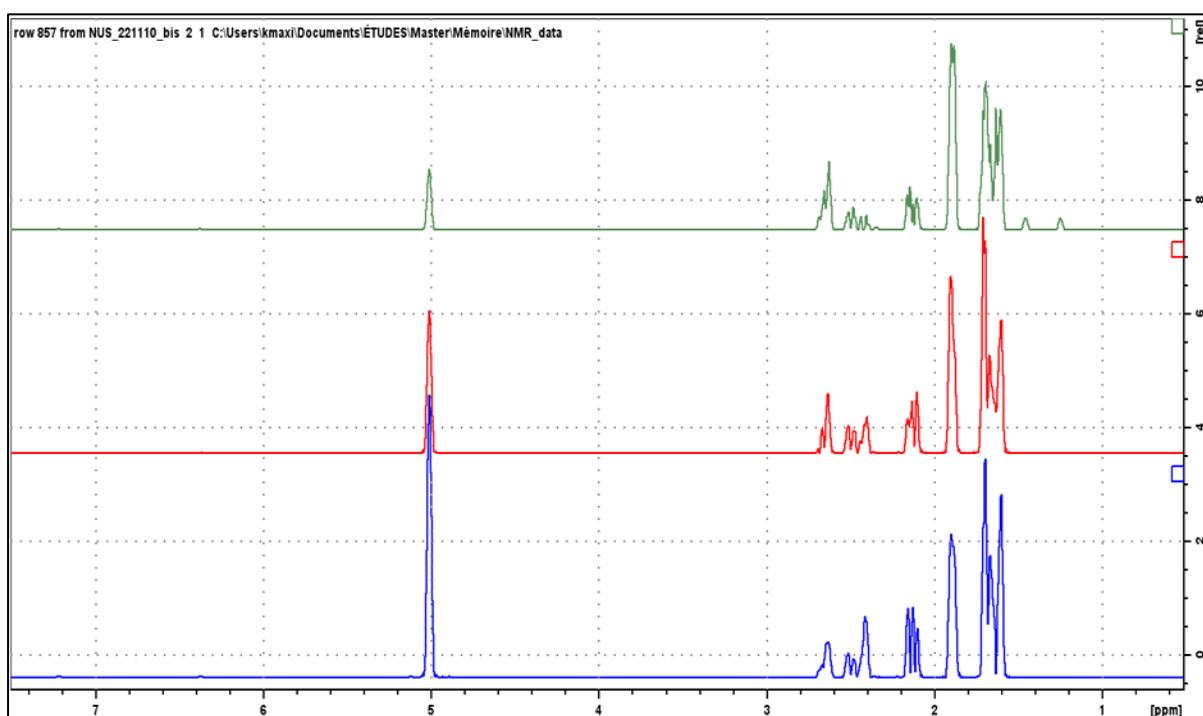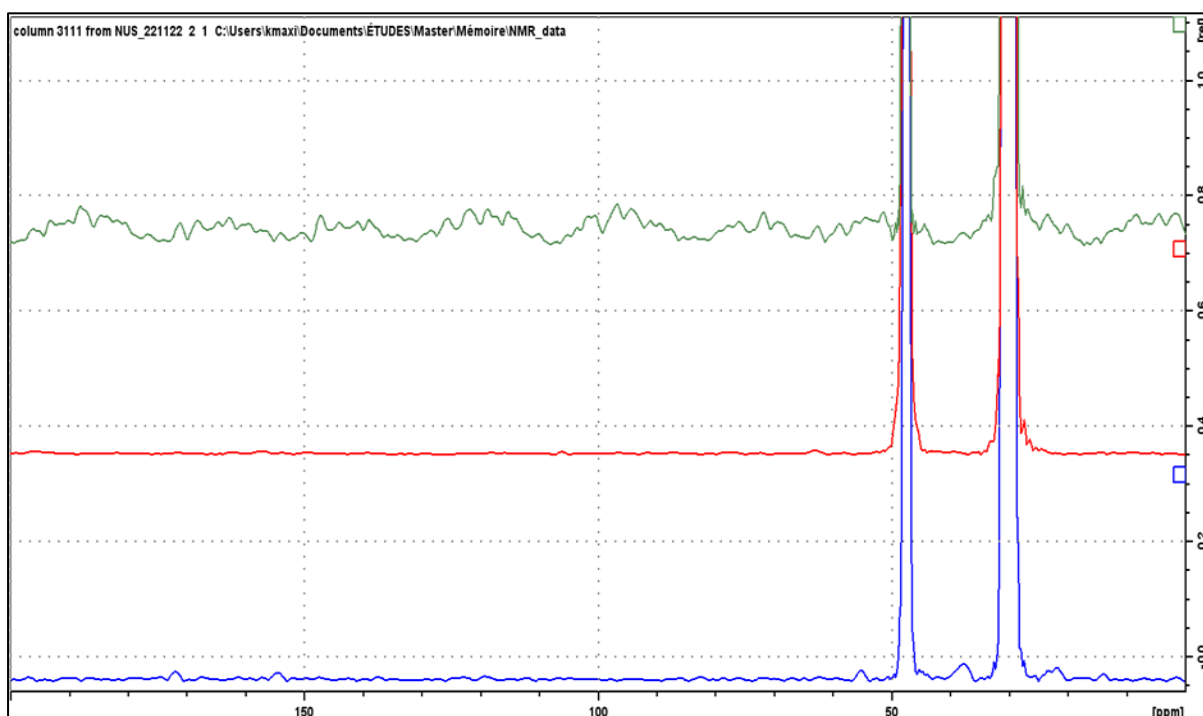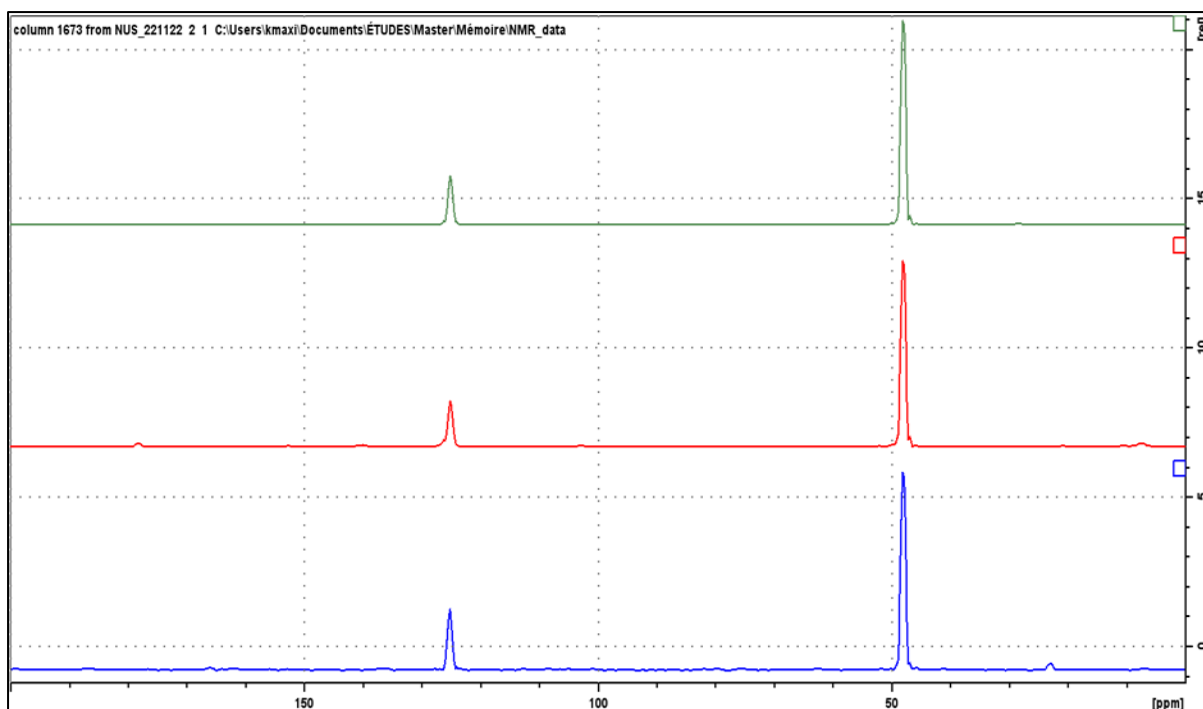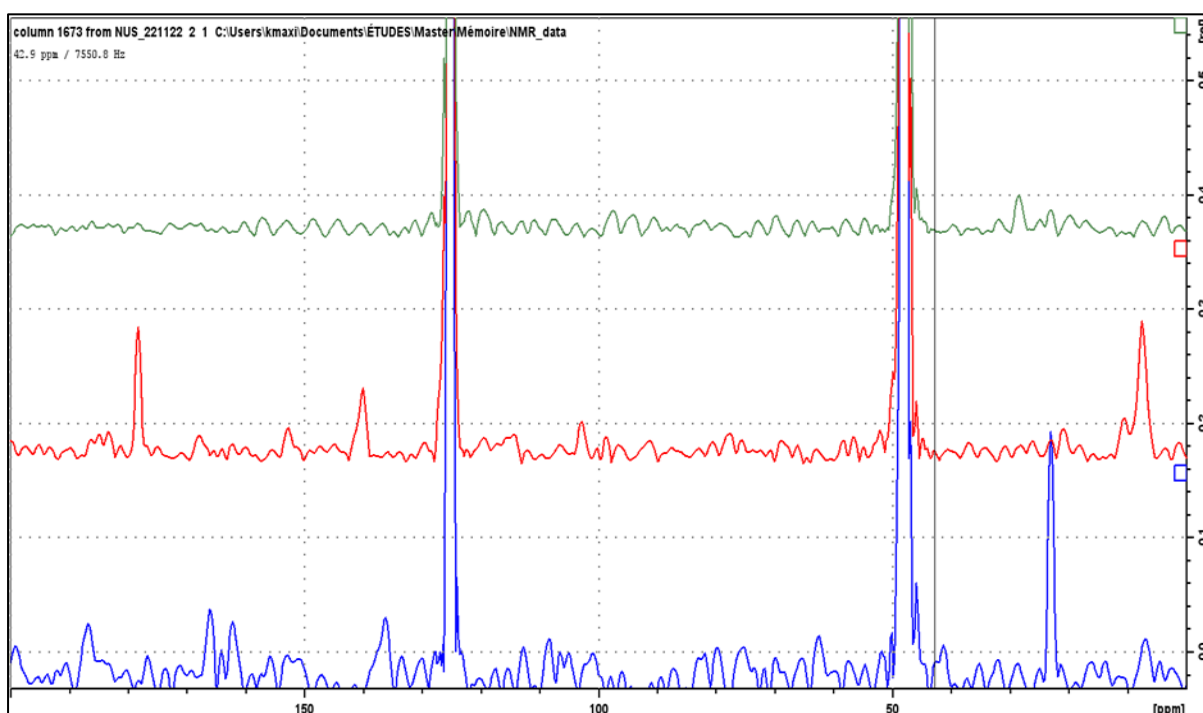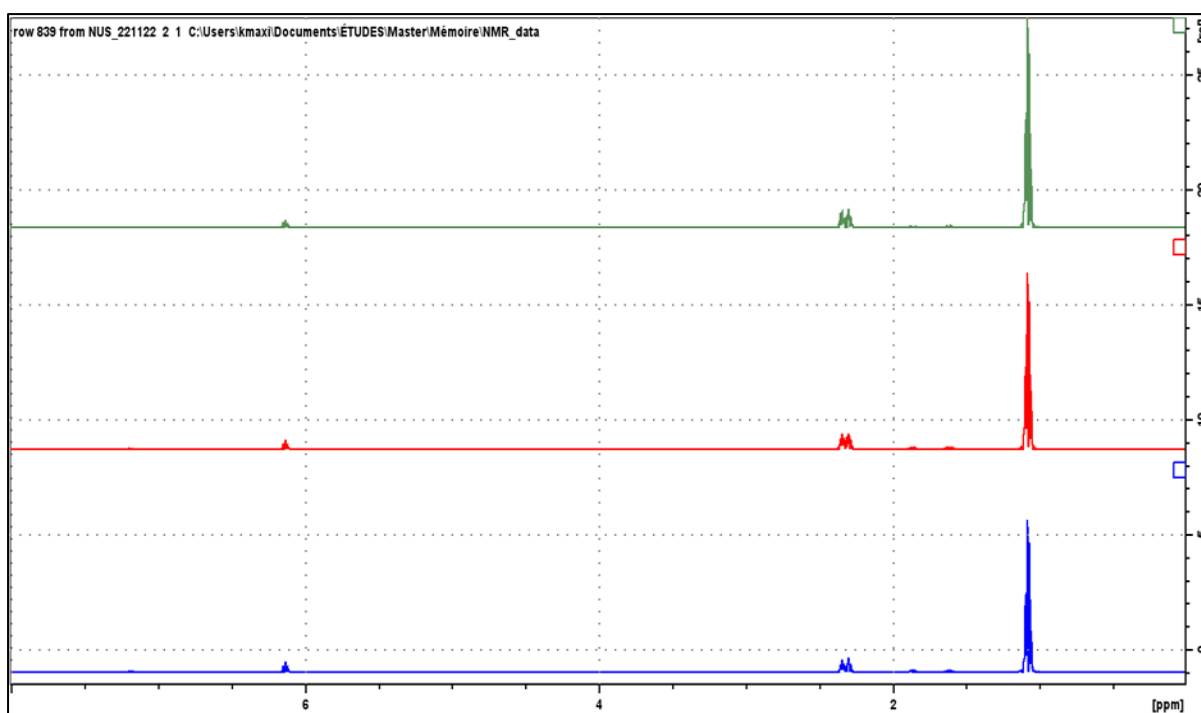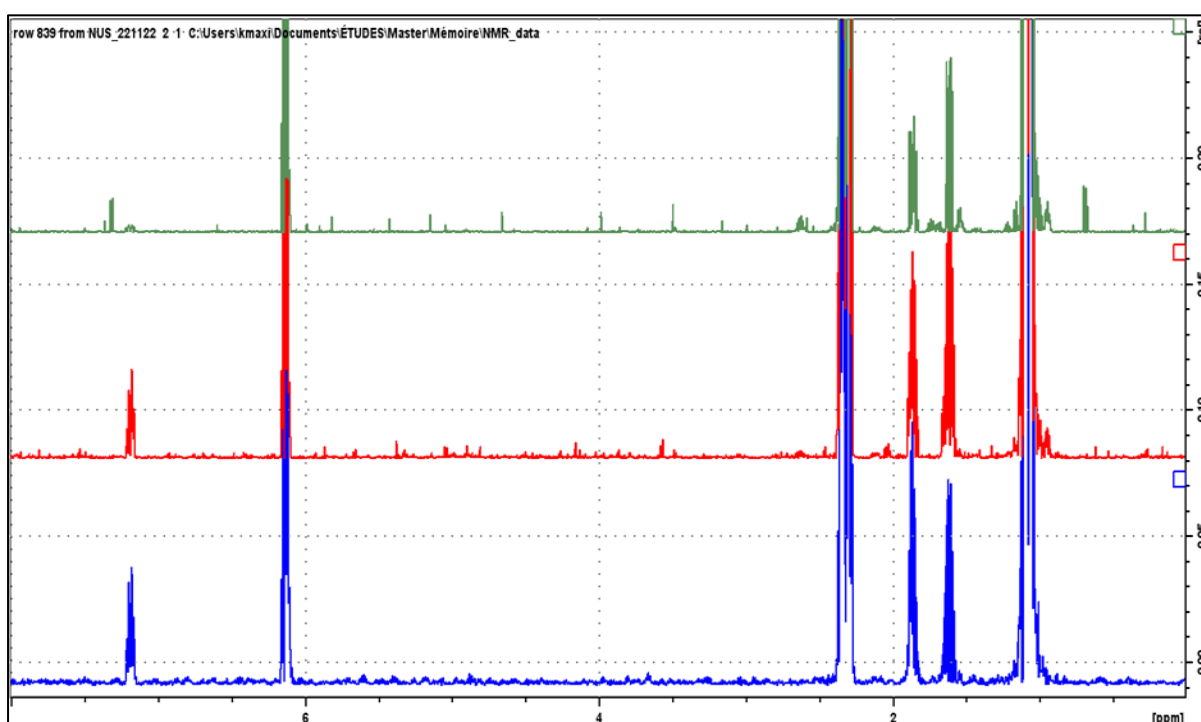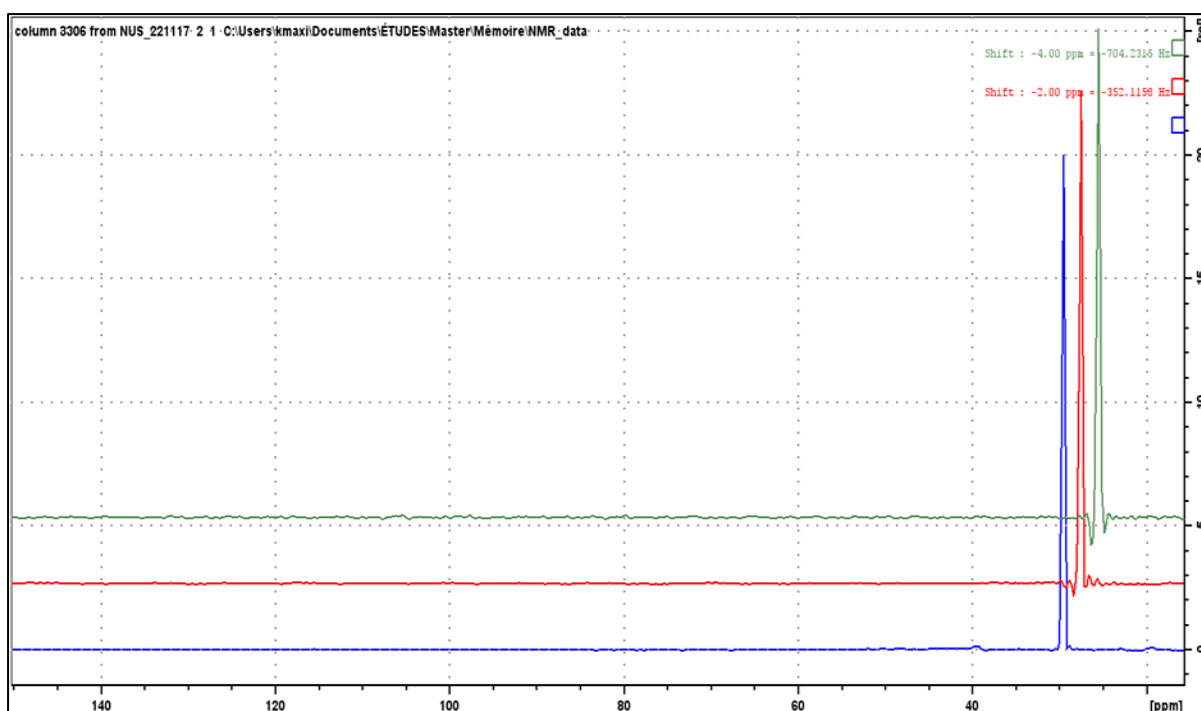


*Figure A2 - Superposition of the 1.65 ppm rows extracted from COSY spectra of a THA sample in CDCl₃ acquired without NUS (blue), with NUS 25% (red) or NUS 10% (green), all acquired with one scan, a resolution of 2k*512. These experiments lasted respectively 14 min 12s, 3 min 39s and 1 min 32s.*
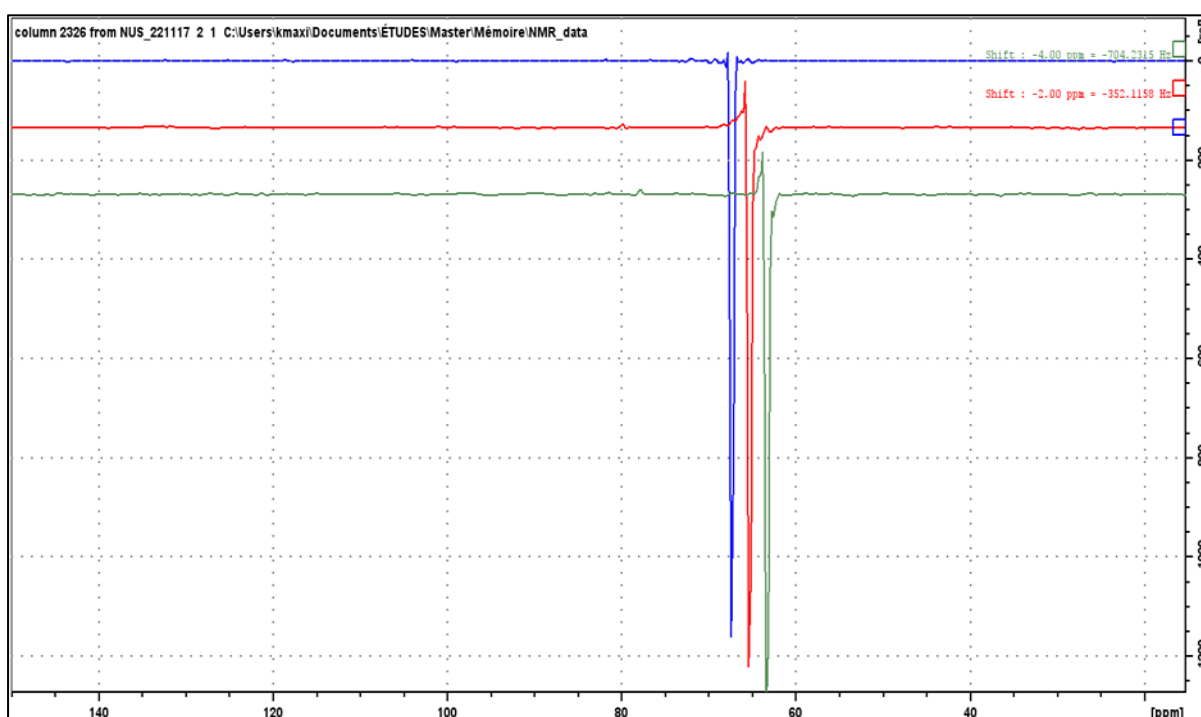
*Kolkman M.*
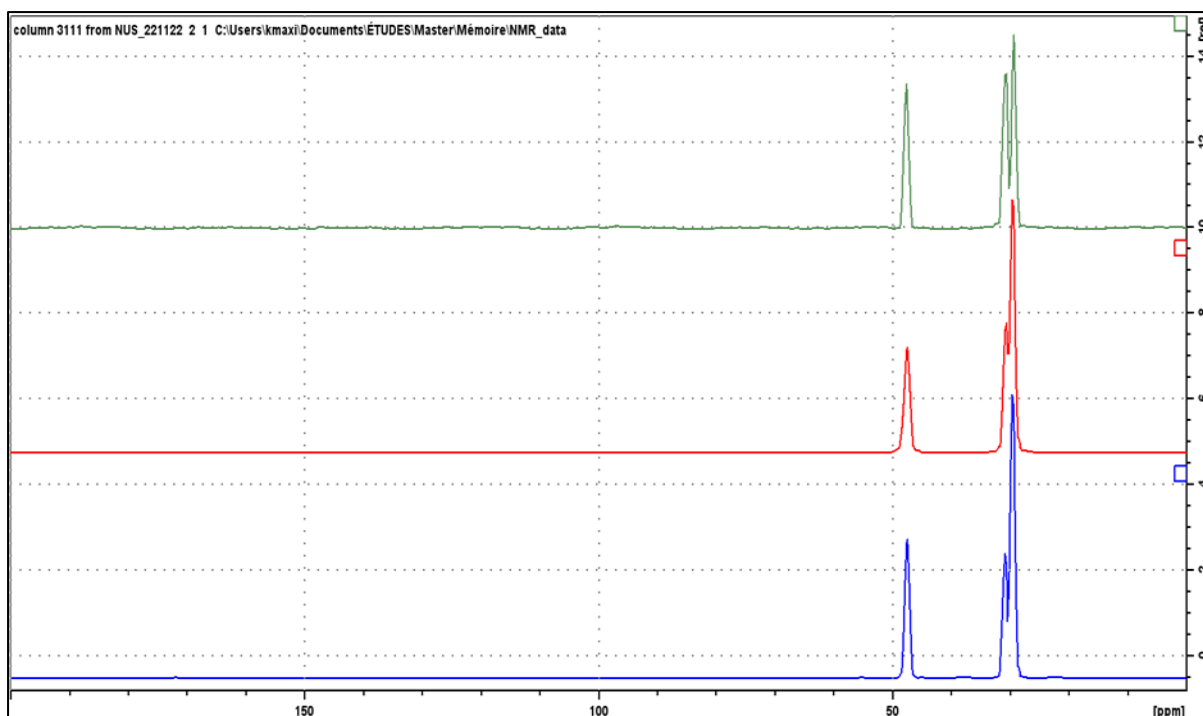
*Figure 20 - Superposition of the 1.09 ppm columns extracted from HMBC spectra of a THA sample in CDCl₃ acquired without NUS (blue), with NUS 25% (red) or NUS 10% (green), all acquired with one scan, a resolution of 2k\*512. These experiments lasted respectively 14 min 49s, 4 min 04s and 1 min 56s.*



*Figure A4 – Zoom of the superposition of the 1.09 ppm columns extracted from HMBC spectra of a THA sample in CDCl₃ acquired without NUS (blue), with NUS 25% (red) or NUS 10% (green), all acquired with one scan, a resolution of 2k\*512. These experiments lasted respectively 14 min 49s, 4 min 04s and 1 min 56s.*
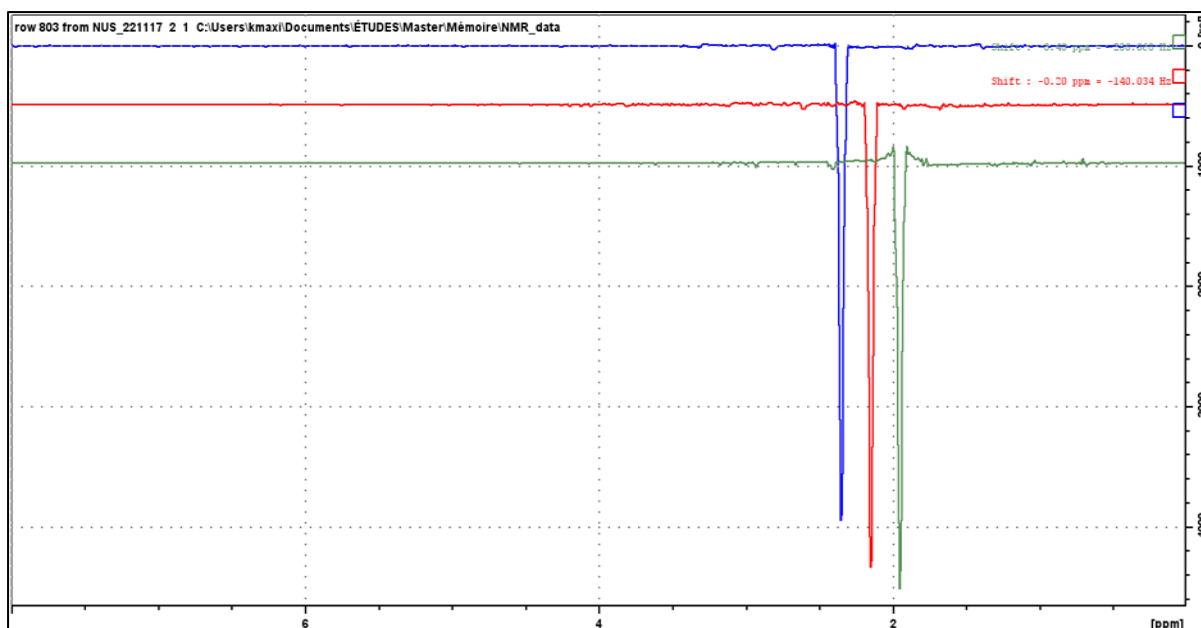
*Figure A5 - Superposition of the 6.35 ppm columns extracted from HMBC spectra of a THA sample in CDCl₃ acquired without NUS (blue), with NUS 25% (red) or NUS 10% (green), all acquired with one scan, a resolution of 2k\*512. These experiments lasted respectively 14 min 49s, 4 min 04s and 1 min 56s.*



*Figure A6 – Zoom of the superposition of the 6.35 ppm columns extracted from HMBC spectra of a THA sample in CDCl₃ acquired without NUS (blue), with NUS 25% (red) or NUS 10% (green), all acquired with one scan, a resolution of 2k\*512. These experiments lasted respectively 14 min 49s, 4 min 04s and 1 min 56s.*

*Figure A7 - Superposition of the 30.9 ppm rows extracted from HMBC spectra of a THA sample in CDCl₃ acquired without NUS (blue), with NUS 25% (red) or NUS 10% (green), all acquired with one scan, a resolution of 2k\*512. These experiments lasted respectively 14 min 49s, 4 min 04s and 1 min 56s.*



*Figure A8 – Zoom of the superposition of the 30.9 ppm rows extracted from HMBC spectra of a THA sample in CDCl₃ acquired without NUS (blue), with NUS 25% (red) or NUS 10% (green), all acquired with one scan, a resolution of 2k\*512. These experiments lasted respectively 14 min 49s, 4 min 04s and 1 min 56s.*

*Figure A9 - Superposition of the 1.09 ppm columns extracted from HSQC spectra of a THA sample in CDCl₃ acquired without NUS (blue), with NUS 25% (red) or NUS 10% (green), all acquired with one scan, a resolution of 2k*512. These experiments lasted respectively 14 min 44s, 4 min 21s and 2 min 18s.*



*Figure A10 - Superposition of the 4.9 ppm columns extracted from HSQC spectra of a THA sample in CDCl₃ acquired without NUS (blue), with NUS 25% (red) or NUS 10% (green), all acquired with one scan, a resolution of 2k*512. These experiments lasted respectively 14 min 44s, 4 min 21s and 2 min 18s.*

*Figure A11 - Superposition of the 47.7 ppm rows extracted from HSQC spectra of a THA sample in CDCl₃ acquired without NUS (blue), with NUS 25% (red) or NUS 10% (green), all acquired with one scan, a resolution of 2k\*512. These experiments lasted respectively 14 min 44s, 4 min 21s and 2 min 18s.*

Figures A12-A19 displays superpositions of slices extracted from spectra acquired with:

- No NUS, $N_s = 1$, $N_2*N_1 = 2k*512$        in blue (reference)
- NUS 10%, $N_s = 1$, $N_2*N_1 = 2k*512$      in red
- NUS 10%, $N_s = 2$, $N_2*N_1 = 2k*512$      in green
- NUS 10%, $N_s = 1$, $N_2*N_1 = 2k*1k$       in purple



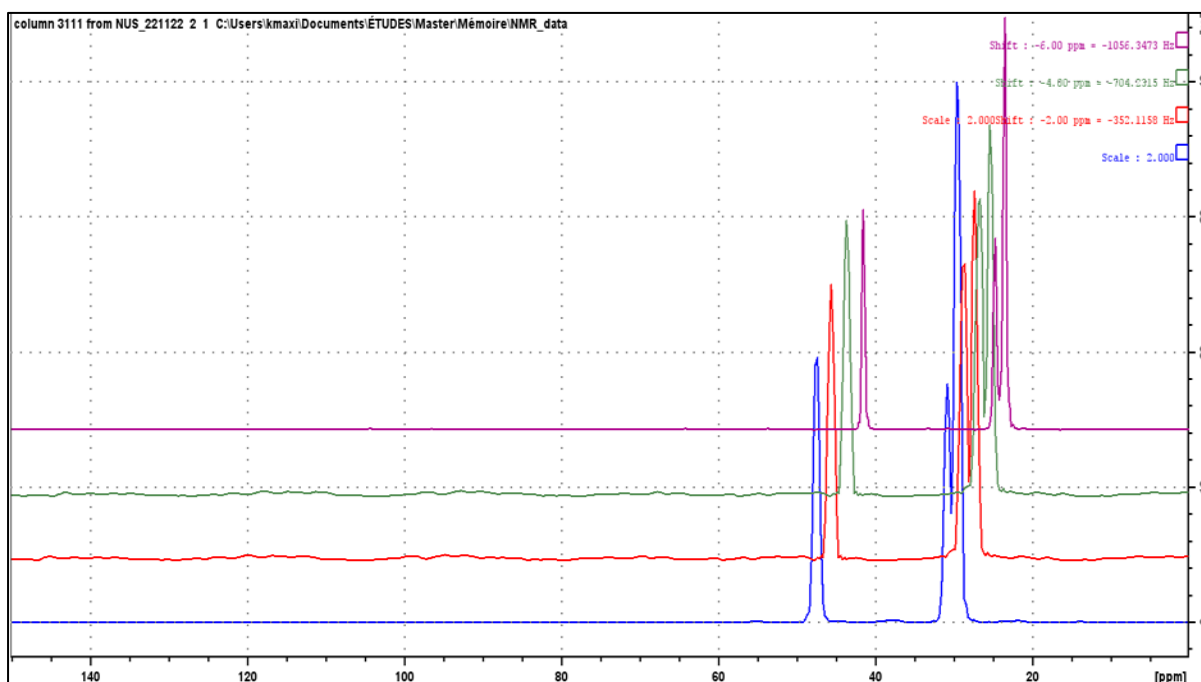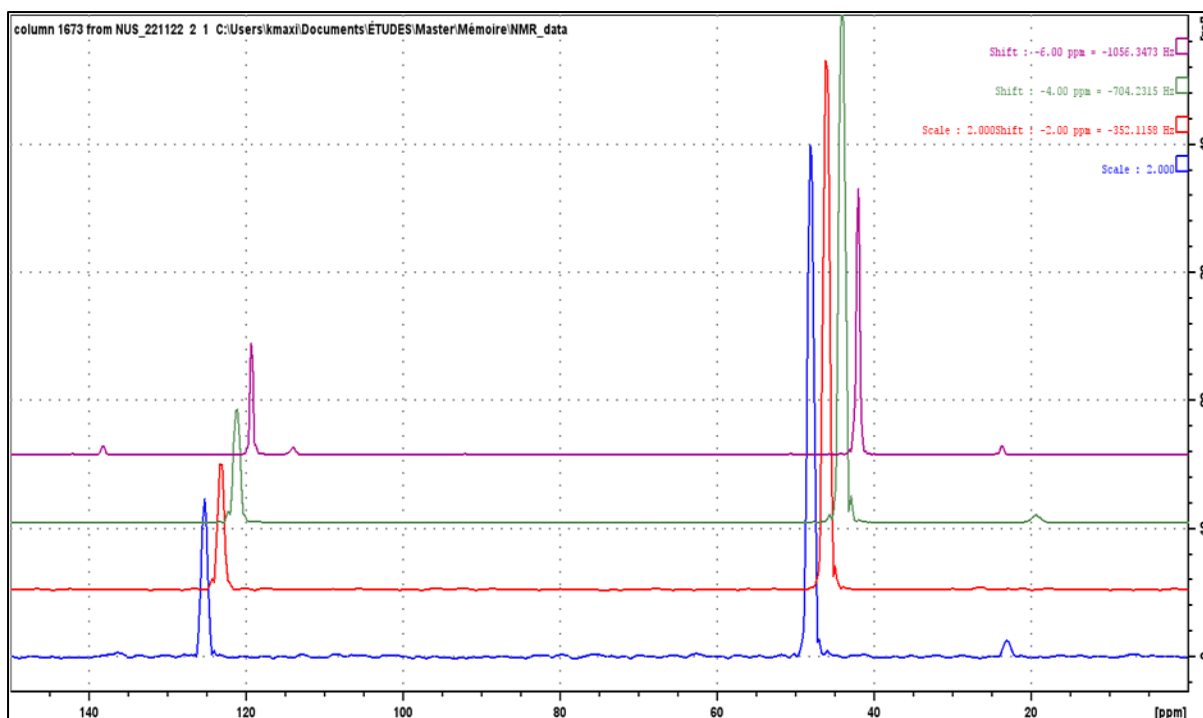*Figure A12 - Superposition of the 1.65 ppm columns extracted from COSY spectra of a THA sample in CDCl₃ acquired with: no NUS, 1 scan, $N_2*N_1 = 2k*512$ in 14 min 1s (blue); NUS 10%, 1 scans, $N_2*N_1 = 2k*512$ in 1 min 32s (red); NUS 10%, 2 scans, $N_2*N_1$ in 2 min 56s (green); and NUS 10%, 1 scan, $N_2*N_1 = 2k*1k$ in 2 min 59s (purple).*

*Kolkman M.*
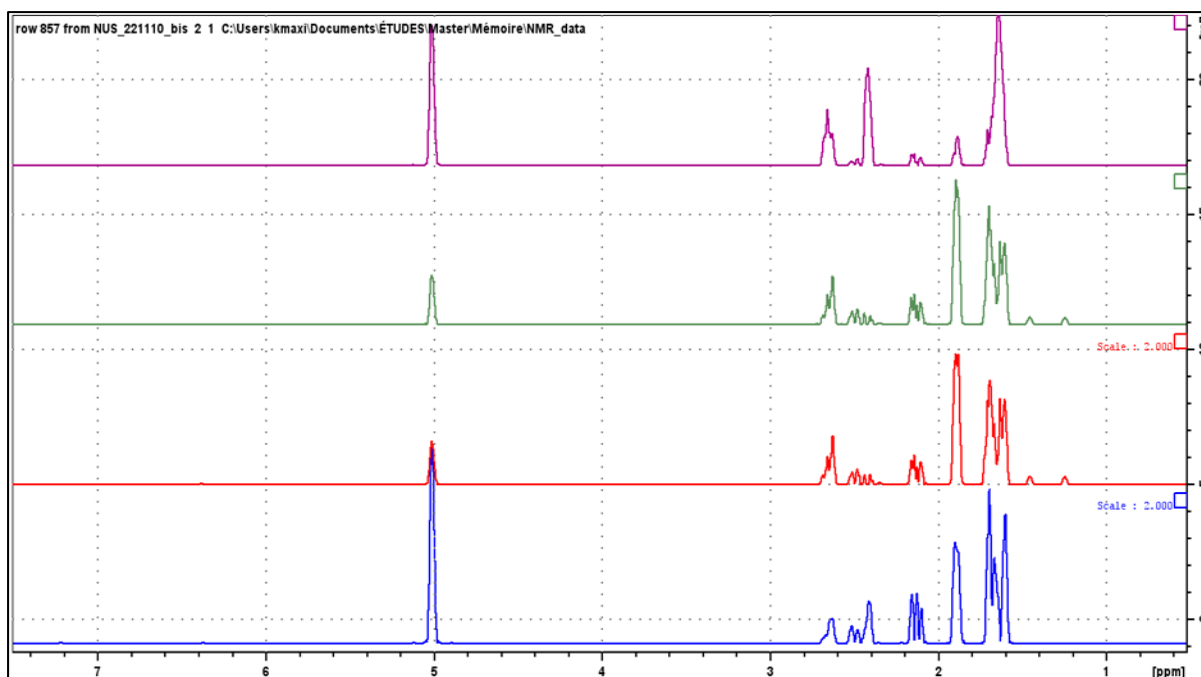
*Figure 21 - Superposition of the 1.65 ppm rows extracted from COSY spectra of a THA sample in CDCl₃ acquired with: no NUS, 1 scan, $N_2*N_1$ = 2k*512 in 14 min 1s (blue); NUS 10%, 1 scans, $N_2*N_1$ = 2k*512 in 1 min 32s (red); NUS 10%, 2 scans, $N_2*N_1$ in 2 min 56s (green); and NUS 10%, 1 scan, $N_2*N_1$ = 2k*1k in 2 min 59s (purple).*

Figures A14-A19 (HMBC-HSQC) are presented a little different than the COSY superpositions (*Figures A12-A13*). The slices are closer and are horizontally shifted to avoid confusion with overlapping peaks.



*Figure 22 - Superposition of the 1.09 ppm columns extracted from HMBC spectra of a THA sample in CDCl₃ acquired with: no NUS, 1 scan, $N_2*N_1$ = 2k*512 in 14 min 49s (blue); NUS 10%, 1 scans, $N_2*N_1$ = 2k*512 in 1 min 56s (red); NUS 10%, 2 scans, $N_2*N_1$ in 3 min 23s (green); and NUS 10%, 1 scan, $N_2*N_1$ = 2k*1k in 3 min 20s (purple).*
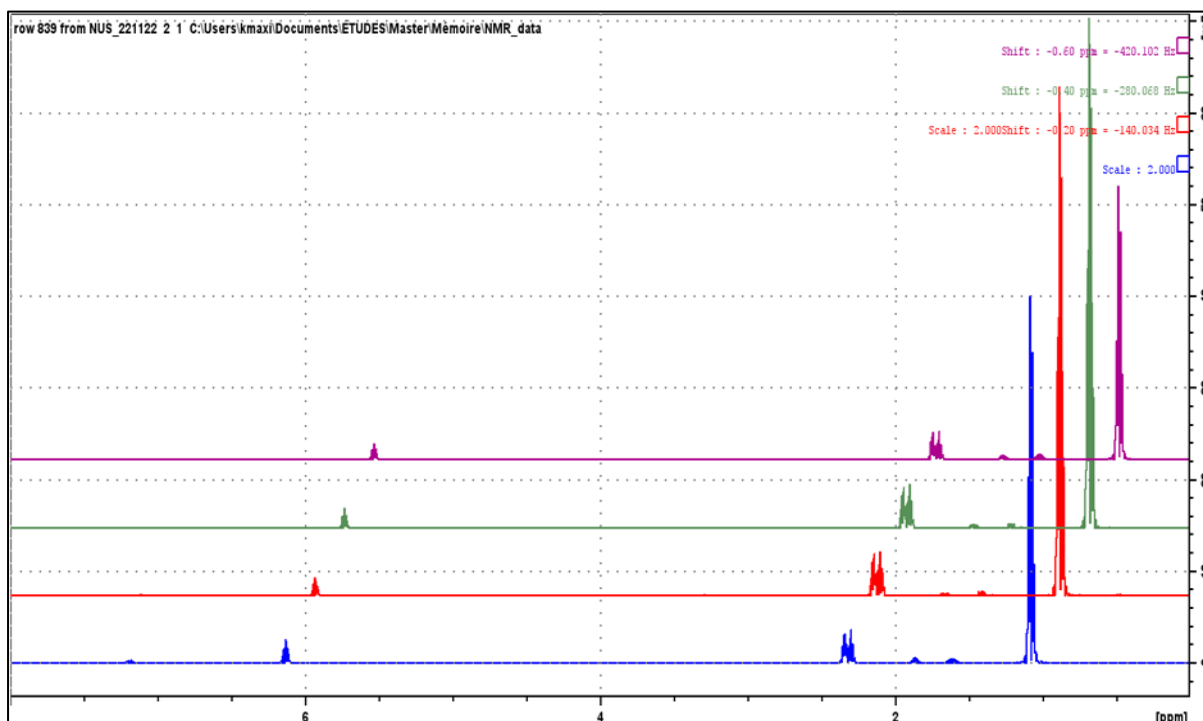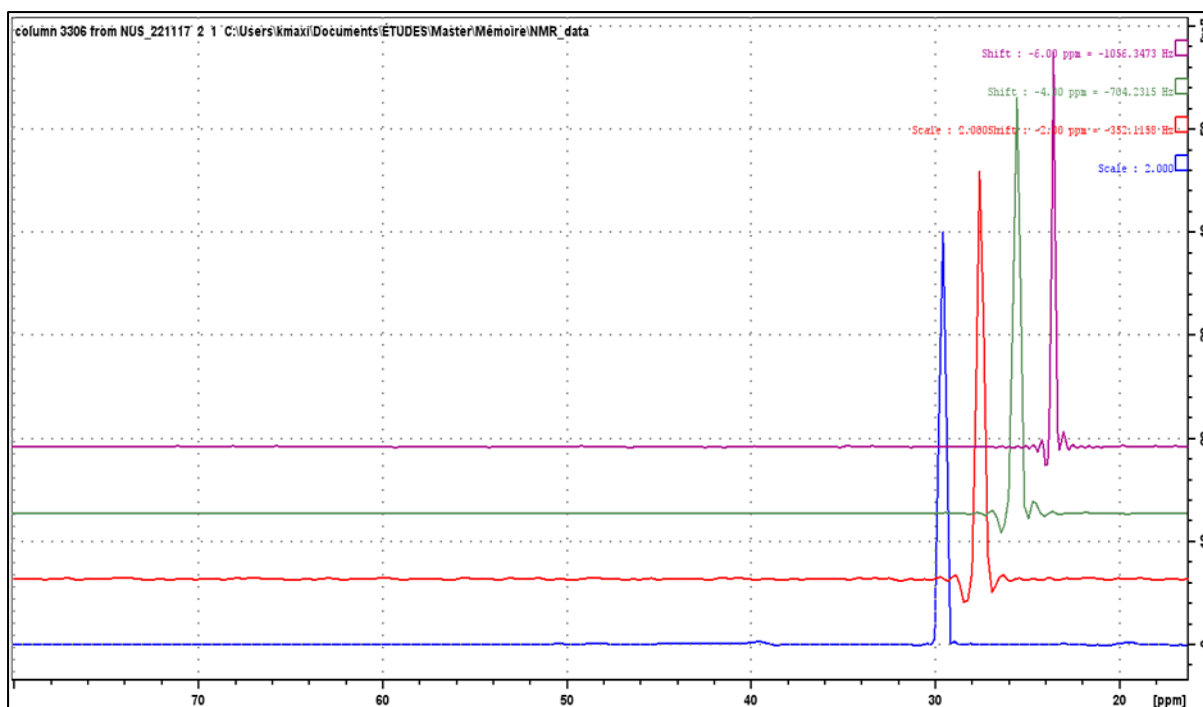
*Figure 23 - Superposition of the 6.35 ppm columns extracted from HMBC spectra of a THA sample in CDCl₃ acquired with: no NUS, 1 scan, $N_2*N_1$ = 2k*512 in 14 min 49s (blue); NUS 10%, 1 scans, $N_2*N_1$ = 2k*512 in 1 min 56s (red); NUS 10%, 2 scans, $N_2*N_1$ in 3 min 23s (green); and NUS 10%, 1 scan, $N_2*N_1$ = 2k*1k in 3 min 20s (purple).*



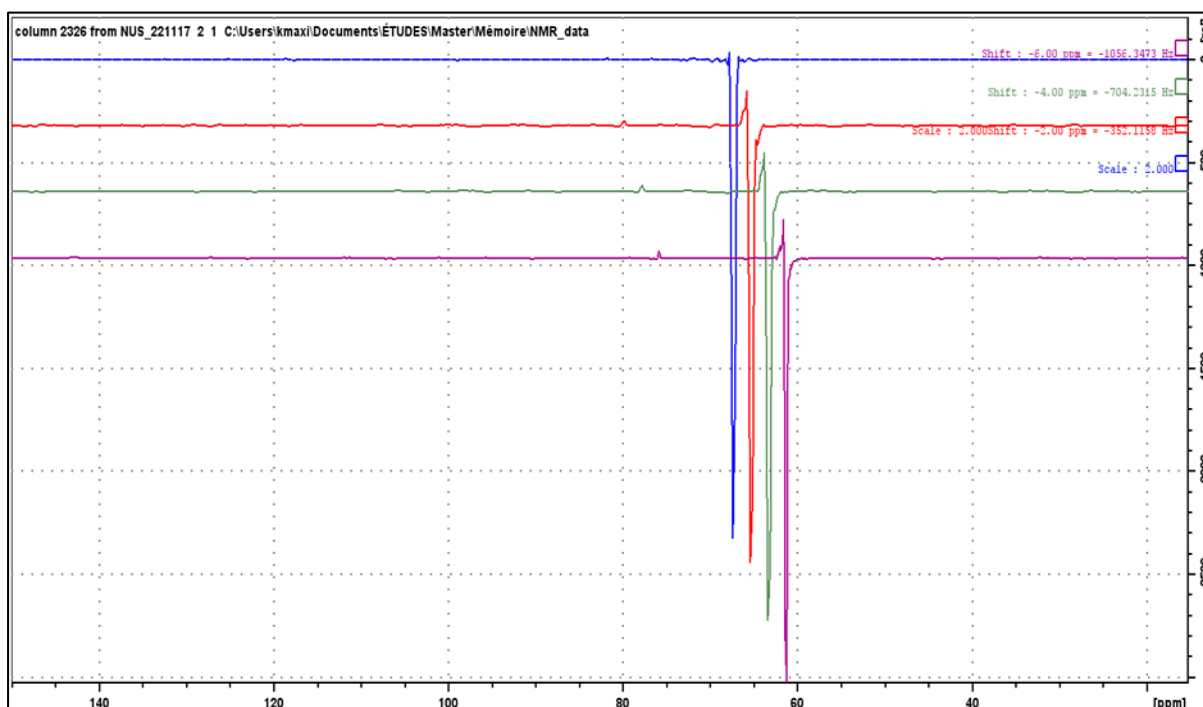*Figure 24 - Superposition of the 30.9 ppm rows extracted from HMBC spectra of a THA sample in CDCl₃ acquired with: no NUS, 1 scan, $N_2*N_1$ = 2k*512 in 14 min 49s (blue); NUS 10%, 1 scans, $N_2*N_1$ = 2k*512 in 1 min 56s (red); NUS 10%, 2 scans, $N_2*N_1$ in 3 min 23s (green); and NUS 10%, 1 scan, $N_2*N_1$ = 2k*1k in 3 min 20s (purple).*

*Figure 25 - Superposition of the 1.09 ppm columns extracted from HSQC spectra of a THA sample in CDCl₃ acquired with: no NUS, 1 scan, $N_2*N_1$ = 2k*512 in 14 min 44s (blue); NUS 10%, 1 scans, $N_2*N_1$ = 2k*512 in 2 min 18s (red); NUS 10%, 2 scans, $N_2*N_1$ in 3 min 42s (green); and NUS 10%, 1 scan, $N_2*N_1$ = 2k*1k in 3 min 39s (purple).*



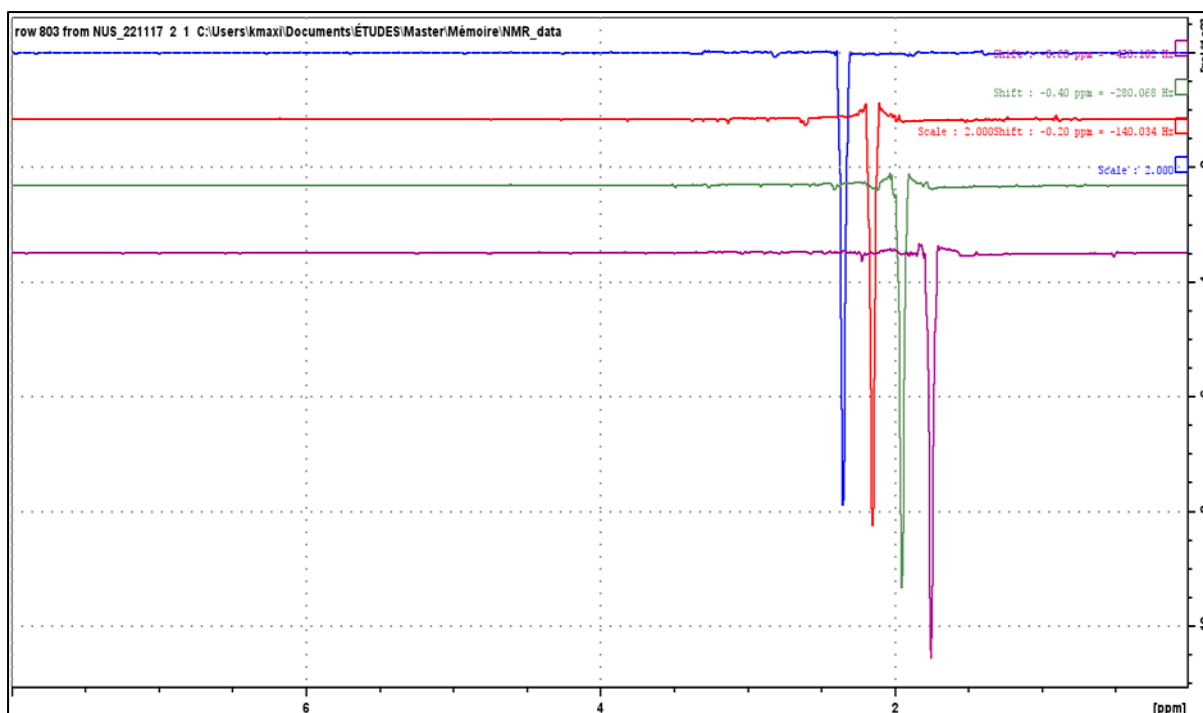*Figure 26 – Superposition of the 4.9 ppm columns extracted from HSQC spectra of a THA sample in CDCl₃ acquired with: no NUS, 1 scan, $N_2*N_1$ = 2k*512 in 14 min 44s (blue); NUS 10%, 1 scans, $N_2*N_1$ = 2k*512 in 2 min 18s (red); NUS 10%, 2 scans, $N_2*N_1$ in 3 min 42s (green); and NUS 10%, 1 scan, $N_2*N_1$ = 2k*1k in 3 min 39s (purple).*

*Figure 27 - Superposition of the 47.7 ppm rows extracted from HSQC spectra of a THA sample in CDCl₃ acquired with: no NUS, 1 scan, $N_2*N_1 = 2k*512$ in 14 min 44s (blue); NUS 10%, 1 scans, $N_2*N_1 = 2k*512$ in 2 min 18s (red); NUS 10%, 2 scans, $N_2*N_1$ in 3 min 42s (green); and NUS 10%, 1 scan, $N_2*N_1 = 2k*1k$ in 3 min 39s (purple).*

Figure A20-A21 are superposition of spectra acquired without NUS, one scan and $N_2*N_1 = 2k*512$ (blue) and with NUS 10%, 4 scans and $N_2*N_1 = 2k*1k$ (red).



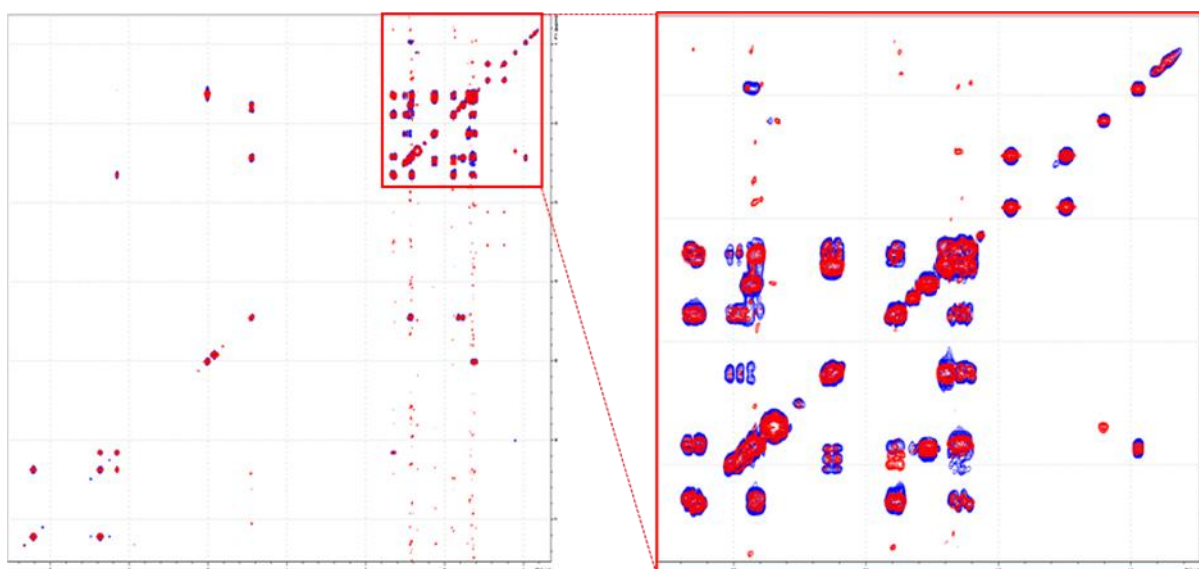*Figure 28 - Superposition of COSY spectra of a THA sample in CDCl₃ acquired with: no NUS, 1 scan, $N_2*N_1 = 2k*512$ in 14 min 12s (blue) and NUS 10%, 4 scans, $N_2*N_1 = 2k*1k$ in 11 min 29s (red). The red box on the right part is a zoom from the left superposition.*
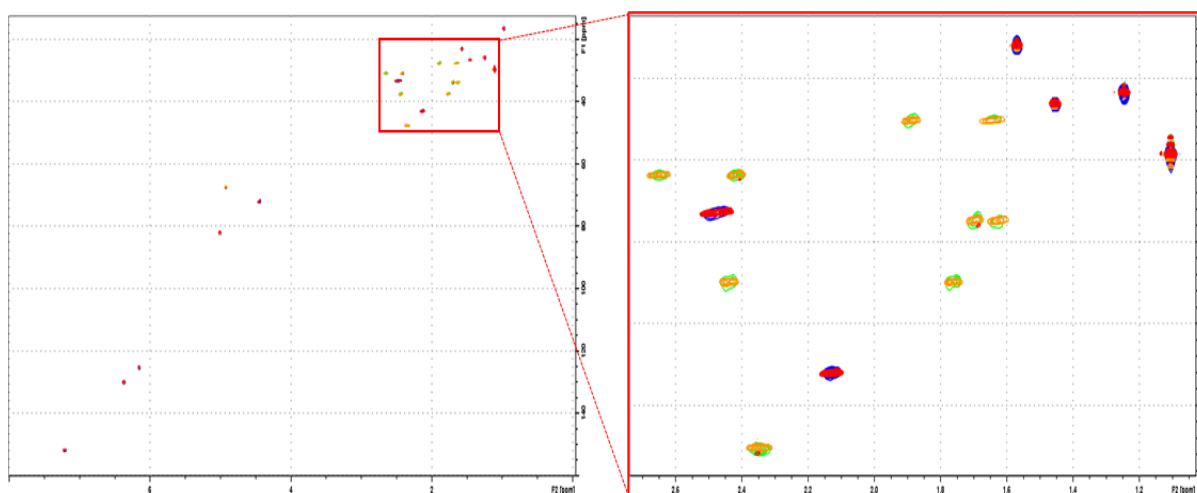
Kolkman M.

*Figure 29 - Superposition of HSQC spectra of a THA sample in CDCl₃ acquired with: no NUS, 1 scan, $N_2*N_1$ = 2k*512 in 14 min 44s (blue) and NUS 10%, 4 scans, $N_2*N_1$ = 2k*1k in 11 min 57s (red). The red box on the right part is a zoom from the left superposition.*

C. <u>Echograd sequence and calibrations</u>

Prior to the optimising both gradient and chirp powers, the command 'ufset' must be applied. That command reads a file which contains definitions for some parameters specific to both launch, processing and lecture of UF experiments, data and spectra. The file was provided by Giraudeau's team from Nantes.
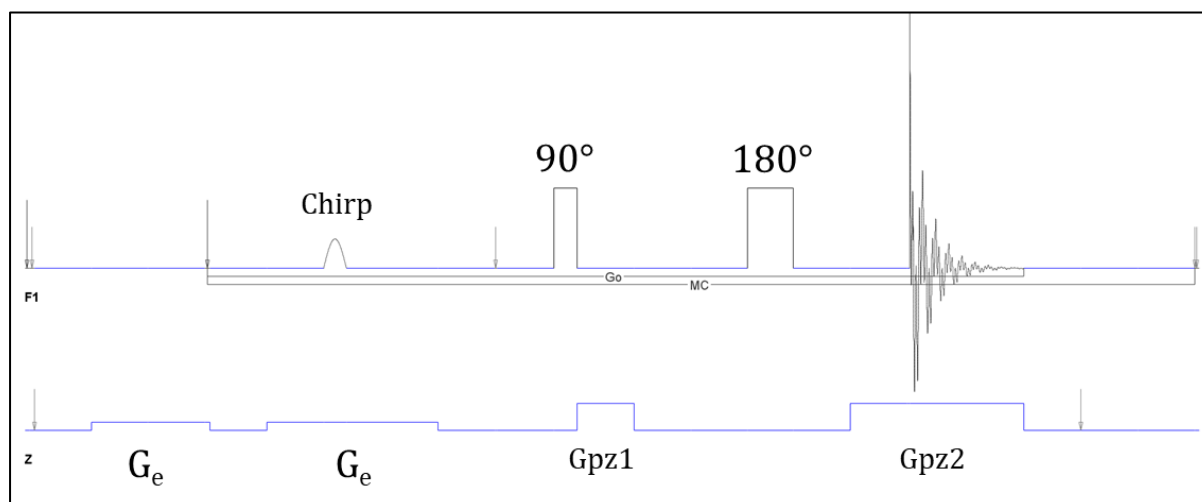


*Figure A22 - Echograd sequence. Here a chirp pulse of 25kHz of frequency range is applied.*

The echograd sequence (*Figure A22*) is used to observe the frequency dispersion generated by the gradients $G_e$ and the one excited by the chirp pulse. An important part in the used of this sequence is the phase correction step. One important feature to begin with is to set the pulse frequency offset (O1P), meaning the middle of the spectrum, because it has a significant impact on the phase corrections. Indeed, for UF experiments, a phase dispersion is caused by the gradients. But, if the O1P of the chirp pulse is modified,

**64** | 69

the phase encoding is modified, and the phase correction must be modified too. Therefore, instead of adapting the phase corrections values each time the chirp pulse parameters are modified, it is easier to calibrate O1P on the first basis. Once the phase corrections adjusted, they are retained through the various experiments used for the calibration of the gradients and the chirp pulse. Minor adjustments might be required but they will not be of a major impact if the first calibration is properly achieved.

It is noteworthy to remember that one of the major drawbacks of the UF experiments is the low SW. Therefore, O1P must be placed in the middle of the observed peaks in a first 1D-proton experiment. This prevents the possibility of missing some signals. As an example, if an aliphatic molecule is observed, with no aromatic signals, there is no need to cover the 10 to 5 ppm band. O1P can be set to 3 ppm so that the final SW will be centred around 3ppm, about 1 to 5 ppm or 0 to 6 ppm. If O1P was placed around 6 ppm, the signals with a low $\delta$ might not be observed. In this case, the experiment was conducted on EtOH, and figure 2a shows the 1D-proton spectrum of EtOH. O1P was set on 3ppm. For THA, sucrose and the metabolites sample, O1P was set to 4 ppm.

Another point is the difference of phase correction between a conventional and an UF experiment. The goal is to make all the oscillations disappear and to obtain a single bump. To achieve such shape, the phase correction in the first order is adjusted in the first place because the phase dispersion depends on the gradient and is different for each slice and thus for each frequency. The correction in the first order has a high value, about 295000 in our case. Afterwards, the zero order correction can be slightly adjusted to optimise the phase correction. Further figures show examples of the end result.

Afterwards, $G_e$ is the next parameter to be optimised. The power of the chirp pulse (CP) is set to 0 watt and both gpz1 and gpz2 are set to 10%. $G_e$ is the gradient which defines the relation between frequency and the z-axis position. The percentage value of $G_e$ will determine its intensity, defining the slope of B(z). It thereby determines the minimum and maximum frequencies, and thus a frequency band that could be manipulated. However, the wanted frequency band is related to the chirp pulse. Here, a chirp pulse with a fixed range of 25kHz is used. On one hand, to use a gradient generating a frequency band tighter than 25 kHz means the chirp pulse is not totally put to profit. A part of the chirp will excite at frequencies that are not generated by $G_e$, with no nuclei having the corresponding Larmor frequency. And on the other hand, if $G_e$ generates a frequency band wider than 25 kHz, it will result in a part of the sample not being excited. Moreover, the use of a more powerful gradient engenders more heating. $G_e$ must thus create a frequency range similar to the one being excited by the chirp pulse.

A first echograd experiment will be achieved with $G_e$ set to 0% and a shape will appear, showing the excitation profile (*Figure A23)*. The goal is to set the value of gpz0 such as the frequency dispersion, the width of the excitation profile, becomes close to 25 kHz. As an example, here, with $G_e$=0% and gpz1=gpz2=10%, a frequency dispersion of ~66 kHz is obtained. To get 25 kHz, we need to multiply it by a factor 25/66 ~0.38. $G_e$

must therefore be around 0.4 times the value of gpz1 & gpz2, here being around 3-4%. This is an approximation, and the value will be further optimised.



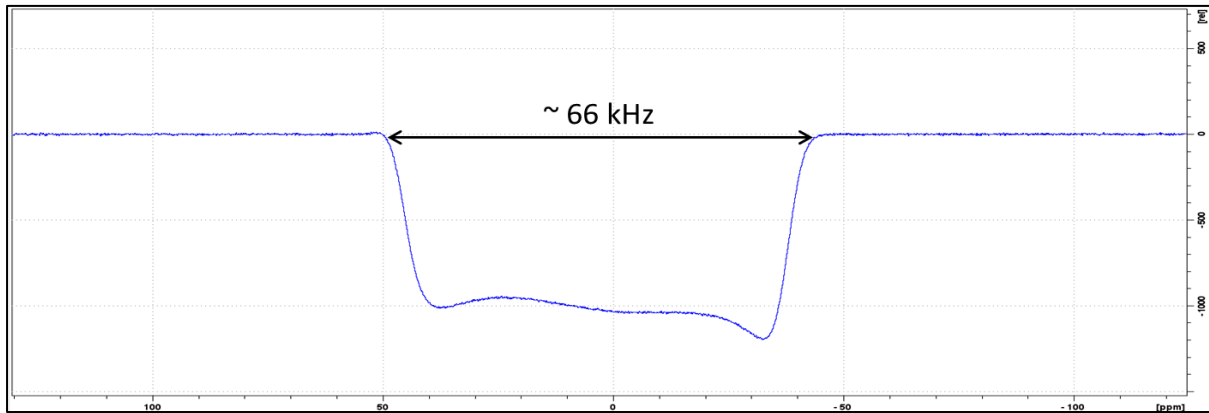*Figure A23 - Echograd for EtOH, with $G_e$=0%, CP = 1000dB and gpz1=-gpz2=10%. A frequency dispersion of ~66kHz is obtained.*

The second step is to activate the chirp pulse. To find an approximation of the value without taking the risk to damage the hardware, the simulation feature can be employed. In the simulation, the frequency range of the chirp pulse must be set a little wider than the actual frequency window which is going to be excited. Here, for a chirp pulse ranging over 25 kHz, a gap of 30 kHz has been set, thus from -15000 to +15000 Hz. (*Figures A24 & A25)* Afterwards, CP is calibrated to perform a 180° rotation. To evaluate the quality of the 180° rotation, it is possible to look at the $M_z$ value, which is standardly set at +1, and must reach towards -1. In general, the higher the power, the better the convergence towards -1. However, as more power equals more risks, CP must be as low as possible. Here, CP is around ~1000 Hz, meaning ~20 dB. The found value can used for the echograd experiment and will be further optimised.
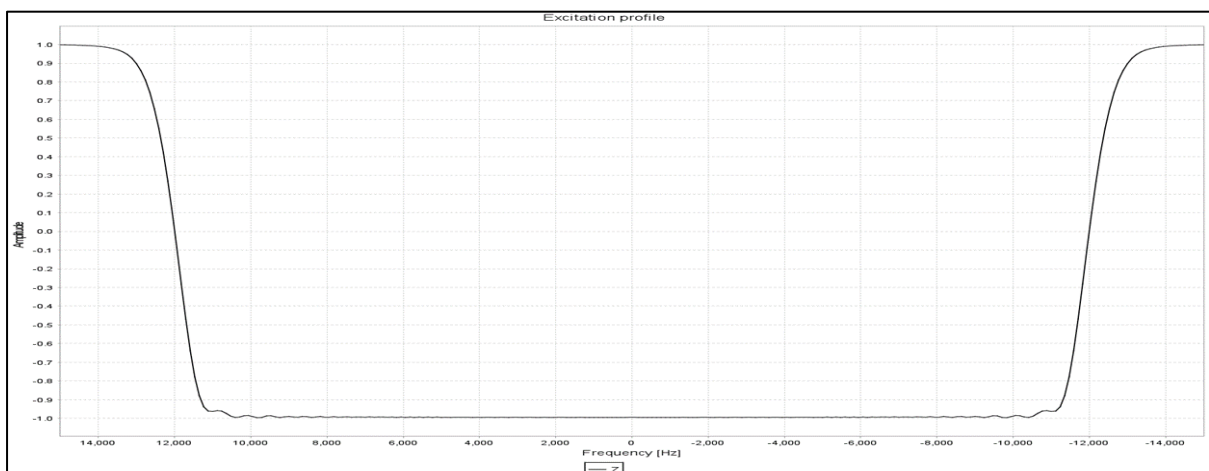


*Figure A24 – Simulation of the magnetisation along the z axis. The black line represent Mz after the chirp has been applied with a power of 1000Hz. A band of 25000Hz has Mz equalling -1 (vertical-axis value of the value of the plateau)*
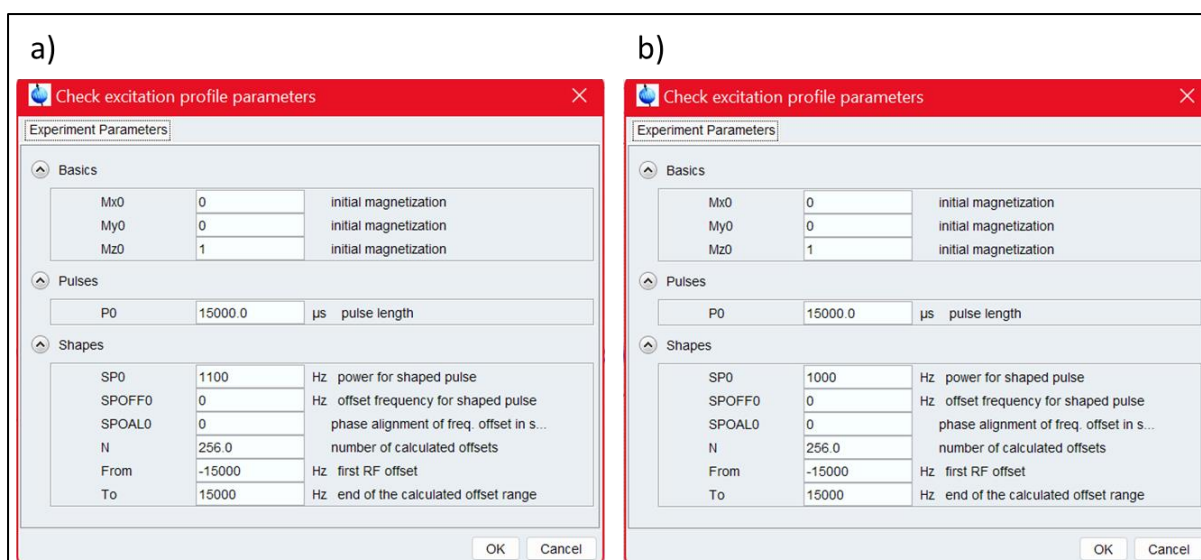
a)

b)



*Figure A25 - Simulations value: from -15000Hz to +15000Hz, pulse length of 15000µs, initial magnetisation fully on Mz (+1) and initial CP (a) or 'optimised' CP (b).*

These found values for $G_e$ and CP can then be applied and an echograd-spectrum is obtained. (*Figure A26*) The same phase corrections are applied in all spectra. As the spectrum is now upwards, and not downwards as in figure 34, it is clear the chirp was executed, engendering a 180° shift for the signals present in the 25kHz frequency band selected by the chirp pulse. Oscillations are present on all the echograd spectrum. These can be reduced by optimising the values de $G_e$ and CP.
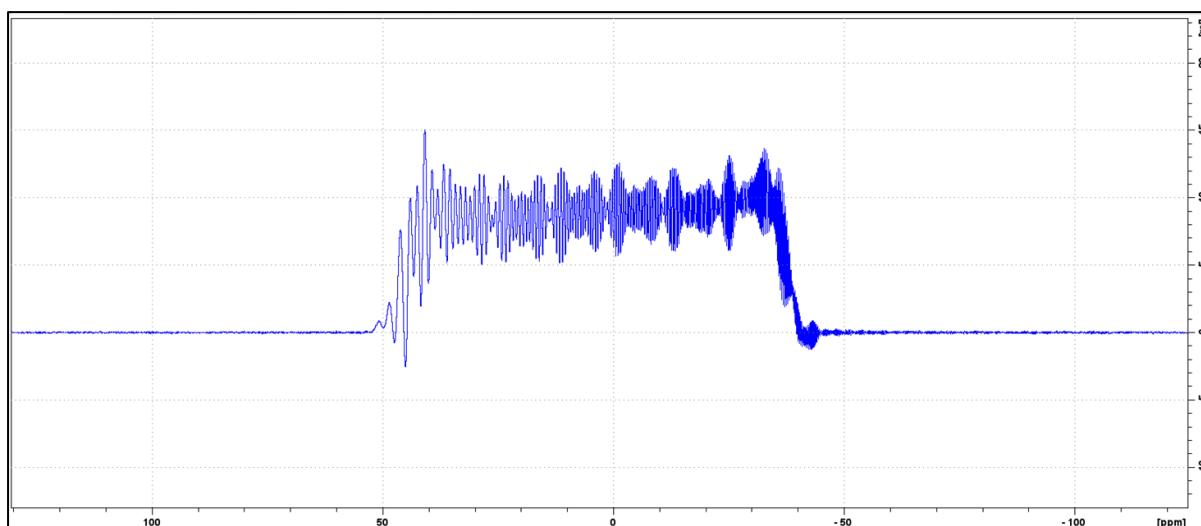


*Figure A26 - Echograd spectrum for an EtOH sample, with $G_e$=3.5% and CP=20dB.*

Various scenarios are possible and require different modifications. (*Figure 38*) Scenarios a, b and c consider the same CP value but were acquired with different $G_e$ values, respectively 3, 3.5 and 4%. In case c, the value of $G_e$ is too high. Indeed, the

*Kolkman M.*

echograd-spectrum shows (red arrows on figure 38) that some parts are still downwards, meaning they are part of the frequency range generated by the gradient but are not correctly excited by the 180° pulse. It is useless to have such high value for $G_e$, and even more since a higher value means more energy. $G_e$ must therefore be lowered. However, on the opposite, $G_e$ value must the highest possible to get the best profit from the chirp pulse. As both cases a and b do not present hollows on the extremities, like in the case c, the highest value is taken, here being 3.5%. This value was set for the 3 following cases d, e and f, which have the same $G_e$ value but were acquired with different CP values, respectively 18, 17 and 16 dB.
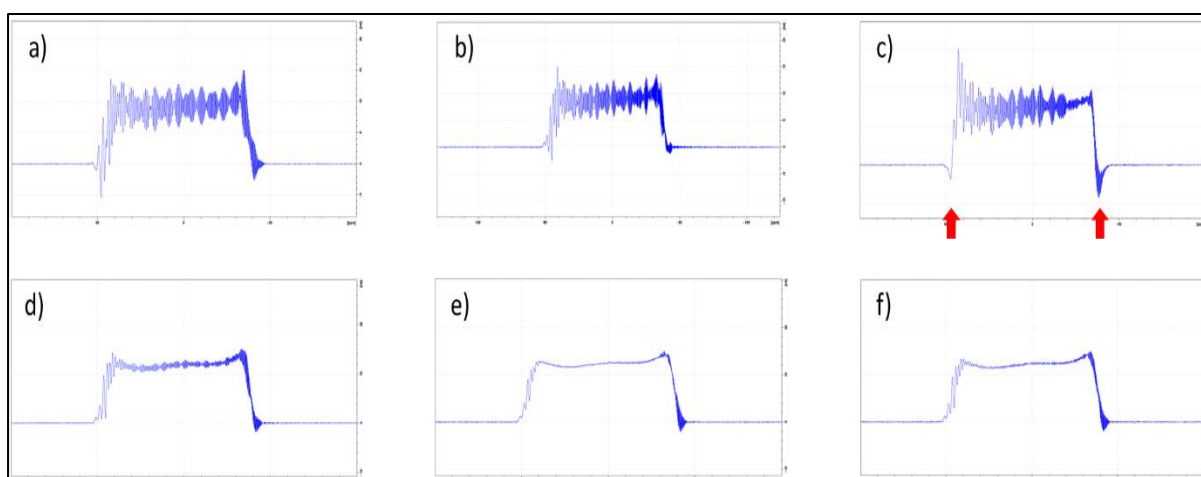


*Figure A27 - Echograd spectra for an EtOH sample. The upper line represents various values for $G_e$ (3% (a), 3.5% (b) and 4% (c)) at a fixed CP of 20dB. The lower line represents various values of CP (18dB (d), 17dB (e) and 16dB (f)) at a fixed $G_e$ value of 3.5%. Red arrows indicate the flaws due to a too high $G_e$ value.*

Oscillations appear on the echograd-spectra, and these can be lowered by increasing CP, thus lowering the value in decibel. However, there is no need to make the oscillations totally disappear because this might result in a unnecessarily high power value, which could endanger the spectrometer. Here, the case d still has a lot of oscillations, and cases e and f do not present relevant differences. Therefore, the value of CP is set to 17dB (case e).

### d. Bruker language/parameters

Here is a correspondence between the terms used in the hereby document and the parameters present in Bruker TopSpin.

IN = td(F1)

$G_e$ = gpz0 (echograd) = gpz0 (UFCOSY) = -gpz1 (UFCOSY)

N = td(F2)

AL = L3

CP = spw1

$N_{UF}$ and $N_{conv}$ do not correlate to parameters in TopSpin, they are calculated. Td(F2) is the total amount of acquired points in one lecture of the sequence. It is set to 18k and is never changed. $N_1$ is the number of points being acquired in one gradient $G_a$. It is calculated by dividing the total number of points by the number of gradients $G_a$:

$$N_{UF} = \frac{N}{2*AL}$$

$N_2$ is the number of points acquired along $t_2$ for a same slice. It is therefore impacted by interleaving. It is calculated by multiplying the number of gradients $G_a$ by the interleaving number:

$$N_{conv} = 2 * AL * IN$$

The multiplication between $N_1$ and $N_2$ gives N times IN, which is coherent. N is the total number of points acquired in one lecture of the sequence and IN is the number of lectures.

e. <u>Presaturation complementary information</u>

As the UFCOSY experiments use only one channel, a second one can be utilized, also to excite protons. The advantage of it is to let O1P on the medium of the spectrum with the first channel but using the other channel to perform the presaturation on the solvent, here water, meaning O2P = 4.7 ppm. If only one channel was used, the middle of the spectrum would have been imposed, and it would be the chemical shift value of the peak which needs to be suppressed.

*Kolkman M.*